PROTEIN NANOPARTICLE VACCINES

A Dissertation
Presented to
The Academic Faculty

by

Timothy Zuchi Chang

In Partial Fulfillment
of the Requirements for the Degree
Doctor of Philosophy in Bioengineering

Georgia Institute of Technology
May 2017

PROTEIN NANOPARTICLE VACCINES

Approved by:

Dr. Julie Champion, Advisor
School of Chemical & Biomolecular Engineering
Georgia Institute of Technology

Dr. Jennifer Leavey
School of Biological Sciences
Georgia Institute of Technology

Dr. Mark Prausnitz
School of Chemical & Biomolecular Engineering
Georgia Institute of Technology

Dr. Baozhong Wang
Institute for Biomedical Sciences
Georgia State University

Dr. Krishnendu Roy
School of Biomedical Engineering
Georgia Institute of Technology

Date Approved: March 13, 2017

ACKNOWLEDGEMENTS

First, I'd like to thank my family for all their support over these past few years. Mom and Dad, thank you for all the unconditional love, encouragement and packages you've given me over these past five years. Uncle Tom, Aunt Mary, thank you for all the motivating phone conversations and refreshing getaways that helped me maintain perspective throughout my time in grad school.

To my advisor, Julie, thank you for taking me on as your student all those years ago. I have been so grateful for your seemingly infinite patience and compassion throughout the learning process. I would like to thank you not only for my scientific and technical training, but for mentoring by example as a forthright and passionate leader of scientific inquiry.

Members of my thesis committee, Dr. Mark Prausnitz, Dr. Krish Roy, and Dr. Jennifer Leavey and Dr. Baozhong Wang, thank you for all your input and suggestions during the preparation of my thesis. Dr. Prausnitz, thank you for the helpful discussions on technology commercialization. Dr. Roy, thank you for giving me access to your cells, protocols, antibodies and more during my research. Dr. Leavey, thank you for teaching me immunology during my first year here.

Dr. Wang, thank you especially for all the advice you've given me at both Emory and Georgia State, and for letting me conduct animal studies in your research labs. Working with insect cells, viruses, and mice brought a whole new dimension of analysis to my thesis, and I am very grateful for the opportunity to have done so.

I'd also like to thank all of the collaborating post-docs I have worked with from Dr. Wang's lab, who taught me techniques that allowed me to conduct my thesis research. Dr. Lei Deng, Dr. Jong Rok Kim, Dr. Yuan He, Dr. Han Zhang, Dr. Li Wang, thank you for all of your assistance and advice on my experiments.

To my fellow soldiers in the trenches, members of the Champion Lab past and present, thank you for your support and camaraderie that make going into lab everyday so enjoyable. Lina, Won, Trudy, Anusha, Kevin, Alex, Adam, Kelly, Anshul, Xingjie, Tianxin, Sung In and Yeongseon, I could not have asked for a more amazing and fun set of characters for coworkers than you guys.

To my mentees who helped me with collecting data for my thesis, Sam, Erika, Siva, and Ishatou, thank you so much for all your hard work, and for working through experimental plans with me. I have become a much better mentor thanks to your help, and I am grateful for having had the opportunity to participate in the scientific process with you.

Finally, to friends near and far, new and old, thank you all for helping me maintain my sanity all these years. Whether you were a phone call away, a stroll down the hall, a walk down the street, or frying seafood in my kitchen at 3am, thank you for being there to celebrate the highs and commiserate during the lows of graduate school. Thank you Jeff, Dee, Perry, Victor, Vicky, Kevin, Julia, Zara, Andrew, Weipeng, Trevor, Joanna, Sylvia, Dalar, Emily, Graham, Chris, Helen, Michael, Jared, Caleb, Christine, Anusha, Trudy, Dan, Monica, Harrison, Troy, Adam, Alex and so many others who weave warm, vibrant colors into the tapestry of life wherever they go.

TABLE OF CONTENTS

LIST OF TABLES

LIST OF FIGURES

LIST OF SYMBOLS AND ABBREVIATIONS

3HA	Trimerized H7 hemagglutinin, stabilized by a GCN4 trimerization motif
APC	Antigen-presenting cell
BMDC	Bone marrow-derived dendritic cell
BSA	Bovine serum albumin
DC	Dendritic cell
dLN	Draining lymph node
DLS	Dynamic light scattering
ELISA	Enzyme-linked immunosorbent assay
ELS	Electrophoretic light scattering
fAiChi	Flagellin-AiChi fusion protein
FBS	Fetal bovine serum
FcγR	Fcγ receptor
FDA	Food and Drug Administration
FDC	Follicular dendritic cell
FliC	Flagellin
fM2e	Flagellin-M2e fusion protein
fPR8	Flagellin-PR8 Hemagglutinin fusion protein
GC	Germinal center
GM-CSF	Granulocyte macrophage colony stimulating factor
HA	Hemagglutinin
HAI	Hemagglutination inhibition
i.m.	Intra-muscular

i.n.	Intra-nasal
IC	Immune complex
IL	Interleukin
IngLN	Inguinal lymph node
LDH	Lactate dehydrogenase
LPS	Lipopolysaccharide
M2e	Influenza matrix protein 2 ectodomain
MHC	Major histocompatibility complex
NA	Neuraminidase
NIAID	National Institute of Allergy and Infectious Diseases
OVA	Ovalbumin
PAMPs	Pathogen-associated molecular patterns
PBS	Phosphate-buffered saline
PdI	Polydispersity index
PLGA	Poly lactic-co-glycolic acid
pMHC	Peptide-loaded major histocompatibility complex
RDE	Receptor-destroying enzyme
SAPN	Self-assembling protein nanoparticle
TCC	Terminal complement complex
TCR	T-cell receptor
TLR	Toll-Like receptor
TNF-α	Tumor necrosis factor α
VLP	Virus-like particle
WHO	World Health Organization
α-MEM	Alpha-modified Eagle's medium

SUMMARY

Highly conserved pathogen proteins are ideal components for broadly cross-protective vaccines, but tend to be poorly immunogenic. The presence of particulates in a vaccine has been known for more than 100 years to enhance a vaccine's efficacy, yet only in recent decades has rational nanoparticle vaccine design emerged from advances in our understanding of immunology. While most vaccine nanoparticles seek to encapsulate or coat antigen onto particles, protein nanoparticles are made entirely of crosslinked antigen. This form of nanoparticulate antigen does not require the addition of stabilizing additives, and the nanoparticle is both the antigen and the immunostimulatory adjuvant. Without added excipients or adjuvants, protein nanoparticles drastically reduce the possibility of off-target immune responses, and their abiotic nature makes them amenable to cold chain-independent storage and use. Protein nanoparticle vaccines have been made from conserved influenza matrix protein 2 peptides (M2e), and triggered specific, adaptive immune responses that soluble protein could not.

Given the enhanced immunogenicity of M2e nanoparticles, we sought to understand the immunological mechanisms behind protein nanoparticle-mediated adjuvancy, whether protein nanoparticles could enhance the immunogenicity of other types of influenza antigens, and whether protein nanoparticle adjuvancy could be further enhanced by the addition of molecular adjuvants. The work described herein (1) tests an expanded range of recombinant influenza proteins as viable components of influenza protein nanoparticle vaccines, (2) examines the

immunological basis behind protein nanoparticle adjuvancy *in vitro* and *in vivo*, (3) assesses long-term, cold chain-independent storage of protein nanoparticle vaccines, and (4) explores using molecular adjuvants as nanoparticle coatings for enhancing vaccine efficacy.

Nanoparticle size and coating were found to be important design criteria for immunogenic protein nanoparticles, and *in vivo* biodistribution and *in vitro* dendritic cell processing of nanoparticles yielded insights into mechanisms of protein nanoparticle adjuvancy. Extended room-temperature wet storage of nanoparticles for up to 3 months was shown to yield no loss in immunogenicity, and the molecular adjuvants flagellin and immunoglobulin were shown to enhance various aspects of the immune response in a mouse immunization model. As cold chain-independent storage is an important goal for disseminating new types of vaccines to the developing world, protein nanoparticles have proven to be an attractive and stable platform technology for the co-delivery of antigen and immunostimulatory adjuvant. Furthermore, the ability of immunoglobulin (Ig) to enhance immune responses to protein nanoparticles underscores the importance of innate immunofeedback mechanisms mediated by this protein, and should be explored further. In addition to providing a host-derived means of enhancing adjuvancy, Ig-opsonized protein nanoparticles could serve as a tool for further investigations in the broader field of immunoengineering. Our work establishes protein nanoparticle vaccines as a promising, versatile platform technology for enhancing the adjuvancy of recombinant subunit protein antigens.

CHAPTER 1. INTRODUCTION

1.1 The Next Generation of Influenza Vaccination

Traditional vaccine development has followed an "isolate-inactivate-inject" paradigm[1], in which whole pathogens are cultured *in vitro*, inactivated to make them less virulent, and injected into a person to induce a protective immune response. This method works well for some pathogens, but the immunology behind why some whole pathogens make good vaccines and others don't remains unclear. The whole pathogen approach is especially ineffective for pathogens that mutate rapidly, such as influenza.

Influenza epidemics affect 5-15% of the world's population every year, and cause approximately 500,000 deaths annually [2]. The traditional approach to generating effective influenza vaccines relies on sampling the currently circulating influenza viruses, and formulating a vaccine with multiple subtypes of the virus. Currently, the World Health Organization (WHO) collects data from more than 120 influenza research centers globally to decide which influenza subtypes need to be included in each year's flu vaccine [3, 4]. As an example, since the H3N2 subtype of the influenza A virus was discovered in 1968, the vaccine strain of H3N2 has been updated almost 30 times, and the WHO analyzes data from approximately 3000 H3N2 viruses every year [3]. This method is labor-intensive, not guaranteed to be effective every year, and requires people to get annual influenza vaccines.

The next generation of influenza vaccines aims to circumvent problems with mutating viruses using recombinant protein expression. Instead of reacting to influenza strains as they emerge, recombinantly-engineered subunit antigens can be rationally

designed with common elements of multiple strains to induce cross-protective immunity. Recombinant protein expression is also an efficient and scalable process for producing these more well-defined antigens [5]. Traditional influenza vaccine virus production requires infection and culturing of virus in embryonated chicken eggs, which is a low-yield process that requires 3-6 months to produce a vaccine, and is unsuitable for responding to pandemic influenza outbreaks [6]. Furthermore, the purification process often results in contaminating egg proteins, such as ovomucoid ovalbumin, that render the vaccine unsuitable for people with egg allergies [7].

1.2 Recombinant Influenza Antigen Choices

Influenza virus subtypes are typically defined by their surface antigens hemagglutinin (HA) and neuraminidase (NA). Hemagglutinin binds sialic acid residues found on mammalian and avian cells, and enables the virus to gain entry into cells via endocytic pathways, where the virus can then replicate [8]. Neuraminidase is responsible for cleaving nascent viruses from infected cells to allow for secondary infection. Generating neutralizing antibodies against HA that can block viral entry is crucial to preventing replication and generating a protective immune response, and HA is considered the most important component of an influenza vaccine [9].

As such, two common assays are used to probe HA structure and function in assessing a vaccine's efficacy. Hemagglutinin's ability to bind to sialic acid residues on cells is used in the hemagglutination assay, in which dilutions of HA are used to crosslink red blood cells (RBCs). Visible detection of crosslinked RBCs can be used as a quick, *in vitro* test of the conformation of recombinantly-expressed HA or the stability of influenza

viruses. The complement of the hemagglutination assay is the hemagglutination inhibition (HAI) assay. In this test, antiserum from individuals vaccinated or infected with influenza is used to block hemagglutination. The number of dilutions that a serum sample can successfully block RBC crosslinking by HA protein or influenza virus is proportional to the concentration of neutralizing antibodies present in the serum.

Currently, there are 18 known subtypes of HA [10], and it is this variability, combined with the high rate of intra-subtype HA mutation, that makes HA such a difficult target to immunize against. Conserved antigens are proteins common to all strains of influenza, and are consequently attractive antigen targets for incorporation into a universal influenza vaccine. The extracellular portion of the influenza matrix protein M2 (M2e) is highly conserved among all strains of influenza. The M2 protein is an ion channel responsible for the virus's endosomal escape, and the small, functional nature of this protein necessitates its conserved sequence [11, 12]. Antibodies to M2e have been found to have neutralizing activity and can prevent influenza infection [13], but are very rarely elicited following an influenza infection or vaccination. The larger HA protein occludes the smaller M2 protein on the outside of the virus, and is considered the more immunodominant epitope, as antibodies are often raised to HA first. A subunit vaccine containing M2e could provide cross-strain protective immunity.

The HA protein also has conserved sequences, but these are on the membrane-proximal "stalk" region. The membrane-distal "head" region is the more immunogenic portion of the protein, and is less conserved. HA stalk proteins fall into two conserved phylogenetic groups [10]. Group 1 contains H1, H2, H5, H6, H8, H9, H11, H12, H13, H16, H17 and H18, while group 2 contains H3, H4, H7, H10, H14 and H15. Antibodies raised

against the HA stalk region can also be neutralizing[14], making the HA stalk also an attractive candidate for a universal influenza vaccine antigen.

Given the conserved portions of M2e and HA can elicit neutralizing antibodies, universal influenza vaccines will most likely contain conserved antigen sequences from M2e and the two HA stalk proteins [10]. Recombinant protein expression allows for customized delivery of vaccine antigens, rather than relying on the native proportions of those antigens found on the pathogen. While recombinant proteins will play an important role in the development of a universal influenza vaccine, recombinant expression of specific, non-conserved influenza proteins will also be useful in developing a rapid response to pandemic influenza outbreaks. We explore vaccines with both types of influenza antigens in Chapter 2.

1.3 The Necessity of Adjuvants

While the antigenic targets for a universal influenza vaccine have been established, these proteins generally have poor immunogenicity on their own [15]. Adjuvants are additives to vaccines that are commonly employed to boost the immune response to vaccine antigens. Adjuvants generally fall into two categories: molecular adjuvants and particulate adjuvants [16]. Molecular adjuvants bind specific immunoreceptors that trigger stimulatory immune cell pathways, enhancing the immune system's perceived danger of the vaccine antigen. Many of the molecular adjuvants are components of bacteria and viruses, such as CpG DNA, double-stranded RNA, lipopolysaccharides, and bacterial proteins such as flagellin [8]. The innate immune system has evolved to recognize many pathogen-associated molecular patterns (PAMPs), and molecules that are perceived as inherently

foreign trigger inflammatory immune responses. Because the underlying cellular pathways these molecules activate are still not fully elucidated, an incorrect or inappropriate amount of inflammation can be triggered by the wrong type or dose of a particular molecular adjuvant. Freund's complete adjuvant, an oil-in-water emulsion of heat-killed mycobacteria, is one of the most potent adjuvants known, and is used to generate polyclonal antibodies in mice [17]. It also generates excessive inflammation and is commonly used as a model inducer of anaphylactic shock, and is thus unsuitable for human use due to its potency [18]. To generate clinically suitable adjuvants, the National Institute of Allergy and Infectious Diseases (NIAID) anticipates spending at least $70 million on vaccine adjuvant research from 2014-2019 [19]. However, as of this writing, only three adjuvants have been approved by the Food and Drug Administration for use in vaccines [19, 20]. Safety concerns over administration of PAMP-based adjuvants have slowed the translation of these adjuvants into the clinic [21]. Currently, only one TLR ligand-based adjuvant, MPL, has been approved for use in humans [22], and its use has been associated with injection-site reactions and transient flu-like symptoms [23].

Particulates are another class of adjuvants. The presence of micro- and nanoparticles in vaccines has been shown to enhance immune responses to co-administered antigen. Since the discovery that aluminum hydroxide crystals, or alum, enhances adjuvancy in influenza vaccines[24], numerous efforts have been made to understand and harness particulate-based vaccine adjuvancy [25-27]. Alum was initially thought to serve as an antigen depot, allowing for sustained release of antigen to the immune system over time [16]. Other hypotheses of alum's mechanism of action include initiating cellular damage [28], consumption by and inflammation of antigen-presenting cells [29, 30], and

adsorption of the innate immune proteins of the complement system [30]. The various proposed mechanisms of alum-mediated adjuvancy have motivated a wide range of engineered micro- and nanoparticle vaccines to mimic the adjuvant effects of alum in a biodegradable and more immunostimulatory form. One common design strategy is to make vaccine particles that imitate the size and shape of pathogens, given the effectiveness of inactivated whole-pathogen vaccines. Since the size of viruses and bacteria generally range from 100 nm – 1 μm, this thesis will focus on the design of nanoparticle vaccines.

Vaccine nanoparticle design generally follows two strategies: internal encapsulation of antigen and/or native antigen display on a particle surface. Biodegradable polymers such as chitosan and poly lactic-co-glycolic acid (PLGA) have been studied extensively for nanoparticle vaccine encapsulation [31], though many different polymers have been investigated [32]. Incorporation of antigens in a nanoparticulate polymer matrix has shown that controlled release of antigen to the immune system gives an advantage over vaccination with soluble antigen [16, 32, 33]. Recently, surface-based display of antigen on nanoparticles, such as on virus-like [32], protein [34] and polymeric [33, 35] particles has gained increasing attention. The shift towards surface antigen display has been driven by two insights: (1) an immunological understanding that surface receptor engagement on antigen presenting cells (APC) is essential for optimal interfacing with the innate and adaptive immune systems [36], and (2) the discovery that APC engagement with nanoparticles themselves triggers inflammatory responses [25, 29, 37].

Vaccine nanoparticles are designed to present specific antigens and epitopes in the context of enhanced immunogenicity conferred by particulate matter. However, the immunomodulatory effects of nanoparticles have been shown to be a function of many

factors, including nanoparticle size [38-40], shape [41, 42], charge [43], surface chemistry [44], and administration route [45]. Given the diversity of vaccine nanoparticle types [36] and immunological responses observed, universal design principles have been difficult to elucidate. Molecular adjuvants are a more well-defined class of immunostimulants, but cannot replicate the exact mechanisms of nanoparticle-mediated adjuvancy. The immunogenic vaccines of the future will most likely contain both molecular and particulate adjuvants, and we explore the interplay between the two types of adjuvants in Chapter 5.

1.4 The Immunology of Vaccine Efficacy

Any rational vaccine design that incorporates molecular and nanoparticulate adjuvants must be based on the principles of immunology. The following sections outline the various components of the immune system we hypothesize to be interacting with nanoparticle vaccines.

1.4.1 Antigen Presentation by Dendritic Cells

While multiple cell types interact with vaccine nanoparticles, dendritic cells (DCs) have been identified as the most potent antigen presenting cells (APCs) [46]. Dendritic cells are characterized by long, branching projections that stem from their cell body, and sample the periphery of the body for foreign antigens. Their ability to process antigens and present them in an immunostimulatory or tolerizing context makes them master regulators of the immune system [47].

Dendritic cell processing and presentation of antigens to B and T cells of the adaptive immune system transforms an innate immune response into an adaptive one. This

bridging of the two arms of the immune system is essential for generating protective immunity [8]. The current model of antigen presentation requires three types of signaling to be initiated by dendritic cells: (1) presentation of antigen-derived peptide on the major histocompatibility complex (MHC), (2) costimulatory surface presentation of maturation factors CD40, CD80, or CD86, and (3) soluble cytokine secretion. Upon encountering foreign protein antigen, a dendritic cell will digest the antigen into smaller peptides to be loaded onto externally-presented MHC I and/or MHC II, and upregulate surface maturation markers. The dendritic cell will then migrate to the nearest lymphatic vessels to reach a lymph node, where the peptide-MHC complex (pMHC) will be presented to T cells. Each T cell has a unique T cell receptor (TCR) that recognizes one type of peptide bound to the MHC complex. Upon correct TCR-pMHC complex binding, and T cell CD28 binding either CD80 or CD86 on the DC, the T cell starts to proliferate and begins the adaptive immune response. $CD4^+$ T cells are known as helper T cells, and are responsible for stimulating antibody production by B cells and triggering proliferation of $CD8^+$ T cells. $CD8^+$ T cells are known as cytotoxic T cells, and are responsible for surveying and killing host cells infected with viruses or intracellular bacteria [8].

While the first two signals are essential for DC maturation and successful antigen presentation, it is hypothesized that the types of cytokines secreted vary in response to the type of antigen being presented, and that this is what allows dendritic cells to effect a wide range of immune responses [48]. In addition to various cytokine signals, different subpopulations of DCs, such as myeloid and lymphoid DCs, can also elicit different types of immune responses [49]. Myeloid DCs are differentiated from the same precursors as macrophages, and are responsible for antigen uptake in the periphery of the body and

transport to the lymphatic system [50]. Lymphoid DCs are lymph node-resident dendritic cells that share a precursor with T cells, and are thought to be involved in promoting immunological tolerance. Recently, lymph node-resident follicular dendritic cells (FDCs) were shown to play an important role in promoting B cell development, but are not related to conventional lymphoid DCs, being derived from vascular endothelium instead [51]. FDCs bind immune complexes, or antibodies associated with antigen. FDCs present these immune complexes to B cells undergoing germinal center reactions, a process that generates antibodies of higher affinity and of diverse effector functions [8, 48].

While dendritic cell stimulation of T cells has been extensively studied and characterized, dendritic cell interactions with B cells are proving to be of great importance as well. Whereas T cell epitopes are linear peptide fragments, B cell epitopes can be conformational and non-linear [8]. B cells can also be stimulated by antigen directly as well, and multimeric epitope display, such as that found on the surface of a nanoparticle, is a known to enhance B cell activation [8]. Nanoparticle vaccines that aim to deliver peptides or proteins to dendritic cells, B cells or T cells should take into account antigen type and appropriate costimulatory molecule delivery.

Peripheral dendritic cell contact with vaccine antigen delivery is not the only means of antigen presentation to the adaptive immune system. Vaccine targeting to the draining lymph nodes using nanoparticle size is a strategy for enhancing antigen delivery to dendritic cells[52], and 100-200 nm has been found to be the upper limit on nanoparticle size for passive drainage to the lymphatic system[52, 53]. Particles in the 500-2000 nm range are actively trafficked to the lymph nodes by antigen presenting cells. At the cellular level, size effects also tend to vary among different nanoparticle materials [38, 39, 54, 55].

However even within the extensively-studied category of polystyrene nanoparticles, nanoparticle sizes ranging from 40 nm [54] to 3 μm [56] have been suggested as optimal. We explore the roles of nanoparticle size and the biodistribution of our nanoparticles further in Chapter 3.

1.4.2 Toll-Like Receptors as Triggers of Inflammation

Pathogen-associated molecular patterns (PAMPs) are macromolecules that interact with specific pattern recognition receptors (PRRs) on or inside dendritic cells and macrophages [8, 27]. Receptors that bind bacterially-derived or virally-derived macromolecules are hypothesized to initiate adaptive immune responses geared toward those particular classes of pathogens [8, 57]. Toll-like receptors (TLRs) are a class of membrane-bound PRRs that have been extensively studied for vaccine adjuvant use [58-60].

For influenza vaccines in particular, flagellin has shown potential as an effective PAMP adjuvant. Flagellin, or FliC, binds to TLR-5 on antigen presenting cells, and its signaling has been associated with enhanced antibody responses [60]. A systems biology analysis of sera samples of humans immunized with a trivalent influenza vaccine showed a strong correlation between serum TLR-5 receptor upregulation 3 days post-vaccination and strong HAI titers 4 weeks post-vaccination [61]. The route of flagellin-mediated adjuvancy is unclear. Flagellin has been anchored into influenza virus-like particles [62], and FliC-antigen fusion proteins have seen promising results in clinical trials [63]. However, mice given flagellated *E. coli* bacteria orally responded better to a subcutaneous influenza vaccine than mice fed unflagellated bacteria, indicating that flagellin may not

need to be incorporated directly into the vaccine [64]. We examine the role of flagellin location in a nanoparticle vaccine formulation in Chapter 5.

1.4.3 T Cell Responses and the T_H1/T_H2 Bias

In studying $CD4^+$ T cell responses upon dendritic cell activation, immunologists found two distinct patterns of T cell activation. In the presence of mature dendritic cells and IL-12, T cells display a T_H1 response, marked by IFN-γ, IL-2 and TNF-β secretion and the activation of macrophages to kill intracellular pathogens. In the presence of mature dendritic cells and IL-4, T cells display a T_H2 response, marked by secretion of IL-4, IL-5, IL-10 and IL-13 and activation of eosinophils and mast cells [8, 65]. T_H1 responses are often referred to as cell-mediated immune responses, due to their predominance during infections involving intracellular bacteria and viruses. T_H2 responses are antibody-predominant responses, and are elicited in response to parasitic worms and allergens. The type of helper T cell response generated by a vaccine or infection is crucial – induction of the correct immune response can be protective, while the inappropriate response can be fatal [66].

Directing appropriate T cell responses is an important feature of nanoparticle vaccine design. Alum adjuvants are known to bias T cell responses towards a T_H2 response, which is inappropriate for influenza and other viral vaccines [16]. Nanoparticle size and shape were recently shown to play a role in determining T_H1 vs T_H2 responses, with 200 nm spherical particles eliciting a T_H1 response and 1500 nm rods eliciting a T_H2 response [67]. To evaluate T_H1 vs T_H2 responses after an immunization, antigen stimulation of

mouse splenocytes in an ELISPOT assay allows for convenient quantification of IFN-γ or IL-4 production in the absence of a pathogen challenge.

1.4.4 The Role of Antibodies and Immunofeedback

Immunoglobulins, or antibodies, play a vital role in the immune response, and there is increasing attention being paid to them in the development of immunotherapeutics. Antibodies are secreted by B cells and have a variety of effector functions. In addition to binding pathogens and neutralizing their surface protein activity, antibodies interact with the host immune system to promote different types of immune responses. Two immunoglobulin G (IgG) proteins can bind to the complement protein C1q to initiate the complement response. The complement system is an innate immune response that initiates on antibody-opsonized pathogens or particles, and results in a membrane-lytic protein complex that can lyse membrane-bound pathogens [8]. Complement is regarded as an innate immune mechanism, and complement-activating nanoparticle vaccines have been proposed as an enhancer of innate danger signals [68, 69]. Recently, however, the complement system has been found to play a role in initiating adaptive immunity and immunological memory, as a child with a genetic defect in the complement system was found to suffer from recurring infections [70].

In addition to activating the complement system, antibodies can serve as an interface between antigen and antigen-presenting cells. Dendritic cells and macrophages have Fc receptors that bind antibodies and antibody-bound antigen. In mice and humans, several different Fc receptors for IgG (FcγRs) have been identified with respect to their ability to activate or suppress immune responses. Targeting vaccine antigens to these

receptors for immunostimulation relies on (1) the FcγR being a well-characterized means of entry into macrophages and dendritic cells [71], and (2) intracellular domains underneath FcγRs leading to pro-inflammatory signaling when crosslinked by IgG [8, 72].

The Fcγ receptors FcγRI, FcγRIIA, FcγRIIC and FcγRIIIA are activating, but FcγRIIB has been identified as an inhibitory Fc receptor, increasing the threshold for B cell, neutrophil and macrophage activation [8, 73]. Genetic deletion of the FcγRIIB receptor in mice leads to an increased likelihood of several autoimmune diseases [74], indicating its importance in regulating a balanced immune response. Furthermore, Fc receptor-targeted vaccine antigen administered to dendritic cells *ex vivo* triggered immune responses in the presence and absence of FcγRIIB, suggesting inhibitory receptors play a minor role in attenuating vaccine responses [75].

Follicular dendritic cells (FDCs) were mentioned previously as holding antigen-antibody immune complexes (ICs) with Fc receptors to present antigen to germinal center B cells to promote somatic hypermutation and class switching. It was recently discovered that immune complexes on FDCs undergo endocytosis to a non-degradative compartment and are recycled back to the FDC surface periodically; antigen was found to be retained in FDCs up to 16 days after immunization [76]. These findings could suggest a possible role for FDCs in mediating immunological memory, and underscore the importance of Ig-bound antigen in promoting an adaptive immune response.

The use of ICs as vaccines has been an area of extensive research. The presence of antibodies on antigen has been seen to increase the resulting antibody response by 1000-fold in the case of soluble antigen, or reduce it by 99% in the case of red blood cells [77,

78]. Despite the apparent negative correlation between antigen size and immunogenicity, there is preliminary evidence that antibody-opsonized nanoparticulates are more inflammatory than soluble immune complexes [79]. Soluble immune complex vaccines have demonstrated efficacy in pre-clinical models for malaria [80], HIV [81], ebola [82], and other diseases. A recent clinical trial of a hepatitis B soluble immune complex vaccines failed, demonstrating that challenges still remain with this type of immunization [83]. It is possible that soluble ICs still face the same problem as recombinant protein antigens; the small size of both lead to rapid clearance and low immunogenicity. We explore the addition of immunoglobulins as adjuvants on our nanoparticle vaccines in Chapter 5.

1.4.5 Integrating Immunology into Nanoparticle Vaccine Design Principles

The various cells of the immune system respond to physical and macromolecular cues differently, and discovering immunostimulatory combinations of both is an active area of research that translates fundamental immunological findings into new types of nanotherapeutics. In Chapter 3 of this work, we explore the effects of nanoparticle size and coating on *in vitro* dendritic cell responses, but dendritic cell stimulation is only one aspect of an effective vaccine response. In Chapter 5, we examine the role of adjuvant coatings in an *in vivo* mouse immunization model, to obtain a more complete image of how molecular and nanoparticulate adjuvants synergize with each other.

1.5 Influenza Vaccine Nanoparticles

Many different strategies have been pursued for generating influenza nanoparticle vaccines. Virus-like particles (VLPs) are most similar to influenza viruses in being bound by a lipid bilayer membrane. VLPs are commonly generated by infection of insect cells

with recombinant baculoviruses expressing the proteins of choice [84, 85]. Hemagglutinin, neuraminidase, and influenza matrix proteins are common antigens inserted into influenza VLPs, and adjuvants such as flagellin can be incorporated into the VLP membrane as well [62, 86]. One of the benefits of VLPs is the stable presentation of membrane-bound antigens on the nanoparticle surface, eliminating the need to engineer membrane-bound antigens into stable, soluble proteins. The membrane-bound nature of the VLP is also a key drawback – these semi-permeable vesicles are unstable to osmotic stresses, and changes in salt concentration can lead to vaccine particle lysis [15].

Self-assembling protein nanoparticles (SAPNs) are composed entirely of protein, which reduces the concern of osmotic stress instability. SAPNs are formed from individual proteins that are genetic fusions of an antigen to a self-assembly tag, which causes a solution of proteins to assemble into higher-order structures upon post-purification refolding [87]. Self-assembly motifs are commonly employed to create protein trimers and tetramers [59, 88], and tetrameric M2e peptide has been used as a type of self-assembling protein vaccine [89]. Larger SAPN self-assembly motifs can enable 24mer [34] and even 60mer [90] self-assembly. Kanekiyo et al. made influenza SAPNs by genetically fusing hemagglutinin to ferritin, a self-assembling 24mer [34]. The 24mer ferritin protein complex consists of 8 junctions where 3 proteins meet. Since hemagglutinin has a trimeric structure in its native form, this base was ideal for assembling native hemagglutinin on the surface. The extensive computation that goes into designing these nanoparticle structures, however, is non-trivial [91]. Furthermore, the incorporation of non-antigenic self-assembly motifs increases the risk of an off-target immune response upon immunization [92].

Both VLPs and SAPNs aim for multimeric antigen display on the nanoparticle surface as a design strategy. This pathogen-mimetic configuration is immunogenic, but achieving it in VLPs and SAPNs comes at the cost of stability and potential off-target immunogenicity, respectively. Our approach to making protein nanoparticle vaccines, desolvation, presents a workaround to both of these problems.

1.6 Desolvated Protein Nanoparticles

Desolvated protein nanoparticles are formed entirely from protein by solvent-directed assembly [93]. Desolvation introduces an unfavorable solvent to a protein solution to increase protein-protein interactions, causing proteins in solution to coalesce into nanoparticles. These protein nanoparticles are easier to form in contrast to those made via a self-assembly sequence in the protein, such as SAPNs [94]. Without an engineered self-assembly tag on the antigen to direct nanoparticle formation, the chances of an off-target immune response[92] to the tag are also decreased. Desolvated protein nanoparticles were originally made from albumin [95, 96]. Recently, protein nanoparticles have been shown capable of intracellular delivery of folded, active enzymes[97]. The delivery of properly folded antigen protein is especially desirable in nanoparticle vaccine design.

The desolvation process in this work uses 100% ethanol dripped in slowly over a solution of stirring protein antigen. The thermodynamically unfavorable interaction between the protein and the solvent force the proteins to cluster together into nanoparticles. A crosslinker is then added to covalently stabilize the nascent nanoparticles and prevent aggregation or disintegration. Glutaraldehyde is a commonly used crosslinker to link primary amines, such as those found on lysines and the N termini of proteins. While

glutaraldehyde has been used in the past to crosslink protein nanoparticles [59, 97], our work uses the crosslinker 3,3'-dithiobis[sulfosuccinimidylpropionate], or DTSSP. DTSSP is an amine-reactive crosslinker like glutaraldehyde, but contains a central disulfide bond that has the potential to break once the particle is inside the cell. Nanoparticle breakup inside antigen presenting cells could facilitate greater proteolytic degradation, and could help enhance the amount of peptides displayed on MHC I and II during antigen presentation.

The first desolvated protein nanoparticles for vaccines were originally made with the conserved, tetrameric influenza matrix protein M2e [59]. In comparison to soluble M2e protein, M2e protein nanoparticles were able to induce strong antibody and T cell responses, and protect mice against $5xLD_{50}$ influenza A Phi/82 and Cal/09 challenges. These results demonstrated that protein nanoparticles could dramatically enhance the immunogenicity of non-immunogenic antigen. Unlike other vaccine nanoparticles, protein nanoparticles are made entirely of biodegradable, crosslinked antigen, minimizing the possibility of off-target immune responses. Their abiotic nature also enhances their amenability to cold chain-independent storage, a desirable property for vaccine transport to the developing world. We will examine the ability of protein nanoparticles to survive cold-chain-independent storage in Chapter 4.

1.7 The Objectives of the Thesis

Our overall goal is to develop protein nanoparticle vaccines as a viable platform technology that can be used to enhance the adjuvancy of different types of protein antigens [98]. To that end, the objectives of this thesis are to (1) translate our initial successes with

M2e protein nanoparticles into other types influenza antigen nanoparticles, (2) understand the mechanism of nanoparticle adjuvancy, (3) explore extended storage of nanoparticle vaccines for the possibility of cold chain-independent storage, and (4) test the ability of molecular adjuvant coatings to boost protein nanoparticle immunogenicity.

Our first goal, in collaboration with Dr. Baozhong Wang's lab, creates nanoparticles with either trimerized H7 hemagglutinin (3HA) or flagellin-fusion proteins with M2e or hemagglutinin (HA) stalk sequences inserted into the hypervariable region of flagellin. Protein nanoparticles made with these proteins immunized mice in an influenza challenge model.

Second, our fundamental mechanistic studies (1) explore the role of nanoparticle size and coating on dendritic cell inflammation and maturation responses *in vitro*, and (2) examine *in vivo* biodistribution and T and B cell responses to nanoparticles and soluble protein. Our *in vitro* studies examining the fundamental properties of size and coating were done with ovalbumin (OVA) as a model antigen, while the *in vivo* studies were performed with trimerized hemagglutinin (3HA) nanoparticles.

Third, our extended nanoparticle storage studies test whether protein nanoparticles can be stored at room temperature or 37°C and retain their immunogenic potential *in vivo*. Since hemagglutinin (HA) has a simple, *in vitro* readout of protein function in the hemagglutination assay, and hemagglutination is a prerequisite for HA immunogenicity, these stability studies were performed with 3HA nanoparticles.

Finally, to examine the potential contributions of molecular adjuvants to enhancing nanoparticle-mediated adjuvancy, we added several types of protein adjuvants as coatings

on model ovalbumin protein nanoparticles. Flagellin (FliC), a *Salmonella*-derived protein, was added as a soluble adjuvant or crosslinked to the nanoparticle surface to determine the role of adjuvant location on the resulting immune response. Immunoglobulin (Ig) is a host-derived protein that is involved in regulating the immune response [77], and could enhance the immune response to the nanoparticles without the addition of a pathogen-derived component. We examined coatings of immunoglobulin G (IgG) and immunoglobulin M (IgM) on our nanoparticles, and whether those could enhance the immune response to ovalbumin nanoparticles.

REFERENCES

[1] G.A. Poland, R.B. Kennedy, I.G. Ovsyannikova, Vaccinomics and Personalized Vaccinology: Is Science Leading Us Toward a New Path of Directed Vaccine Development and Discovery?, Plos Pathog 7(12) (2011).

[2] K. Stohr, Influenza - WHO cares, Lancet Infect Dis 2(9) (2002) 517-517.

[3] C.A. Russell, T.C. Jones, I.G. Barr, N.J. Cox, R.J. Garten, V. Gregory, I.D. Gust, A.W. Hampson, A.J. Hay, A.C. Hurt, J.C. de Jong, A. Kelso, A.I. Klimov, T. Kageyama, N. Komadina, A.S. Lapedes, Y.P. Lin, A. Mosterin, M. Obuchi, T. Odagiri, A.D.M.E. Osterhaus, G.F. Rimmelzwaan, M.W. Shaw, E. Skepner, K. Stohri, M. Tashiro, R.A.M. Fouchier, D.J. Smith, Influenza vaccine strain selection and recent studies on the global migration of seasonal influenza viruses, Vaccine 26 (2008) D31-D34.

[4] K. Stöhr, The Global Agenda on Influenza Surveillance and Control, Vaccine 21(16) (2003) 1744-1748.

[5] T.A. Kost, J.P. Condreay, D.L. Jarvis, Baculovirus as versatile vectors for protein expression in insect and mammalian cells, Nat Biotech 23(5) (2005) 567-575.

[6] K. Wang, K.M. Holtz, K. Anderson, R. Chubet, W. Mahmoud, M.M.J. Cox, Expression and purification of an influenza hemagglutinin—one step closer to a recombinant protein-based influenza vaccine, Vaccine 24(12) (2006) 2176-2185.

[7] R.S. Zeiger, Current issues with influenza vaccination in egg allergy, J. Allergy Clin. Immunol. 110(6) (2002) 834-840.

[8] K. Murphy, P. Travers, M. Walport, C. Janeway, Janeway's immunobiology, Garland Science, New York, 2012.

[9] W.C. Weldon, B.Z. Wang, M.P. Martin, D.G. Koutsonanos, I. Skountzou, R.W. Compans, Enhanced Immunogenicity of Stabilized Trimeric Soluble Influenza Hemagglutinin, Plos One 5(9) (2010).

[10] H. Zhang, L. Wang, R.W. Compans, B.Z. Wang, Universal Influenza Vaccines, a Dream to Be Realized Soon, Viruses-Basel 6(5) (2014) 1974-1991.

[11] M. De Filette, W. Martens, K. Roose, T. Deroo, F. Vervalle, M. Bentahir, J. Vandekerckhove, W. Fiers, X. Saelens, An influenza A vaccine based on tetrameric ectodomain of matrix protein 2, J Biol Chem 283(17) (2008) 11382-11387.

[12] L.H. Pinto, L.J. Holsinger, R.A. Lamb, INFLUENZA-VIRUS M2 PROTEIN HAS ION CHANNEL ACTIVITY, Cell 69(3) (1992) 517-528.

[13] J.J. Treanor, E.L. Tierney, S.L. Zebedee, R.A. Lamb, B.R. Murphy, Passively Transferred Monoclonal-Antibody to the M2 Protein Inhibits Influenza-a Virus-Replication in Mice, J Virol 64(3) (1990) 1375-1377.

[14] D.C. Ekiert, R.H.E. Friesen, G. Bhabha, T. Kwaks, M. Jongeneelen, W.L. Yu, C. Ophorst, F. Cox, H. Korse, B. Brandenburg, R. Vogels, J.P.J. Brakenhoff, R. Kompier, M.H. Koldijk, L. Cornelissen, L.L.M. Poon, M. Peiris, W. Koudstaal, I.A. Wilson, J. Goudsmit, A Highly Conserved Neutralizing Epitope on Group 2 Influenza A Viruses, Science 333(6044) (2011) 843-850.

[15] O.S. Kumru, S.B. Joshi, D.E. Smith, C.R. Middaugh, T. Prusik, D.B. Volkin, Vaccine instability in the cold chain: Mechanisms, analysis and formulation strategies, Biologicals 42(5) (2014) 237-259.

[16] S. Manmohan, Vaccine adjuvants and delivery systems, Wiley-Interscience, Hoboken, N.J., 2007.

[17] R. Cevenini, V. Sambri, S. Pileri, G. Ratti, M. La Placa, Development of transplantable ascites tumours which continuously produce polyclonal antibodies in pristane primed BALB/c mice immunized with bacterial antigens and complete Freund's adjuvant, J Immunol Methods 140(1) (1991) 111-118.

[18] N. Inagaki, T. Miura, H. Nagai, A. Koda, ACTIVE CUTANEOUS ANAPHYLAXIS (ACA) IN THE MOUSE EAR, Jpn. J. Pharmacol. 59(2) (1992) 201-208.

[19] H. Hoffman, NIH awards seven new vaccine adjuvant discovery contracts, National Institute of Allergy and Infectious Diseases, 2014.

[20] NIAID, NIAID Strategic Plan for Research on Vaccine Adjuvants, National Institutes of Health, 2010.

[21] M. Kwissa, H.I. Nakaya, H. Oluoch, B. Pulendran, Distinct TLR adjuvants differentially stimulate systemic and local innate immune responses in nonhuman primates, Blood 119(9) (2012) 2044-2055.

[22] S. Lee, Nguyen, M.T., Recent Advances of Vaccine Adjuvants for Infectious Diseases, Immune Network 15(2) (2015) 51-57.

[23] A.M. Krieg, Toll-free vaccines?, Nat Biotech 25(3) (2007) 303-305.

[24] M. Kool, K. Fierens, B.N. Lambrecht, Alum adjuvant: some of the tricks of the oldest adjuvant, Journal of Medical Microbiology 61(7) (2012) 927-934.

[25] V. Hornung, F. Bauernfeind, A. Halle, E.O. Samstad, H. Kono, K.L. Rock, K.A. Fitzgerald, E. Latz, Silica crystals and aluminum salts activate the NALP3 inflammasome through phagosomal destabilization, Nat Immunol 9(8) (2008) 847-856.

[26] D.R. Getts, L.D. Shea, S.D. Miller, N.J.C. King, Harnessing nanopartricles for immune modulation, Trends Immunol 36(7) (2015) 419-427.

[27] J. Leleux, K. Roy, Micro and Nanoparticle-Based Delivery Systems for Vaccine Immunotherapy: An Immunological and Materials Perspective, Adv Healthc Mater 2(1) (2013) 72-94.

[28] T. Marichal, K. Ohata, D. Bedoret, C. Mesnil, C. Sabatel, K. Kobiyama, P. Lekeux, C. Coban, S. Akira, K.J. Ishii, F. Bureau, C.J. Desmet, DNA released from dying host cells mediates aluminum adjuvant activity, Nat Med 17(8) (2011) 996-U118.

[29] F.A. Sharp, D. Ruane, B. Claass, E. Creagh, J. Harris, P. Malyala, M. Singh, D.T. O'Hagan, V. Petrilli, J. Tschopp, L.A.J. O'Neill, E.C. Lavelle, Uptake of particulate vaccine adjuvants by dendritic cells activates the NALP3 inflammasome, P Natl Acad Sci USA 106(3) (2009) 870-875.

[30] R.K. Gupta, Aluminum compounds as vaccine adjuvants, Adv Drug Deliver Rev 32(3) (1998) 155-172.

[31] B. Slutter, L. Plapied, V. Fievez, M.A. Sande, A. des Rieux, Y.J. Schneider, E. Van Riet, W. Jiskoot, V. Preat, Mechanistic study of the adjuvant effect of biodegradable nanoparticles in mucosal vaccination, J Control Release 138(2) (2009) 113-121.

[32] A.E. Gregory, R. Titball, D. Williamson, Vaccine delivery using nanoparticles, Front Cell Infect Mi 3 (2013).

[33] L. Liu, P. Ma, H. Wang, C. Zhang, H. Sun, C. Wang, C. Song, X. Leng, D. Kong, G. Ma, Immune responses to vaccines delivered by encapsulation into and/or adsorption onto cationic lipid-PLGA hybrid nanoparticles, J Control Release 225 (2016) 230-239.

[34] M. Kanekiyo, C.J. Wei, H.M. Yassine, P.M. McTamney, J.C. Boyington, J.R.R. Whittle, S.S. Rao, W.P. Kong, L.S. Wang, G.J. Nabel, Self-assembling influenza

nanoparticle vaccines elicit broadly neutralizing H1N1 antibodies, Nature 499(7456) (2013) 102-+.

[35] S.D. Xiang, K. Wilson, S. Day, M. Fuchsberger, M. Plebanski, Methods of effective conjugation of antigens to nanoparticles as non-inflammatory vaccine carriers, Methods 60(3) (2013) 232-241.

[36] L. Zhao, A. Seth, N. Wibowo, C.-X. Zhao, N. Mitter, C. Yu, A.P.J. Middelberg, Nanoparticle vaccines, Vaccine 32(3) (2014) 327-337.

[37] H.F. Li, S.B. Willingham, J.P.Y. Ting, F. Re, Cutting edge: Inflammasome activation by alum and alum's adjuvant effect are mediated by NLRP3, J Immunol 181(1) (2008) 17-21.

[38] S.D. Xiang, A. Scholzen, G. Minigo, C. David, V. Apostolopoulos, P.L. Mottram, M. Plebanski, Pathogen recognition and development of particulate vaccines: Does size matter?, Methods 40(1) (2006) 1-9.

[39] A. Stano, C. Nembrini, M.A. Swartz, J.A. Hubbell, E. Simeoni, Nanoparticle size influences the magnitude and quality of mucosal immune responses after intranasal immunization, Vaccine 30(52) (2012) 7541-7546.

[40] P.L. Mottram, D. Leong, B. Crimeen-Irwin, S. Gloster, S.D. Xiang, J. Meanger, R. Ghildyal, N. Vardaxis, M. Plebanski, Type 1 and 2 immunity following vaccination is influenced by nanoparticle size: Formulation of a model vaccine for respiratory syncytial virus, Mol Pharmaceut 4(1) (2007) 73-84.

[41] S. Kumar, A.C. Anselmo, A. Banerjee, M. Zakrewsky, S. Mitragotri, Shape and size-dependent immune response to antigen-carrying nanoparticles, J Control Release 220(Pt A) (2015) 141-148.

[42] C.A. Vaine, M.K. Patel, J.T. Zhu, E. Lee, R.W. Finberg, R.C. Hayward, E.A. Kurt-Jones, Tuning Innate Immune Activation by Surface Texturing of Polymer Microparticles: The Role of Shape in Inflammasome Activation, J Immunol 190(7) (2013) 3525-3532.

[43] S. Neumann, K. Burkert, R. Kemp, T. Rades, P.R. Dunbar, S. Hook, Activation of the NLRP3 inflammasome is not a feature of all particulate vaccine adjuvants, Immunol Cell Biol 92(6) (2014) 535-542.

[44] R.X. Huang, R.P. Carney, F. Stellacci, B.L.T. Lau, Protein-nanoparticle interactions: the effects of surface compositional and structural heterogeneity are scale dependent, Nanoscale 5(15) (2013) 6928-6935.

[45] B.S. Zolnik, A. Gonzalez-Fernandez, N. Sadrieh, M.A. Dobrovolskaia, Minireview: Nanoparticles and the Immune System, Endocrinology 151(2) (2010) 458-465.

[46] C. Thery, S. Amigorena, The cell biology of antigen presentation in dendritic cells, Curr Opin Immunol 13(1) (2001) 45-51.

[47] E. Gatti, P. Pierre, Understanding the cell biology of antigen presentation: the dendritic cell contribution, Curr Opin Cell Biol 15(4) (2003) 468-473.

[48] J. Banchereau, R.M. Steinman, Dendritic cells and the control of immunity, Nature 392(6673) (1998) 245-252.

[49] J. Leleux, A. Atalis, K. Roy, Engineering immunity: Modulating dendritic cell subsets and lymph node response to direct immune-polarization and vaccine efficacy, J Control Release 219 (2015) 610-621.

[50] R.M. Steinman, K. Inaba, Myeloid dendritic cells, J Leukocyte Biol 66(2) (1999) 205-208.

[51] A. Aguzzi, J. Kranich, N.J. Krautler, Follicular dendritic cells: origin, phenotype, and function in health and disease, Trends Immunol 35(3) 105-113.

[52] S.T. Reddy, A.J. van der Vlies, E. Simeoni, V. Angeli, G.J. Randolph, C.P. O'Neill, L.K. Lee, M.A. Swartz, J.A. Hubbell, Exploiting lymphatic transport and complement activation in nanoparticle vaccines, Nat Biotechnol 25(10) (2007) 1159-1164.

[53] V. Manolova, A. Flace, M. Bauer, K. Schwarz, P. Saudan, M.F. Bachmann, Nanoparticles target distinct dendritic cell populations according to their size, Eur J Immunol 38(5) (2008) 1404-1413.

[54] T. Fifis, A. Gamvrellis, B. Crimeen-Irwin, G.A. Pietersz, J. Li, P.L. Mottram, I.F.C. McKenzie, M. Plebanski, Size-dependent immunogenicity: Therapeutic and protective properties of nano-vaccines against tumors, J Immunol 173(5) (2004) 3148-3154.

[55] J.M. Brewer, K.G.J. Pollock, L. Tetley, D.G. Russell, Vesicle size influences the trafficking, processing, and presentation of antigens in lipid vesicles, J Immunol 173(10) (2004) 6143-6150.

[56] K.K. Tran, H. Shen, The role of phagosomal pH on the size-dependent efficiency of cross-presentation by dendritic cells, Biomaterials 30(7) (2009) 1356-1362.

[57] D.T. Fearon, R.M. Locksley, Elements of immunity - The instructive role of innate immunity in the acquired immune response, Science 272(5258) (1996) 50-54.

[58] S.P. Kasturi, I. Skountzou, R.A. Albrecht, D. Koutsonanos, T. Hua, H.I. Nakaya, R. Ravindran, S. Stewart, M. Alam, M. Kwissa, F. Villinger, N. Murthy, J. Steel, J. Jacob, R.J. Hogan, A. Garcia-Sastre, R. Compans, B. Pulendran, Programming the magnitude and persistence of antibody responses with innate immunity, Nature 470(7335) (2011) 543-U136.

[59] L. Wang, A. Hess, T.Z. Chang, Y.C. Wang, J.A. Champion, R.W. Compans, B.Z. Wang, Nanoclusters self-assembled from conformation-stabilized influenza M2e as broadly cross-protective influenza vaccines, Nanomed-Nanotechnol 10(2) (2014) 473-482.

[60] S.B. Mizel, J.T. Bates, Flagellin as an Adjuvant: Cellular Mechanisms and Potential, J Immunol 185(10) (2010) 5677-5682.

[61] H.I. Nakaya, J. Wrammert, E.K. Lee, L. Racioppi, S. Marie-Kunze, W.N. Haining, A.R. Means, S.P. Kasturi, N. Khan, G.M. Li, M. McCausland, V. Kanchan, K.E. Kokko, S.Z. Li, R. Elbein, A.K. Mehta, A. Aderem, K. Subbarao, R. Ahmed, B. Pulendran, Systems biology of vaccination for seasonal influenza in humans, Nat Immunol 12(8) (2011) 786-U149.

[62] B.Z. Wang, F.S. Quan, S.M. Kang, J. Bozja, I. Skountzou, R.W. Compans, Incorporation of Membrane-Anchored Flagellin into Influenza Virus-Like Particles Enhances the Breadth of Immune Responses, J Virol 82(23) (2008) 11813-11823.

[63] C.B. Turley, R.E. Rupp, C. Johnson, D.N. Taylor, J. Wolfson, L. Tussey, U. Kavita, L. Stanberry, A. Shaw, Safety and immunogenicity of a recombinant M2e-flagellin influenza vaccine (STF2.4xM2e) in healthy adults, Vaccine 29(32) (2011) 5145-5152.

[64] J.Z. Oh, R. Ravindran, B. Chassaing, F.A. Carvalho, M.S. Maddur, M. Bower, P. Hakimpour, K.P. Gill, H.I. Nakaya, F. Yarovinsky, R.B. Sartor, A.T. Gewirtz, B. Pulendran, TLR5-Mediated Sensing of Gut Microbiota Is Necessary for Antibody Responses to Seasonal Influenza Vaccination, Immunity 41(3) (2014) 478-492.

[65] S. Romagnani, Th1/Th2 cells, Inflammatory bowel diseases 5(4) (1999) 285-94.

[66] H.J. van den Ham, A.C. Andeweg, R.J. de Boer, Induction of appropriate Th-cell phenotypes: cellular decision-making in heterogeneous environments, Parasite Immunol 35(11) (2013) 318-330.

[67] S. Kumar, A.C. Anselmo, A. Banerjee, M. Zakrewsky, S. Mitragotri, Shape and size-dependent immune response to antigen-carrying nanoparticles, J Control Release 220 (2015) 141-148.

[68] P.M. Pacheco, B. Le, D. White, T. Sulchek, TUNABLE COMPLEMENT ACTIVATION BY PARTICLES WITH VARIABLE SIZE AND Fc DENSITY, Nano LIFE 3(2) (2013) 1341001.

[69] S.T. Reddy, A.J. van der Vlies, E. Simeoni, V. Angeli, G.J. Randolph, C.P. O'Neil, L.K. Lee, M.A. Swartz, J.A. Hubbell, Exploiting lymphatic transport and complement activation in nanoparticle vaccines, Nat Biotech 25(10) (2007) 1159-1164.

[70] A. Ghannam, M. Pernollet, J.L. Fauquert, N. Monnier, D. Ponard, M.B. Villiers, J. Peguet-Navarro, A. Tridon, J. Lunardi, D. Gerlier, C. Drouet, Human C3 deficiency associated with impairments in dendritic cell differentiation, memory B cells, and regulatory T cells, J Immunol 181(7) (2008) 5158-5166.

[71] Y.X. Zhang, A.D. Hoppe, J.A. Swanson, Coordination of Fc receptor signaling regulates cellular commitment to phagocytosis, P Natl Acad Sci USA 107(45) (2010) 19332-19337.

[72] L.J. Cruz, F. Rueda, B. Cordobilla, L. Simon, L. Hosta, F. Albericio, J.C. Domingo, Targeting Nanosystems to Human DCs via Fc Receptor as an Effective Strategy to Deliver Antigen for Immunotherapy, Mol Pharmaceut 8(1) (2011) 104-116.

[73] M. Guilliams, P. Bruhns, Y. Saeys, H. Hammad, B.N. Lambrecht, The function of Fc gamma receptors in dendritic cells and macrophages, Nat Rev Immunol 14(2) (2014) 94-108.

[74] T. Yuasa, S. Kubo, T. Yoshino, A. Ujike, K. Matsumura, M. Ono, J.V. Ravetch, T. Takai, Deletion of Fc gamma receptor IIB renders H-2(b) mice susceptible to collagen-induced arthritis, J Exp Med 189(1) (1999) 187-194.

[75] G. Pham, B. Iglesias, S. Rosa, E. Gosselin, Fc receptor-targeting of immunogen as a strategy for enhanced antigen loading, vaccination, and protection using intranasally-administered ex vivo antigen-pulsed dendritic cells, J Immunol 190 (2013).

[76] B.A. Heesters, P. Chatterjee, Y.A. Kim, S.F. Gonzalez, M.P. Kuligowski, T. Kirchhausen, M.C. Carroll, Endocytosis and Recycling of Immune Complexes by Follicular Dendritic Cells Enhances B Cell Antigen Binding and Activation, Immunity 38(6) (2013) 1164-1175.

[77] A. Getahun, B. Heyman, How antibodies act as natural adjuvants, Immunol Lett 104(1-2) (2006) 38-45.

[78] F. Hjelm, F. Carlsson, A. Getahun, B. Heyman, Antibody-mediated regulation of the immune response, Scand J Immunol 64(3) (2006) 177-184.

[79] G. Fossati, R.C. Bucknall, S.W. Edwards, Insoluble and soluble immune complexes activate neutrophils by distinct activation mechanisms: changes in functional responses induced by priming with cytokines, Ann Rheum Dis 61(1) (2002) 13-19.

[80] P.G. Harte, A. Cooke, J.H.L. Playfair, Specific Monoclonal Igm Is a Potent Adjuvant in Murine Malaria Vaccination, Nature 302(5905) (1983) 256-258.

[81] C.E. Hioe, M.L. Visciano, R. Kumar, J. Liu, E.A. Mack, R.E. Simon, D.N. Levy, M. Tuen, The use of immune complex vaccines to enhance antibody responses against neutralizing epitopes on HIV-1 envelope gp120, Vaccine 28(2) (2009) 352-360.

[82] K. Konduru, S.B. Bradfute, J. Jacques, M. Manangeeswaran, S. Nakamura, S. Morshed, S.C. Wood, S. Bavari, G.G. Kaplan, Ebola virus glycoprotein Fc fusion protein confers protection against lethal challenge in vaccinated mice, Vaccine 29(16) (2011) 2968-2977.

[83] D.Z. Xu, K. Zhao, L.M. Guo, X.Y. Chen, H.F. Wang, J.M. Zhang, Q. Xie, H. Ren, W.X. Wang, L.J. Li, M. Xu, P. Liu, J.Q. Niu, X.F. Bai, X.L. Shen, Z.H. Yuan, X.Y. Wang, Y.M. Wen, A Randomized Controlled Phase IIb Trial of Antigen-Antibody Immunogenic Complex Therapeutic Vaccine in Chronic Hepatitis B Patients, Plos One 3(7) (2008).

[84] E.V.L. Grgacic, D.A. Anderson, Virus-like particles: Passport to immune recognition, Methods 40(1) (2006) 60-65.

[85] B.Z. Wang, H.S. Gill, S.M. Kang, L. Wang, Y.C. Wang, E.V. Vassilieva, R.W. Compans, Enhanced Influenza Virus-Like Particle Vaccines Containing the Extracellular Domain of Matrix Protein 2 and a Toll-Like Receptor Ligand, Clin Vaccine Immunol 19(8) (2012) 1119-1125.

[86] B.Z. Wang, R. Xu, F.S. Quan, S.M. Kang, L. Wang, R.W. Compans, Intranasal Immunization with Influenza VLPs Incorporating Membrane-Anchored Flagellin Induces Strong Heterosubtypic Protection, Plos One 5(11) (2010).

[87] Y.K. Yang, P. Ringler, S.A. Muller, P. Burkhard, Optimizing the refolding conditions of self-assembling polypeptide nanoparticles that serve as repetitive antigen display systems, J Struct Biol 177(1) (2012) 168-176.

[88] L. Wang, T.Z. Chang, Y. He, J.R. Kim, S. Wang, T. Mohan, Z. Berman, S.M. Tompkins, R.A. Tripp, R.W. Compans, J.A. Champion, B.-Z. Wang, Coated protein nanoclusters from influenza H7N9 HA are highly immunogenic and induce robust protective immunity, Nanomedicine: Nanotechnology, Biology and Medicine 13(1) (2016) 253-262.

[89] S. Babapoor, T. Neef, C. Mittelholzer, T. Girshick, A. Garmendia, H. Shang, M.I. Khan, P. Burkhard, A Novel Vaccine Using Nanoparticle Platform to Present Immunogenic M2e against Avian Influenza Infection, Influenza Research and Treatment 2011 (2011) 12.

[90] J. Jardine, J.P. Julien, S. Menis, T. Ota, O. Kalyuzhniy, A. McGuire, D. Sok, P.S. Huang, S. MacPherson, M. Jones, T. Nieusma, J. Mathison, D. Baker, A.B. Ward, D.R. Burton, L. Stamatatos, D. Nemazee, I.A. Wilson, W.R. Schief, Rational HIV Immunogen Design to Target Specific Germline B Cell Receptors, Science 340(6133) (2013) 711-716.

[91] T. Doll, T. Neef, N. Duong, D.E. Lanar, P. Ringler, S.A. Muller, P. Burkhard, Optimizing the design of protein nanoparticles as carriers for vaccine applications, Nanomed-Nanotechnol 11(7) (2015) 1705-1713.

[92] T.A. Willett, A.L. Meyer, E.L. Brown, B.T. Huber, An effective second-generation outer surface protein A-derived Lyme vaccine that eliminates a potentially autoreactive T cell epitope, P Natl Acad Sci USA 101(5) (2004) 1303-1308.

[93] C. Weber, C. Coester, J. Kreuter, K. Langer, Desolvation process and surface characterisation of protein nanoparticles, Int J Pharmaceut 194(1) (2000) 91-102.

[94] L.P.H. Estrada, J.A. Champion, Protein nanoparticles for therapeutic protein delivery, Biomater Sci-Uk 3(6) (2015) 787-799.

[95] K. Langer, S. Balthasar, V. Vogel, N. Dinauer, H. von Briesen, D. Schubert, Optimization of the preparation process for human serum albumin (HSA) nanoparticles, Int J Pharmaceut 257(1-2) (2003) 169-180.

[96] C. Weber, J. Kreuter, K. Langer, Desolvation process and surface characteristics of HSA-nanoparticles, Int J Pharmaceut 196(2) (2000) 197-200.

[97] L.H. Estrada, S. Chu, J.A. Champion, Protein nanoparticles for intracellular delivery of therapeutic enzymes, J Pharm Sci-Us 103(6) (2014) 1863-71.

[98] T. Mamo, G.A. Poland, Nanovaccinology: The next generation of vaccines meets 21st century materials science and engineering, Vaccine 30(47) (2012) 6609-6611.

CHAPTER 2. RECOMBINANT INFLUENZA PROTEIN NANOPARTICLES

2.1 Hemagglutinin and M2e as Influenza Antigens

The finding that desolvated M2e nanoparticles could protect mice against a lethal influenza challenge demonstrated that protein nanoparticles could enhance subunit antigen immunogenicity. M2e is only one of the antigens found on influenza, and incorporating additional antigens into protein nanoparticles could broaden the repertoire of anti-influenza antibodies generated after a vaccine. In particular, the incorporation of hemagglutinin into an influenza vaccine increases the chances that the vaccine will generate neutralizing antibodies that can protect the host from viral infection. Unlike M2e, hemagglutinin is a full-length protein with a functional tertiary structure. Exposing a full-length protein to ethanol could cause protein denaturation, and a loss of conformational epitopes could reduce the vaccine's efficacy. Though desolvation is a fairly simple process for generating peptide nanoparticles [1], it poses challenges for generating nanoparticles of full-length proteins, which we explore in the studies below.

The following chapter is divided into two subsections, each examining protein nanoparticles made with a different type of antigen. We first look at protein nanoparticles made with a trimerized form of H7 hemagglutinin (3HA), and examine the role of immunization route in generating effective immune responses. The second half of the chapter is devoted to hemagglutinin stalk proteins and M2e expressed in genetic fusion with flagellin, a TLR-5-activating protein adjuvant, and examining the role that the

molecular adjuvant flagellin can play in enhancing the immunogenicity of protein nanoparticles.

2.2 H7 Hemagglutinin

In 2013, a new strain of influenza A H7N9 emerged in eastern China with a mortality rate of 35% [2], the highest mortality rate ever reported for H7 viruses [3]. The virus's spread was fortunately limited by its avian-to-human transmission route. Were the virus to acquire the sustained ability to spread from person-to-person, it could result in widespread infection and mortality [4, 5].

Preventing influenza infection requires the formation of neutralizing antibodies against hemagglutinin. The hemagglutinin protein is 63 kDa, contains a variable head and a conserved stalk domain, and is responsible for facilitating the virus's entry into cells [6]. The head domain binds sialic acids on the surface of mammalian and avian cells, and antibodies against this head domain are ideal for blocking infection.

H7 hemagglutinin is known to be an especially poor immunogen, and inactivated virus vaccines require the use of adjuvants to boost their efficacy [4]. Recombinant H7 hemagglutinin has been produced, and its use in place of whole virus or virus-like particles[7] could decrease the chance of off-target immune responses [2]. Unlike the H7 20nm sub-viral particles described by Pushko et al [2], our protein nanoparticles are an order of magnitude bigger (~270 nm) and deliver more antigen per nanoparticle. Given the urgency of developing an effective vaccine for this new strain of influenza, and the prevailing paradigm of pathogen-mimetic vaccine nanoparticle design, our virus-sized

protein nanoparticles seem well-suited to enhance the adjuvancy of recombinant H7 hemagglutinin.

2.3 Materials and Methods

2.3.1 3HA Synthesis

Recombinant, trimerized H7 hemagglutinin (3HA) was synthesized by baculovirus infection of Sf9 and Tni cells, and purified by nickel-NTA (Ni-NTA) affinity chromatography as described previously [1].

2.3.2 Hemagglutination assay

To test the hemagglutinating activity of 3HA and 3HA nanoparticles, a modified hemagglutination assay (Virapur, San Diego, CA) was performed with turkey red blood cells (RBCs) (Lampire Biological Labs, Pipersville, PA). Briefly, 5 μg of protein or protein nanoparticles in 100 μL of phosphate-buffered saline was serially diluted by half across 11 wells of a 96-well plate. 50 μL of 0.5% turkey RBCs were then added to each well, and incubated at room temperature for 1 hour. The hemagglutination titer was read as the last well in the serial dilution that did not form a red button of settled RBCs.

2.3.3 Nanoparticle Synthesis

The assembly of 3HA into protein nanoparticles by desolvation was performed as previously described with modification . In brief, ethanol was dropped into the 3HA solution at a rate of 1 mL/min under constant stirring at 600 rpm. The solution contained 1.6 mg/ml of protein in PBS and was desolvated with a 4:1 volume ratio of ethanol to

protein solution. The particles were collected by centrifugation, and resuspended in sterile PBS with sonication. To coat an additional layer of 3HA molecules onto the 3HA nanoclusters, 800 µg soluble 3HA protein was added at a concentration of 1.6 mg/mL to 480 µg desolvated 3HA nanoclusters and an amine crosslinking reaction was performed using 3 mM 3,3´-Dithiobis[sulfosuccinimidylpropionate (DTSSP, Thermo Scientific, Waltham, MA) for 12 hours while stirring to stabilize the nanoparticles. Coated nanoclusters were collected by centrifugation, and protein concentration was measured by a BCA assay according to the manufacturer's instructions (Thermo Scientific) to estimate the total protein content in nanoparticles. Dynamic light scattering (DLS) was performed in PBS with a Malvern Zetasizer Nano ZS (Malvern Instruments, Westborough, MA) to assess nanoparticle size distributions. For scanning election microscopy studies, coated 3HA nanoparticles were resuspended in water, dried, and sputter coated with carbon prior to visualization with a Zeiss Ultra60 FE scanning electron microscope at 5.0 kV.

2.3.4 In vitro Characterization

JAWS II murine dendritic cells (DCs, passages 6-15) were cultured in α-Minimal Essential Media (α-MEM) with 10% fetal bovine serum (FBS) and 5 ng/mL murine GM-CSF (Peprotech, Rocky Hill, NJ). Cells were plated at a density of 10^5 cells/mL in 24-well plates for *in vitro* measurement of inflammation and maturation responses. After 24 hours of incubation post-plating, cells were stimulated with 10 µg/mL of soluble 3HA or coated 3HA nanoclusters in fresh complete media. 1 µg/mL of LPS in complete media was used as a positive control treatment. TNF-α, a secreted marker of inflammation, was assessed in supernatants after 6 hours of stimulation by ELISA according to the manufacturer's instructions (R&D Systems, Minneapolis, MN).

A cell surface marker of DC maturation, CD86, was assessed by flow cytometry after 24 hours of stimulation. Cells were harvested and washed with PBS. Fc receptors were blocked by TruStain fcX (Biolegend) for 10 minutes on ice. Cells were then incubated with PE-conjugated rat anti-mouse CD86 (clone GL-1) or isotype control (clone RTK2758) antibodies for 30 minutes on ice. After two washes, cells were fixed with 1% paraformaldehyde and analyzed with a BD Accuri C6 flow cytometer (BD Biosciences, San Jose, CA). Data were analyzed with FlowJo software (FlowJo LLC, Ashland, OR).

Bone marrow-derived dendritic cells were harvested and cultured as previously described [8]. Briefly, bone marrow progenitor cells were collected from femurs and tibias from 6-8 week old female Balb/c mice and cultured in RPMI 1640 (ATCC, Manassas, VA) supplemented with 10% heat-inactivated FBS, 50 μM β-mercaptoethanol, 1% penicillin-streptomycin, 2mM sodium pyruvate, 1x non-essential amino acids (Thermo Scientific, Grand Island, NY), and 25 ng/mL each of IL-4 and GM-CSF (Peprotech, Rocky Hill, NJ). Cells were matured for one week, and the media was changed on days 2, 4 and 6. On Day 7, cells were harvested by scraping and plated for experiments at a density of $1*10^5$ cells/mL in 24-well plates. The next day, BMDCs were stimulated with either 10 μg/mL soluble 3HA or 3HA nanoparticles for 24 hours. Supernatants were collected and tested for IL-1β by ELISA according to the manufacturer's instructions (R&D Systems).

2.3.5 Immunization and Challenge

All animal studies were approved by the Emory University Institutional Animal Care and Use Committee (IACUC) under protocol number 2001659. Female, 6-8 week old Balb/c mice (Jackson Labs, Bar Harbor, ME) were immunized with 10 μg 3HA

nanoparticles in 100 μL PBS once or twice at 4 week intervals through the intra-nasal(i.n.) or intra-muscular(i.m.) routes. Blood samples were collected 3 weeks after priming and boosting by submandibular venipuncture to test for serum antibodies. Four weeks after the priming or boosting immunization, mice were challenged with a $10xLD_{50}$ i.n. challenge of mouse-adapted influenza A/Anhui. Body weight loss and survival rates were monitored daily over a 2 week period post-infection. Weight loss of ≥25% was used as a humane endpoint for euthanasia per IACUC guidelines.

2.3.6 Sample collection and analysis

Blood collected from immunized mice by submandibular venipuncture was allowed to clot at 4°C for at least 30 minutes, and was centrifuged at 2700 x g for 5 minutes to collect serum. Serum samples were decanted and stored at -20°C for further analysis. Anti-HA serum antibody concentration was determined by ELISA as described previously [1] using 1μg/mL 3HA in PBS as a coating antigen.

2.3.7 Statistical analysis

Statistical significance was determined by a two-tailed Student's *t*-test in comparing two different conditions. Two-way ANOVA was used to analyze the significant difference among 3 or more groups. P-values less than 0.05 was considered to be significant (*, $p < 0.05$; **, $p < 0.005$; ***, $p < 0.001$). The analysis was performed with GraphPad Prism (version 5.0) software for Windows (GraphPad Software, San Diego, CA).

2.4 Results and Discussion

Protein nanoparticles made from trimerized hemagglutinin (3HA) were 273 ± 125 nm in diameter by DLS (Figure 1). The smaller average size observed by scanning electron microscopy in comparison to dynamic light scattering could be explained by the drying process used to prepare an SEM sample, indicating that the nanoparticles are porous in their hydrated state.

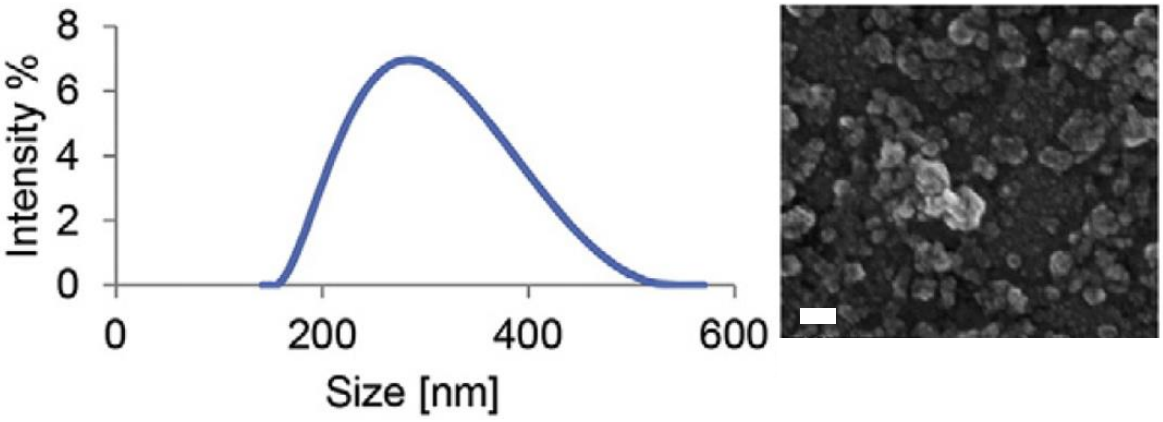

Figure 1. Representative size distribution of 3HA nanoparticles as determined by dynamic light scattering (DLS) (left), and SEM micrograph of the nanoparticles (right), scale bar = 200 nm.

After observing the lower hemagglutinating potential of monomeric HA compared to 3HA, it was decided that nanoparticles would be made from the trimeric 3HA (Figure 2). Coated 3HA nanoparticles were also shown to possess an 8-fold greater agglutinating capability than uncoated 3HA nanoparticles (agglutinating 3 more wells, and thus possessing a 2^3-fold greater agglutinating capacity). Since greater agglutinating capability is indicative of greater preservation of functional protein structure, which is critical for

neutralizing antibody development, our immunization studies proceeded with coated 3HA nanoparticles.

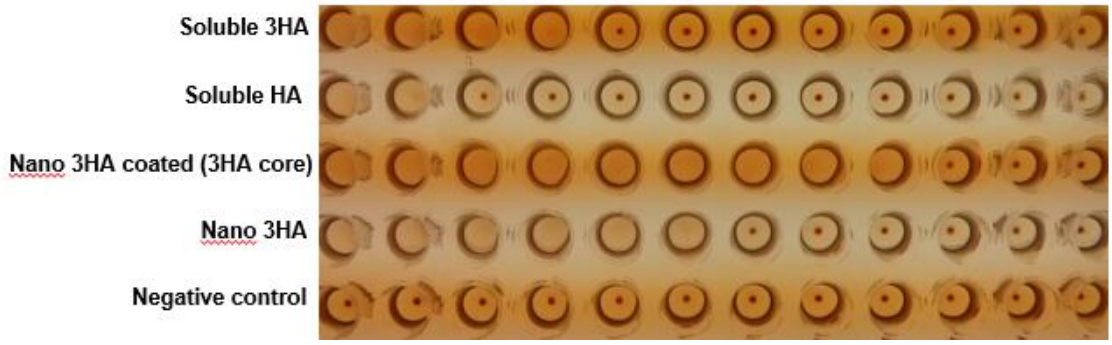

Figure 2. Hemagglutination assay results showing relative hemagglutinating potential of (from top) trimeric HA, monomeric HA, coated and uncoated 3HA protein nanoparticles, and PBS. (Courtesy of Dr. Li Wang)

To further underscore the superiority of coated 3HA nanoparticles to uncoated 3HA nanoparticles, we examined TNF-α responses in dendritic cells. TNF-α is an inflammatory cytokine released by antigen presenting cells, and is important in increasing vascular permeability around the site of injection, leading to even greater recruitment of antigen presenting cells [9]. Coated 3HA nanoparticles performed significantly better than uncoated nanoparticles, which both performed better than soluble protein in eliciting TNF-α responses from dendritic cells (Figure 3).

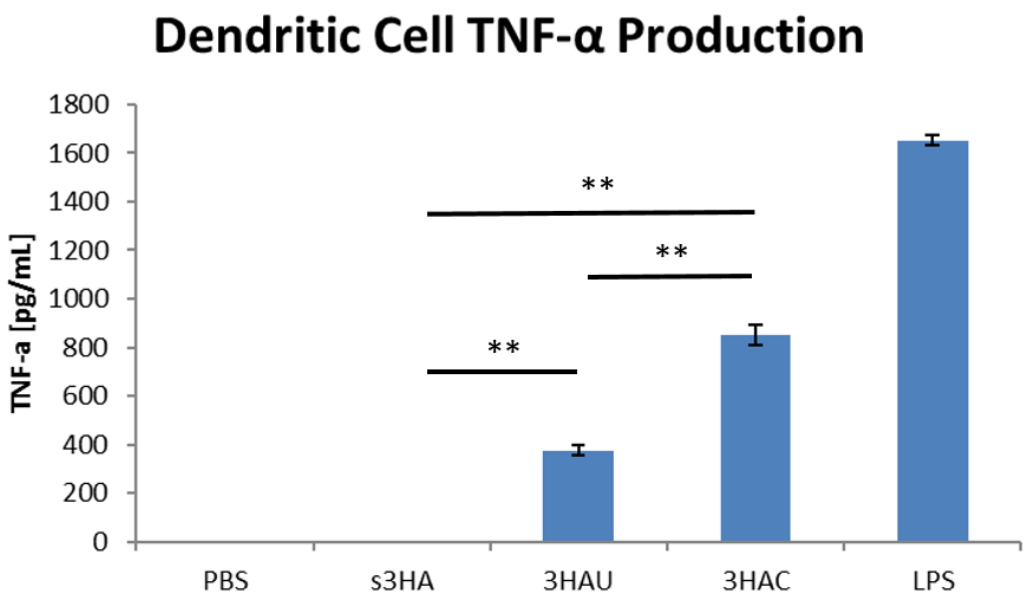

Figure 3. TNF-α secretion by JAWS II dendritic cells after 6 hours of stimulation. s3HA = soluble 3HA, 3HAU = uncoated 3HA nanoparticles, 3HAC = coated 3HA nanoparticles, LPS = lipopolysaccharide control. Error bars represent the standard deviation of 3 samples.

Upon intra-muscular (i.m.) or intra-nasal (i.n.) administration of coated 3HA nanoparticles, two i.m. injections was found to be the best method of nanoparticle administration, and thus this immunization scheme was used for this and future studies (Figure 4).

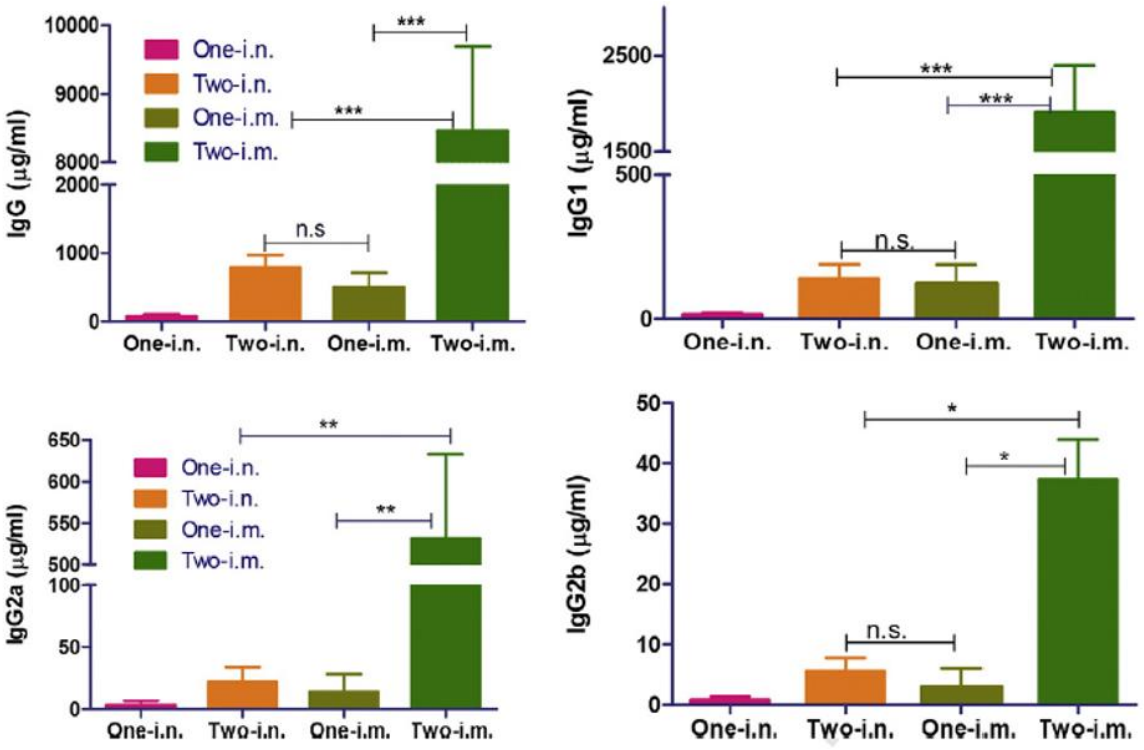

Figure 4. Total IgG and IgG subtype concentrations after various administrations of 3HA nanoparticles. Error bars represent one standard deviation from the average (n = 7-8 samples each). (Courtesy of Dr. Jong Rok Kim).

Following a 10xLD_{50} challenge of influenza A H7N9 virus, almost all of the mice given H7N9 nanoparticles survived (Figure 5). In the single i.n. immunization group, one mouse died following the challenge. Mice given 1 immunization i.m. or i.n. lost approximately 10% body weight 4-8 days post-challenge, but eventually recovered. Since the 3HA nanoparticles were able to provide protective immune responses and induce high antibody levels, and since 3HA has a convenient, *in vitro* readout of function in the hemagglutination assay, we chose these nanoparticles to be our model for extended cold-chain-independent storage in our Chapter 4 studies.

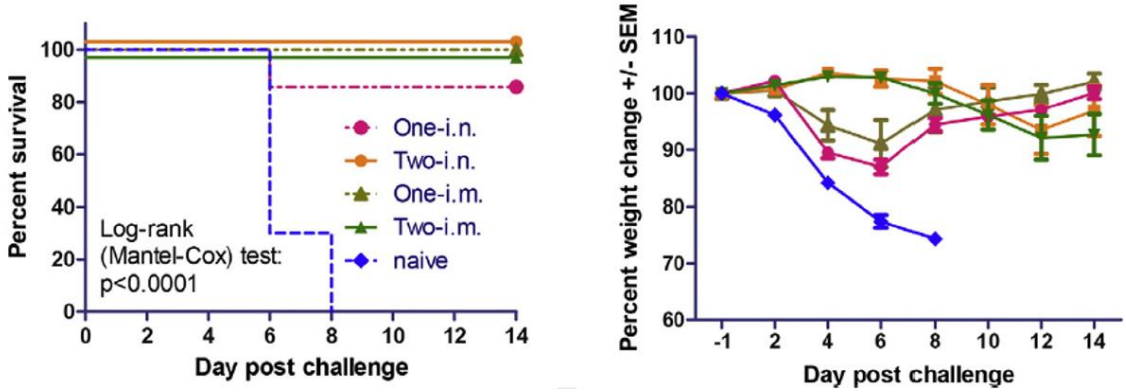

Figure 5. Percent survival (left) and percent weight change (right) following a 10xLD$_{50}$ intranasal challenge of H7N9 influenza A virus. Error bars on the right represent the standard error of the mean of 7-8 mice per group. (Courtesy of Dr. Ralph Tripp (UGA), Dr. Jong Rok Kim)

To better understand the mechanism of nanoparticle adjuvancy, we looked at the production of IL-1β by dendritic cells stimulated with our nanoparticles. Like TNF-α, IL-1β is also an inflammatory cytokine that acts on the vascular endothelium. Although many types of antigens from viral RNA to bacterial toxins can trigger IL-1β release [10], particulate antigens and adjuvants in particular have been associated with its release from antigen presenting cells via activation of the NLRP3 inflammasome [11]. Our finding that 3HA nanoparticles trigger greater IL-1β release than soluble 3HA protein (Figure 6) is consistent with previous findings in the literature, and suggests that the NLRP3 inflammasome may be an important part of 3HA nanoparticle-mediated adjuvancy.

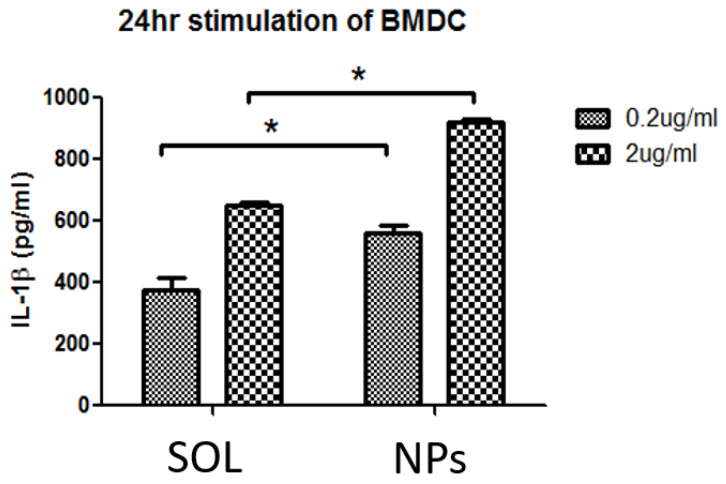

Figure 6. BMDC production of IL-1β after 24 hours of stimulation. SOL = Soluble 3HA, NPs = Coated 3HA nanoparticles. Error bars represent the standard deviation of 3 samples. (Courtesy of Dr. Jong Rok Kim)

Surface CD86 expression of dendritic cells was measured to assess dendritic cell maturation. CD86 is upregulated in dendritic cells undergoing maturation, a process crucial for antigen presentation to the adaptive immune system. We found that soluble 3HA protein was unable to trigger dendritic cell maturation, while 3HA nanoparticles could (Figure 7). The finding that dendritic cell maturation occurs in response to nanoparticulate, but not soluble antigen signifies the enhanced adjuvancy of protein nanoparticles is at least partly mediated at the level of antigen-presenting cell interactions. Although the 3HA nanoparticles were protective, our *in vitro* studies with dendritic cells presented here have only scratched the surface in determining the mechanism of nanoparticle adjuvancy. We continued our mechanism studies by testing biodistribution and adaptive immune cell activation in Chapter 3.

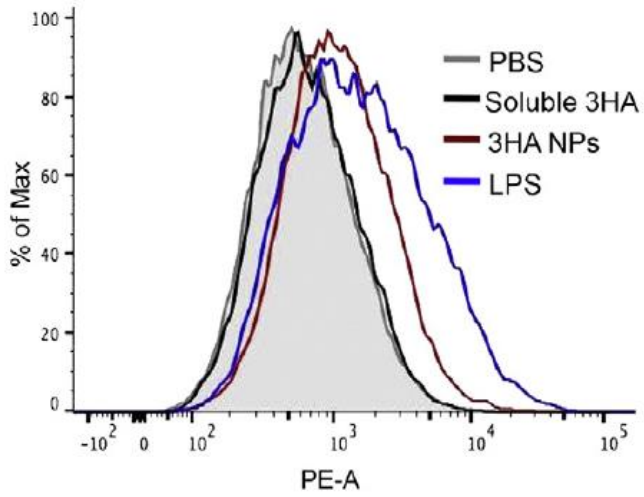

Figure 7. CD86 expression on JAWS II dendritic cells after 24 hours of stimulation. Each curve represents the fluorescence distribution of 10,000 cells. (Courtesy of Dr. Jong Rok Kim)

2.5 Flagellin-HA Stalk Fusion Proteins

Toll-like receptors are devoted to recognizing pathogen-associated molecular patterns (PAMPs), and are a key component of the innate immune system [9]. Stimulation of specific TLR receptors on dendritic cells provokes an innate immune response, and is a commonly employed strategy used to guide development of new types of PAMP and PAMP-derived adjuvants [12]. Flagellin, or FliC, is a toll-like receptor 5 (TLR-5) agonist, but can also bind to the intracellular receptors Naip5 and NLRC4 to trigger inflammatory responses [13, 14]. FliC has been extensively studied as an adjuvant for influenza vaccines. Influenza virus-like particles (VLPs) made with FliC enhanced virus-specific IgG responses in comparison to VLPs lacking FliC [15]. VLPs containing FliC-M2e fusion proteins also enhanced systemic and mucosal IgG and IgA production, respectively [16]. Currently, a FliC-fusion protein with 4 tandem copies of M2e (STF2.4xM2e) has completed a Phase II clinical trial successfully [17].

Replacing the hypervariable region of FliC with an antigen protein sequence is known to boost the humoral immune response to the protein sequence inserted [18]. Given the conserved nature of M2e and the HA stalk protein, it is hypothesized that protein nanoparticles made from M2e and HA stalk FliC-fusion proteins would enhance the adjuvancy of these component antigens. The HA stalk domain is highly conserved across influenza viruses, and HA stalk types fall under two phylogenetic groups of influenza viruses, group 1 (H1-like) and group 2 (H3-like) [19]. To obtain a set of antigens that could immunize against all types of influenza viruses, an H1-FliC fusion protein (fPR8) and an H3-FliC fusion protein (fAiChi) were used in conjunction with an H3N2 M2e-FliC fusion protein (fM2e) to make protein nanoparticles.

2.6 Materials and Methods

2.6.1 Protein Expression and Purification

Plasmids for FliC-fusion proteins fPR8 and fAiChi were obtained from the lab of Dr. Baozhong Wang, and the protein was expressed in *E. coli BL21*. The inclusion body-bound proteins were purified by non-native Ni-NTA purification, dialyzed against refolding buffer and PBS for 1.5 days each, and stored at -80°C for further use [20].

2.6.2 Nanoparticle Synthesis

To preserve TLR-5 stimulating activity, a desolvation-free method for creating the nanoparticles was used. Nanoparticles were formed by DTSSP crosslinking (Thermo Scientific, Waltham, MA), followed by diafiltration to remove excess soluble protein. 500 µL of fM2e or a mixture of fM2e and fPR8 or fAiChi at a 1:1 mass ratio was stirred at

speed of 600 rotations per minute with final protein concentration of 2.2 mg/mL and 0.197 mM final concentration of DTSSP at 4°C for 1 hour. Soluble protein and excess crosslinker was then removed by buffer exchange with fresh PBS using a 300 kDa diafiltration tube (Pall Corporation, Port Washington, NY). Dynamic light scattering (DLS) was performed in PBS with a Malvern Zetasizer Nano ZS to assess the size distribution of the collected nanoparticles.

2.6.3 TLR-5 Stimulation Assay

FliC fusion activity was characterized by a TLR-5-dependent luciferase activation assay *in vitro*. HEK 293T cells (ATCC, Manassas, VA) were grown in DMEM supplemented with 10% fetal bovine serum (FBS), and cultured in humidified 5% CO_2 at 37°C. Cells were incubated overnight at a density of $2*10^6$ cells/well in a 6-well plate, and transfected the following day with 10 μg pUNO1-hTLR5, 2 μg pGL4.32-[Luc2/Nf-κB/Hygro] (Invivogen, San Diego, CA) and 15 μL Lipofectamine 2000 (Invitrogen, Grand Island, NY) in DMEM with 1% FBS. Transfected cells were plated the following day at a density of $5*10^4$ cells/well in a 96-well plate in DMEM with 1% FBS. Cells were then stimulated for 5 hours by 1:5 serially diluted nanoparticles and FliC protein in serum-free media. Bright-Glo Luciferase Assay reagent (Promega, Madison, WI) was diluted 1:1 with serum-free DMEM and used to assess luciferase activity according to the manufacturer's instructions. Luminescence was measured using LUMAT LB9501 (Berthold, TN).

2.6.4 BMDC Culture and IL-1β Activity

Bone marrow-derived dendritic cells were harvested and cultured as previously described [8]. Briefly, bone marrow progenitor cells were collected from femurs and tibias from 6-8

week old female Balb/c mice and cultured in RPMI 1640 (ATCC, Manassas, VA) supplemented with 10% heat-inactivated FBS, 50 μM β-mercaptoethanol, 1% penicillin-streptomycin, 2mM sodium pyruvate, 1x non-essential amino acids (Thermo Scientific, Grand Island, NY), and 25 ng/mL each of IL-4 and GM-CSF (Peprotech, Rocky Hill, NJ). Cells were matured for one week, and the media was changed on days 2, 4 and 6. On Day 7, bone marrow-derived dendritic cells were plated at 10^5 cells/mL in 24-well plates for *in vitro* measurement of secreted IL-1β levels. After 24 hours of incubation, cells were stimulated with 10 μg/mL of fM2e, fM2e/fPR8 or fM2e/AiChi nanoparticles in fresh complete medium. IL-1β was assessed in supernatants after 24 hours of stimulation by ELISA (R&D Systems, Minneapolis, MN).

2.6.5 Immunization and Challenge studies

Female, 6-8 week old Balb/c mice (Charles River, Wilmington, MA) were intranasally immunized with 10 μg fM2e nanoparticles, 10 μg fM2e/fPR8 nanoparticles, 10 μg fM2e/AiChi nanoparticles, or PBS as a control. Ten mice per group were immunized twice i.m. at 4-week intervals. To compare antibody responses, sera were collected 2 weeks after each immunization by submandibular venipuncture. For challenge infections, mice from the fM2e, fM2e/fAiChi, and PBS groups were anesthetized with isoflurane, then intranasally infected with a $4xLD_{50}$ dose of A/Aichi/2/68 (H3N2) 4 weeks after the boost immunization. Mice were observed daily to monitor changes in survival rate and body weight, with 25% body weight loss being the humane endpoint for euthanasia according to IACUC guidelines. All animal studies were approved by the Emory University Institutional Animal Care and Use Committee (IACUC) under protocol number 2001659.

2.6.6 Serum Antibody Assessment

Serum was collected as described above and as in Section 2.1.2.6, and assessed for anti-M2e and anti-H1/H3 HA responses. M2e sequences from influenza H1N1, H3N2, H5N1, and H7N9 viruses were tested, and their sequences can be found in Appendix A. 1 μg/mL antigen was used for ELISA, and was carried out as described previously [1].

2.6.7 Statistical analysis

Statistical significance was determined by a two-tailed Student's *t*-test in comparing two different conditions. Two-way ANOVA was used to analyze the significant difference among 3 or more groups. A *P*-value less than 0.05 was considered to be significant. The analysis was done by using GraphPad Prism (version 5.0) software for Windows (GraphPad Software, San Diego, CA).

2.7 Results and Discussion

In these studies, desolvation-free protein nanoparticle synthesis was used to preserve FliC-fusion proteins' ability to activate TLR-5. Of the protein nanoparticle types tested so far, these proteins tested were the first ones to have a molecular adjuvant expressed in genetic fusion to the antigen of interest.

Desolvation of the fPR8 and fAiChi proteins resulted in a loss of TLR-5 stimulating activity, and coating the nanoparticles by the method used to make 3HA nanoparticles resulted in extremely poor yields. A new type of desolvation-free protein nanoparticle was designed for this study; one that consisted of crosslinker and antigen with no ethanol added

to compact the nanoparticles together. Because of this, the desolvation-free nanoparticles were considerably smaller than those made by desolvation, as shown in Table 1.

Table 1. Desolvation-free nanoparticle size and zeta potential

Nanoparticle Type	Size [nm]	Stdev [nm]	ζ Pot. [mV]	St dev [mV]
fM2e	54	13.5	-7.1	0.26
fM2e/fPR8	46.7	24.1	-10.9	1.43
fM2e/fAiChi	81.7	18.9	-7.94	0.83

The ability of the nanoparticles to activate TLR-5 was demonstrated by TLR-5-dependent NF-κB luciferase production (Figure 8). All nanoparticle types were able to stimulate luciferase production on a similar order of magnitude to soluble flagellin (FliC), indicating that the TLR-5 binding domains of fM2e, fPR8, and fAiChi were preserved in our nanoparticles.

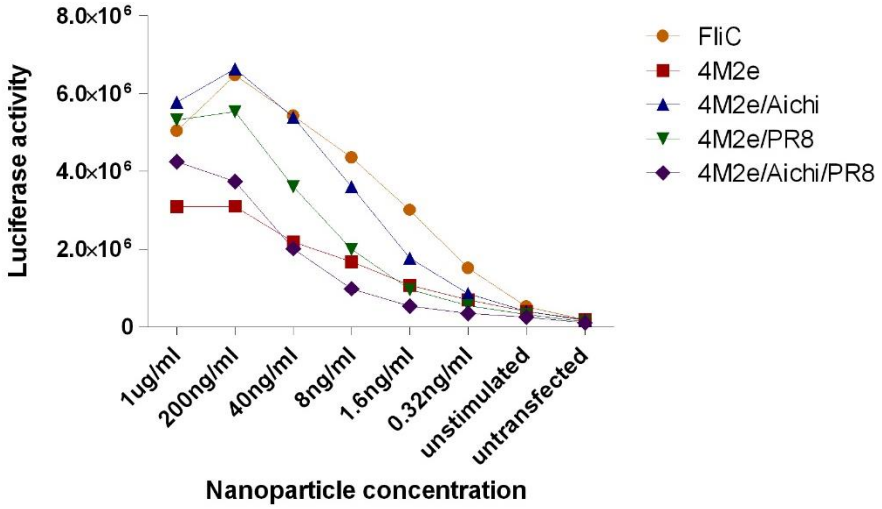

Figure 8. Luciferase activity in cells transfected with NF-κB-promoted luciferase and TLR-5. 4M2e = fM2e (Courtesy of Dr. Jong Rok Kim)

The various desolvation-free nanoparticle types were incubated with JAWS dendritic cells and tested for IL-1β stimulating activity (Figure 9). All nanoparticle types were found to significantly upregulate IL-1β production. Due to flagellin's inherent ability to activate the inflammasome and subsequent IL-1β production through NLRC4 binding [21], we cannot conclude whether the IL-1β production is a result of the nanoparticle-activated NLRP3 inflammasome, the flagellin-activated NLRC4 inflammasome, or a combination of both.

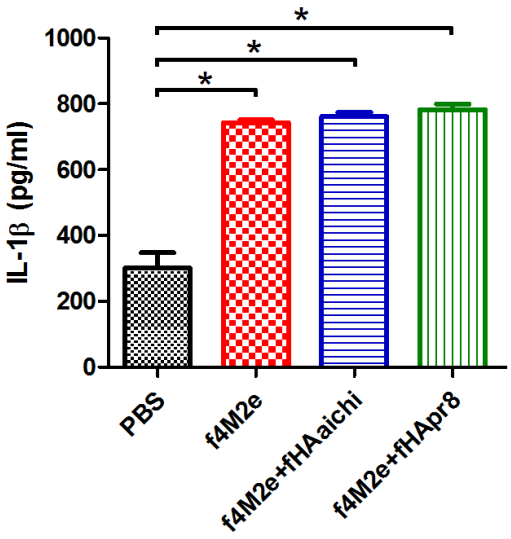

Figure 9. IL-1β production in JAWS dendritic cells 24 hours after stimulation with various nanoparticle types. Error bars represent the standard deviation of 3 samples. (Courtesy of Dr. Lei Deng)

Following two i.m. immunizations of 10 μg of each of the nanoparticle types, the ability of the desolvation-free nanoparticles to elicit antibodies to various M2e peptides was assessed. Since all particle types contained fM2e, it was of interest to see if this protein could elicit cross-reactive antibodies against different sequences of M2e. All types of nanoparticles were able to induce antibodies against all sequences of M2e tested (Figure 10).

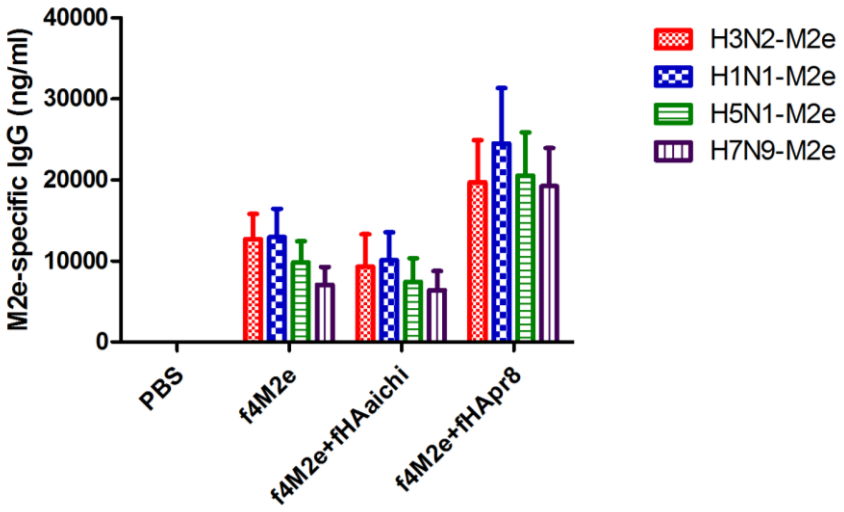

Figure 10. M2e-specific IgG concentrations as assessed by ELISA. Error bars represent the standard deviation of 6 serum samples. (Courtesy of Dr. Lei Deng)

In addition to measuring M2e-specific responses, hemagglutinin-specific responses were also assessed after immunization. As expected, each nanoparticle type containing hemagglutinin induced antibodies against its particular strain of hemagglutinin, but not the other one (Figure 11). These findings are consistent with the conserved nature of M2e, but not of the HA stalk across these phylogenetic groups.

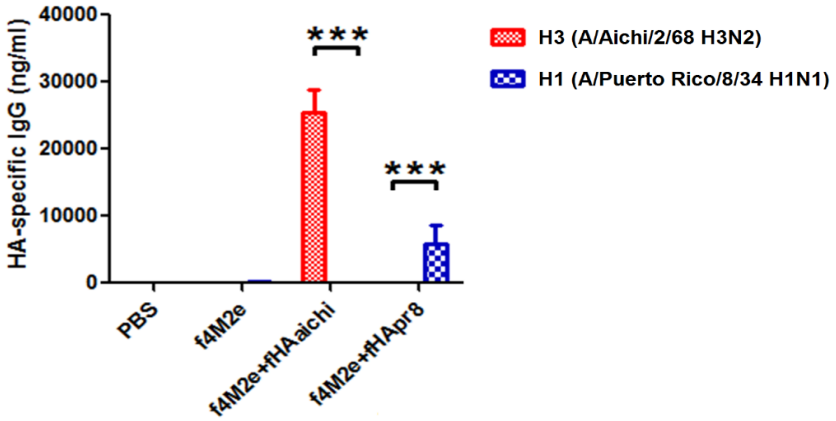

Figure 11. H1- and H3-hemagglutinin-specific IgG responses induced by each type of nanoparticle. Error bars represent the standard deviation of 6 serum samples. (Courtesy of Dr. Lei Deng).

Four weeks after a boost immunization, mice in groups immunized with fM2e and fM2e/fAiChi nanoparticles were challenged i.n. with a 4xLD_{50} dose of an H3N2 influenza virus. All mice given nanoparticles survived this challenge (Figure 12), and the addition of fAiChi into the nanoparticles did not improve post-challenge survival or weight loss (Figure 13).

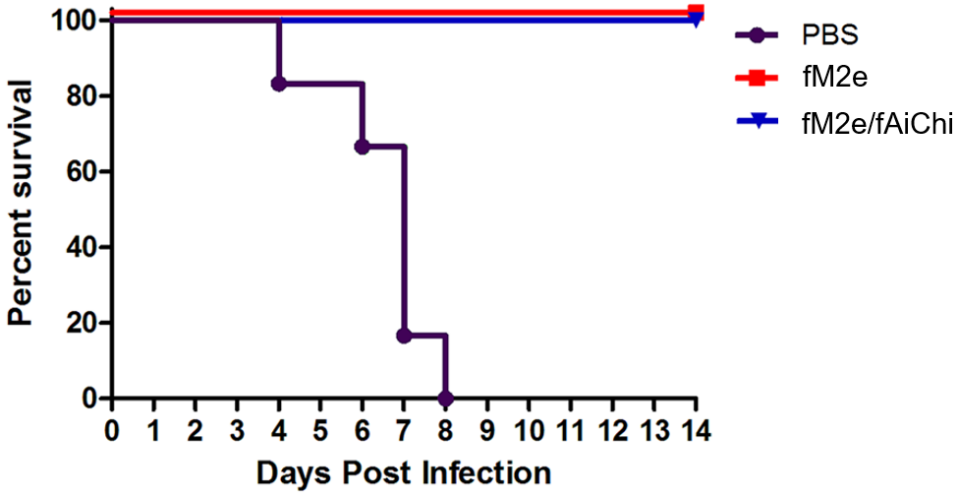

Figure 12. Post-H3N2 challenge survival of mice immunized with fM2e or fM2e/fAiChi nanoparticles. (Courtesy of Dr. Lei Deng)

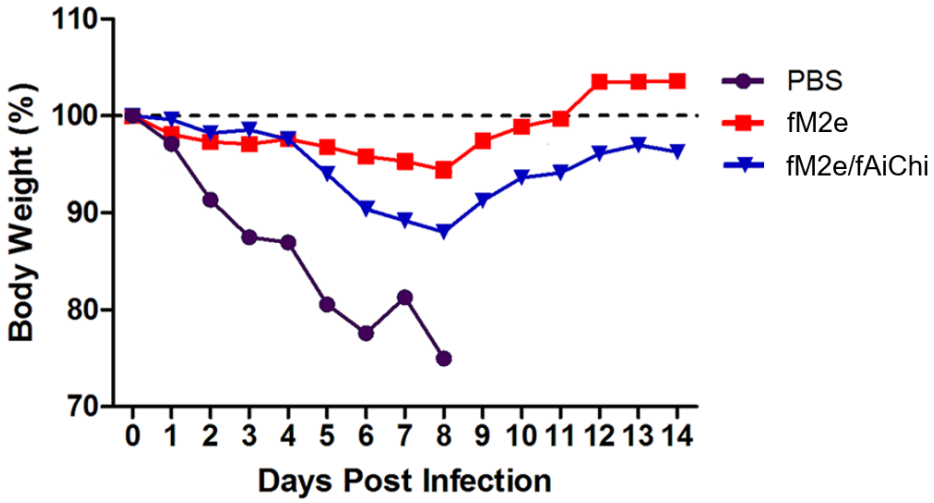

Figure 13. Post-H3N2 challenge body weight change of mice immunized with fM2e or fM2e/fAiChi nanoparticles. Data shown is the average weight of 11 mice. (Courtesy of Dr. Lei Deng)

The comparable ability of fM2e and fM2e/fAiChi nanoparticles to protect mice from a 4xLD_{50} challenge suggests that the flagellin-adjuvanted M2e may be sufficient for providing protection (Figure 12, Figure 13). This is supported by the ability of fM2e nanoparticles to induce antibodies against M2e peptides from an H3N2 influenza virus (Figure 10), and also by the finding that H3N2-challenged mice immunized with M2e nanoparticles lost on average twice as much weight as mice given fM2e nanoparticles. Although the fAiChi fusion protein was able to activate TLR-5 and induce anti-HA antibodies, these additional antibodies were not necessary for protection against infection.

Flagellin-fusion proteins have been reported to have sequence-dependent stability issues with protein aggregation [18], limiting their viability as a platform technology for immunization. Since a nanoparticle can co-localize antigen and adjuvant proteins together, it may not be necessary to use FliC-fusion proteins to co-deliver antigen and adjuvant. Furthermore, whether a 1:1 molar ratio of antigen:adjuvant is necessary has not been

established, and decreasing the amount of adjuvant used with the nanoparticles could improve the vaccine safety profile. To examine whether co-administration of soluble FliC with protein nanoparticles or coating of protein nanoparticles with FliC enhances the immune response, we explore the role of adjuvant location in Chapter 5.

2.8 Overall Conclusions

In the preceding studies, we modified the protein nanoparticle synthesis procedure to accommodate two additional types of proteins – trimerized hemagglutinin, and flagellin-fusion proteins. Overall, this chapter has explored ways of creating protein nanoparticles from full-length proteins. Challenges associated with desolvant-mediated denaturation of proteins were overcome by avoiding protein-desolvant contact – either by crosslinking proteins to the surface of desolvated 3HA protein nanoparticles or by crosslinking fM2e, fPR8 or fAiChi together in PBS.

Uncoated 3HA nanoparticles made by the original desolvation method showed less hemagglutination than coated 3HA nanoparticles, and this difference in hemagglutination was reflected in correspondingly lower TNF-α production by dendritic cells. These preliminary results highlighted the importance of the outer nanoparticle coat layer in making protein nanoparticles with conformational antigens.

Immunizing mice with 3HA-coated 3HA nanoparticles provided protection against a $10xLD_{50}$ influenza challenge. Although a challenge was not performed on mice immunized with soluble 3HA protein, we performed an immunization experiment with soluble 3HA protein in our evaluation of nanoparticle stability in Chapter 4. The ability of a non-conserved HA antigen, H7, to induce protection in nanoparticulate form

complements earlier M2e data demonstrating that conserved antigens in nanoparticles provide protective immune responses. Taken together, these data suggest that protein nanoparticles are a promising technology for developing both universal influenza vaccines and strain-specific influenza vaccines.

An alternative approach to universal influenza vaccine development was explored by augmenting M2e with flagellin in an M2e-FliC fusion protein construct. To preserve this protein's adjuvant activity and obtain substantial yields of nanoparticles, a desolvation-free method was used to create nanoparticles, and these desolvation-free nanoparticles were able to protect against a $4xLD_{50}$ influenza challenge. The strong efficacy of the fM2e fusion protein nanoparticles suggests that genetic fusion of FliC to M2e in a 1:1 ratio may add more adjuvant than necessary to the nanoparticles. Given that protein nanoparticles colocalize antigen and adjuvant proteins, incorporating full-length flagellin alongside antigen in protein nanoparticles could sidestep the issue of generating potentially unstable fusion proteins, and allow for independent control of antigen and adjuvant ratios. Along with incorporating less adjuvant, determining optimal adjuvant location, on or off the nanoparticle, is a critical question for nanoparticle vaccine design, and is addressed in the studies in Chapter 5.

REFERENCES

[1] L. Wang, A. Hess, T.Z. Chang, Y.C. Wang, J.A. Champion, R.W. Compans, B.Z. Wang, Nanoclusters self-assembled from conformation-stabilized influenza M2e as broadly cross-protective influenza vaccines, Nanomed-Nanotechnol 10(2) (2014) 473-482.

[2] P. Pushko, L.M. Pujanauski, X.J. Sun, M. Pearce, R. Hidajat, T. Kort, L.M. Schwartzman, I. Tretyakova, C.Q. Liu, J.K. Taubenberger, T.M. Tumpey, Recombinant H7 hemagglutinin forms subviral particles that protect mice and ferrets from challenge with H7N9 influenza virus, Vaccine 33(38) (2015) 4975-4982.

[3] Q. Liu, L. Lu, Z. Sun, G.-W. Chen, Y. Wen, S. Jiang, Genomic signature and protein sequence analysis of a novel influenza A (H7N9) virus that causes an outbreak in humans in China, Microbes Infect 15(6–7) (2013) 432-439.

[4] L.A. Jackson, J.D. Campbell, S.E. Frey, K.M. Edwards, W.A. Keitel, K.L. Kotloff, A.A. Berry, I. Graham, R.L. Atmar, C.B. Creech, I.P. Thomsen, S.M. Patel, A.F. Gutierrez, E.L. Anderson, H.M. El Sahly, H. Hill, D.L. Noah, A.R. Bellamy, Effect of Varying Doses of a Monovalent H7N9 Influenza Vaccine With and Without AS03 and MF59 Adjuvants on Immune Response A Randomized Clinical Trial, Jama-J Am Med Assoc 314(3) (2015) 237-246.

[5] X. Qi, Y.H. Qian, C.J. Bao, X.L. Guo, L.B. Cui, F.Y. Tang, H. Ji, Y. Huang, P.Q. Cai, B. Lu, K. Xu, C. Shi, F.C. Zhu, M.H. Zhou, H. Wang, Probable person to person transmission of novel avian influenza A (H7N9) virus in Eastern China, 2013: epidemiological investigation, Bmj-Brit Med J 347 (2013).

[6] J.J. Skehel, D.C. Wiley, Receptor binding and membrane fusion in virus entry: The influenza hemagglutinin, Annu. Rev. Biochem. 69 (2000) 531-569.

[7] G.E. Smith, D.C. Flyer, R. Raghunandan, Y. Liu, Z.P. Wei, Y.Y. Wu, E. Kpamegan, D. Courbron, L.F. Fries, G.M. Glenn, Development of influenza H7N9 virus like particle (VLP) vaccine: Homologous A/Anhui/1/2013 (H7N9) protection and heterologous A/chicken/Jalisco/CPA1/2012 (H7N3) cross-protection in vaccinated mice challenged with H7N9 virus, Vaccine 31(40) (2013) 4305-4313.

[8] T.Z. Chang, S.S. Stadmiller, E. Staskevicius, J.A. Champion, Effects of ovalbumin protein nanoparticle vaccine size and coating on dendritic cell processing, Biomater Sci-Uk (2017).

[9] K. Murphy, P. Travers, M. Walport, C. Janeway, Janeway's immunobiology, Garland Science, New York, 2012.

[10] O. Gross, C.J. Thomas, G. Guarda, J. Tschopp, The inflammasome: an integrated view, Immunol Rev 243(1) (2011) 136-151.

[11] V. Hornung, F. Bauernfeind, A. Halle, E.O. Samstad, H. Kono, K.L. Rock, K.A. Fitzgerald, E. Latz, Silica crystals and aluminum salts activate the NALP3 inflammasome through phagosomal destabilization, Nat Immunol 9(8) (2008) 847-856.

[12] S. Manmohan, Vaccine adjuvants and delivery systems, Wiley-Interscience, Hoboken, N.J., 2007.

[13] K.L. Lightfield, J. Persson, S.W. Brubaker, C.E. Witte, J. von Moltke, E.A. Dunipace, T. Henry, Y.H. Sun, D. Cado, W.F. Dietrich, D.M. Monack, R.M. Tsolis, R.E. Vance, Critical function for Naip5 in inflammasome activation by a conserved carboxy-terminal domain of flagellin, Nat Immunol 9(10) (2008) 1171-1178.

[14] L. Franchi, A. Amer, M. Body-Malapel, T.D. Kanneganti, N. Ozoren, R. Jagirdar, N. Inohara, P. Vandenabeele, J. Bertin, A. Coyle, E.P. Grant, G. Nunez, Cytosolic flagellin requires Ipaf for activation of caspase-1 and interleukin 1 beta in salmonella-infected macrophages, Nat Immunol 7(6) (2006) 576-582.

[15] B.Z. Wang, F.S. Quan, S.M. Kang, J. Bozja, I. Skountzou, R.W. Compans, Incorporation of Membrane-Anchored Flagellin into Influenza Virus-Like Particles Enhances the Breadth of Immune Responses, J Virol 82(23) (2008) 11813-11823.

[16] B.Z. Wang, H.S. Gill, S.M. Kang, L. Wang, Y.C. Wang, E.V. Vassilieva, R.W. Compans, Enhanced Influenza Virus-Like Particle Vaccines Containing the Extracellular Domain of Matrix Protein 2 and a Toll-Like Receptor Ligand, Clin Vaccine Immunol 19(8) (2012) 1119-1125.

[17] C.B. Turley, R.E. Rupp, C. Johnson, D.N. Taylor, J. Wolfson, L. Tussey, U. Kavita, L. Stanberry, A. Shaw, Safety and immunogenicity of a recombinant M2e-flagellin influenza vaccine (STF2.4xM2e) in healthy adults, Vaccine 29(32) (2011) 5145-5152.

[18] S.B. Mizel, J.T. Bates, Flagellin as an Adjuvant: Cellular Mechanisms and Potential, J Immunol 185(10) (2010) 5677-5682.

[19] R.D. de Vries, A.F. Altenburg, G.F. Rimmelzwaan, Universal influenza vaccines, science fiction or soon reality?, Expert Rev Vaccines 14(10) (2015) 1299-1301.

[20] I. Skountzou, P. Martin Mdel, B. Wang, L. Ye, D. Koutsonanos, W. Weldon, J. Jacob, R.W. Compans, Salmonella flagellins are potent adjuvants for intranasally administered whole inactivated influenza vaccine, Vaccine 28(24) (2010) 4103-12.

[21] A. Ketko, C.H. Lin, A.M. LeVine, Surfactant Protein-a Mediates Flagellin Induced Interleukin-1-Beta Expression through the Inflammasome, Crit Care Med 40(12) (2012) U57-U57.

CHAPTER 3. FUNDAMENTAL STUDIES OF PROTEIN NANOPARTICLE ADJUVANCY

3.1 Introduction

In prior work, protein nanoparticles made with the conserved influenza peptide M2e were found to induce protective immune responses in mice against two subtypes of influenza[1]. Mice immunized with M2e protein nanoparticles showed anti-M2e IgG and IgA responses in lung and nasal washes as well as M2e-inducible splenic IL-4 and IFN-γ responses, indicating both strong humoral and T-cell mediated immune responses. In contrast, immunization with soluble M2e triggered no protective immunity or immune correlates. In Chapter 2, we also found nanoparticles made from trimerized, H7 hemagglutinin confer protection against an H7 influenza challenge, and that coating the hemagglutinin nanoparticles with an additional layer of hemagglutinin protein increased the nanoparticles' hemagglutinating capabilities [2]. To understand how protein nanoparticles confer protective immunity and how particle properties, such as size and coating, affect the resulting immune response, an *in vitro* examination of nanoparticulate antigen processing is needed.

In this chapter, we examine protein nanoparticle and soluble ovalbumin (OVA) uptake and processing, and the resulting markers of inflammation and maturation in dendritic cells *in vitro*. Protein nanoparticle size and coating were varied due to the immunomodulatory importance of particle size [3] and properly-conformed surface antigen [4]. Protein nanoparticle size and coating are the two controllable parameters of

protein nanoparticles made entirely from antigen, while other nanoparticle properties such as charge and hydrophobicity are intrinsically linked to the antigen protein of choice. We found both protein nanoparticle size and coating to be important modifiers of DC inflammatory cytokine production. Other aspects of protein nanoparticle antigen processing, such as uptake and acidification, were found to be significantly different from soluble antigen processing, but particle size- and coating-independent.

Although dendritic cells are one of the key regulators of the adaptive immune response, other aspects of the nanoparticle-mediated immune response arise only from multiple cell types or even whole organs interacting with nanoparticles and soluble protein differently. To explore these interactions, we also looked at different *in vivo* responses to our coated 3HA nanoparticles and soluble 3HA protein. By assessing biodistribution, as well as lymph node and spleen cell responses, we sought to answer if (1) antigen persistence at the site of injection or in draining lymphatic organs could explain protein nanoparticles' enhanced adjuvancy, and (2) whether germinal center B cell responses were enhanced by nanoparticulate antigen.

To initiate an adaptive immune response, antigen must be presented by antigen presenting cells in an immunostimulatory context to cognate B and T cells of the adaptive immune system. Activated B cells can undergo proliferation in the lymph nodes or spleen to form a germinal center, a region of high B cell proliferation and somatic hypermutation that generates high affinity antibodies to antigens presented. Germinal centers grow in size in the presence of antigen from a vaccine or infection, and can last up to 3 or 4 weeks after initial antigen exposure [5]. Germinal center formation is crucial for high-affinity antibody

responses, B cell class switching to generate diverse antibody effector functions, and memory B cell formation to ensure lasting protection.

Before a vaccine nanoparticle can stimulate effective germinal center formation, it must be presented to the adaptive immune system. Small nanoparticles in the range of 20-200 nm in size can drain directly to the lymph nodes, while larger particles (500-2000 nm) have been found to associate with injection-site dendritic cells [6, 7]. Better injection site retention of large vaccine particles has also been reported [6]. Our 3HA nanoparticles lie between these two ranges. Although they are closer in size to the small range of nanoparticles, the order-of-magnitude size difference between soluble protein and protein nanoparticles will allow us to probe the difference between direct LN drainage and APC-mediated antigen presentation.

3.2 Materials and Methods

3.2.1 Protein Nanoparticle Synthesis

Nanoparticles were made by a modified desolvation method [1], and size was adjusted through the exact conditions as listed in Table 2. To make the particles, 0.4 mL pure ethanol was added at a constant rate to 0.1 mL of 6.2 mg/mL OVA (Invivogen, San Diego, CA) in phosphate-buffered saline (PBS) under constant stirring at 600 rpm. The amine-reactive crosslinker 3,3’-dithiobis[sulfosuccinimidylpropionate] (DTSSP) (ThermoFisher Scientific, Waltham, MA) was used to stabilize the resulting nanoparticles. The nanoparticles were crosslinked while stirring at room temperature for one hour, followed by centrifugation to collect the particles. Nanoparticles were resuspended by sonication in either 1 mL of 6.2 mg/mL OVA in PBS or 1 mL of PBS for coating or non-

coating, respectively. Coating was performed for 2 hours while stirring at 4°C. Following collection by centrifugation, particles were resuspended in 0.5 mL of PBS, and additional DTSSP was added to a concentration of 6.18 mM to stabilize the outer coating. Coat crosslinking was performed for 2 hours while stirring at 4°C. The coat crosslinking reaction was quenched with 50 mM Tris base, and particles were collected by centrifugation and resuspended in 0.5 mL PBS.

3.2.2 Protein Nanoparticle Characterization

Nanoparticle size distribution and zeta potential were assessed by dynamic light scattering (DLS) and electrophoretic light scattering (ELS) respectively with a Malvern Zetasizer Nano ZS (Malvern Instruments, Westborough, MA). Protein concentration in the nanoparticle solution was assessed with a BCA assay according to the manufacturer's instructions (Thermo Scientific, Waltham, MA). Nanoparticles were resuspended in water, air-dried, and sputter-coated with carbon prior to visualization with a Zeiss Ultra60 FE (Carl Zeiss Microscopy, Cambridge, UK) scanning electron microscope at 5.0 kV.

Fluorescent protein nanoparticle coating was confirmed by flow cytometry. Coat antigenicity was assessed with ELISA using a horseradish peroxidase (HRP)-conjugated polyclonal anti-ovalbumin antibody (Thermo Scientific, Rockford, IL). 5.4 µg/mL OVA protein nanoparticles in PBS were coated on a 96-well plate overnight at room temperature. Each reagent incubation step was followed by three washes with 0.05% Tween-20 in PBS. Non-specific binding was blocked by a 1 hour incubation of the plate at 4°C with 1% bovine serum albumin (BSA) in PBS. The HRP-conjugated anti-OVA antibody in PBS was incubated at 1 µg/mL on the plate for 2 hours at 4°C. Chromogenic quantification was

assessed by the oxidation of tetramethylbenzidine by hydrogen peroxide (R&D Systems, Minneapolis, MN) according to the manufacturer's instructions.

3.2.3 Cell Culture

The JAWS II immature dendritic cell line was obtained from the American Type Culture Collection (Manassas, VA) and cultured in MEM-alpha (Corning, Manassas, VA) supplemented to 4 mM glutamine and 5 ng/mL GM-CSF (Peprotech, Rocky Hill, NJ), 20% fetal bovine serum (FBS), and 1% penicillin/streptomycin (Amresco, Solon, OH). Cells were grown in a humidified incubator at 37°C in 5% CO_2. For all experiments, cells were plated at a density of 10^5 cells/mL and incubated for 24 hours prior to stimulation unless indicated otherwise.

3.2.4 Nanoparticle Uptake

Nanoparticle uptake was assessed by flow cytometry. Fluorescent nanoparticles were made as described but with OVA containing 5 wt% AlexaFluor 488-conjugated OVA (Life Technologies, Grand Island, NY). JAWS II dendritic cells were plated in 24-well plates, and stimulated with 20 µg/mL fluorescent OVA nanoparticles or fluorescent soluble OVA. Cells were washed once with PBS, briefly trypsinized, collected by centrifugation, and resuspended in chilled trypan blue (Corning, Manassas, VA) to quench external green fluorescence. Cell fluorescence was measured at 6, 15 and 24 hours post-stimulation with a BD Accuri C6 flow cytometer (BD Biosciences, San Jose, CA). Nanoparticle internalization was confirmed by confocal microscopy.

3.2.5 Endosomal pH

Endosomal pH was assessed by ratiometric fluorescence. FITC-(pH-sensitive fluorophore) and AlexaFluor 647-(pH insensitive fluorophore) conjugated OVA (Life Technologies, Grand Island, NY) were added to a final concentration of 15 wt% and 1 wt%, respectively, to non-fluorescent OVA to make green/red-fluorescent nanoparticles as described above. Standard curves were generated in pH-adjusted PBS to correlate fluorescent intensity ratios to pH (Figure 20). 100 μg/mL green/red protein nanoparticles were incubated with JAWS DCs in 96-well plates for 2 hours. The nanoparticle solution was removed, the cells were washed with PBS, and fresh media was added. Following an additional incubation for 0-6 hours, the media was replaced with PBS, and fluorescence measurements were taken on a plate reader (BioTek, Winooski, VT) or a flow cytometer (BD Biosciences, San Jose, CA). Fluorescent intensities were calculated as averages of either a 5x5 fluorescent area scan of each well or the median fluorescence intensity, respectively.

3.2.6 Nanoparticle Uptake Inhibition

Fluorescent nanoparticle uptake was assessed in the presence of 42 μM chlorpromazine or 49 μM cytochalasin D. Concentrations of inhibitors were chosen based on (1) maximizing positive control uptake inhibition of fluorescent transferrin or 3 μm polystyrene beads as assessed by flow cytometry or confocal microscopy, respectively, and (2) minimizing cytotoxicity as assessed by a lactate dehydrogenase assay (LDH). Percent inhibition of positive control and nanoparticle uptake was calculated by normalizing inhibited uptake by uninhibited uptake. Uptake inhibition studies were performed in 48-

well plates. Cells were first pre-treated with uptake inhibitors for one hour. Afterwards, complete media containing fluorescent protein nanoparticles or soluble OVA at a concentration of 20 μg/mL and each appropriate uptake inhibitor was added. After 3 hours of incubation, the cells were washed once with PBS, fixed with 3.7% paraformaldehyde, washed with PBS again, and resuspended in trypan blue to quench extracellular fluorescence. Cells were scraped from the plate and their fluorescence measured by flow cytometry. Degree of uptake inhibition was calculated by median fluorescence intensities of 10,000 cells (Equation 1).

3.2.7 In Vitro Inflammatory and Maturation Markers

JAWS DCs were plated in either 24- or 48-well plates for measuring *in vitro* maturation and inflammation markers, respectively. Cells were stimulated with 20 μg/mL of soluble OVA or OVA protein nanoparticles. CD86 was assessed by flow cytometry after 24 hours of stimulation. Cells were fixed with 3.7% paraformaldehyde and blocked with 1% BSA in PBS for 1 hour. Cells were then incubated with 2 μg/mL rat-anti-mouse CD86 (clone GL-1) or isotype control (clone aRTK2758) primary antibodies for 30 minutes, washed twice with 1% BSA in PBS, then stained with 1 μg/10^6 cells polyclonal PE-conjugated goat-anti-rat Fc secondary antibody for 30 minutes. All antibodies were purchased from Abcam (Cambridge, MA). Cells were washed twice with PBS, scraped from the plate, and analyzed by flow cytometry. TNF-α was assessed in supernatants after 6 hours of stimulation by ELISA (R&D Systems, Minneapolis, MN) according to the manufacturer's instructions.

3.2.8 Bone Marrow Derived Dendritic Cell (BMDC) Generation and Cell Culture

Bone marrow from euthanized, ten-week old Balb/c mouse femurs and tibias was collected and cultured as previously described [8]. All animal work was compliant with the NIH Guide for the Care and Use of Laboratory Animals. Bone marrow progenitor cells were cultured in RPMI 1640 (ATCC, Manassas, VA) supplemented with 10% heat-inactivated FBS, 50 μM β-mercaptoethanol, 1% penicillin-streptomycin, 2mM sodium pyruvate, 1x non-essential amino acids (Thermo Scientific, Grand Island, NY), and 25 ng/mL each of IL-4 and GM-CSF (Peprotech, Rocky Hill, NJ). Cells were matured for one week, and the media was changed on days 2, 4 and 6. On Day 7, cells were harvested by scraping and plated for experiments.

3.2.9 IL-1β Measurement

BMDCs were plated at a density of $5x10^5$ cells/mL in 24-well plates. Cells were stimulated with 20 μg/mL of soluble OVA or protein nanoparticles. Supernatants were collected after 48 hours and stored at -80°C. IL-1β was assessed by ELISA (R&D Systems, Minneapolis, MN).

3.2.10 BSA Coating of Nanoparticles

100 μg of small coated and uncoated OVA protein nanoparticles were incubated stirring in 0.5 mL of 10 mg/mL bovine serum albumin (BSA) in PBS for 2 hours at 4°C, collected by centrifugation, resuspended in PBS and crosslinked as described in Table 2. Nanoparticles were then assessed for BSA presence with an HRP-conjugated anti-BSA

antibody (Life Technologies, Grand Island, NY) using a standard ELISA protocol (R&D Systems, Minneapolis, MN).

3.2.11 Confocal Microscopy

Jaws II Dendritic cells were incubated with 100 μg/mL small, uncoated, green-fluorescent protein nanoparticles for 6 hours. Cells were then washed with PBS, permeablized with 1% Triton-X in PBS, and washed twice more. Rhodamine-phalloidin (1:40) was used to stain the actin cytoskeleton, and incubated with the cells for 15 minutes at room temperature. After 3 more PBS washes, the cells were imaged using a Zeiss confocal laser-scanning microscope.

3.2.12 MHC I/II Upregulation

C57BL/6 bone marrow was cultured and matured into BMDCs as described in Section 3.2.8, and seeded at a density of $3*10^5$ cells/mL in 96-well plates. After 24 hours of stimulation with OVA protein nanoparticles, soluble OVA, or soluble OVA + 1 μg/mL LPS, cells were blocked with anti-CD16/32 (TruStain FcX, Biolegend), and incubated with APC-conjugated anti-H-$2K^b$-SIINFEKL (MHC I) and FITC-conjugated anti-I-A^b (MHC II) according to the manufacturer's instructions (Biolegend). Cells were analyzed by flow cytometry (BD Accuri).

3.2.13 3HA Nanoparticle Synthesis

Coated 3HA nanoparticles were made according to the protocol in Section 2.1.2.3. To make fluorescent 3HA, 10 μL of 10 mg/mL Alexa Fluor 700 succinimidyl ester dye (Life Technologies, Grand Island, NY) in dimethyl sulfoxide (DMSO) was added to 50 μL

of 5 mg/mL 3HA protein in sterile 0.1 M sodium bicarbonate buffer (pH 8.3). The reaction was stirred at 800 rpm for 1 hour at room temperature on a Thermoshaker (Grant Instruments, Cambridge, UK), and excess dye was removed by buffer exchanging with PBS in a 3 kDa diafiltration tube until the filtrate was colorless. Protein concentration was measured by the BCA assay, and conjugated dye concentration was measured by fluorescence against a standard curve of the free dye on a spectrophotometer (BioTek, Winooski, VT). To make fluorescent nanoparticles, 144 μg fluorescent 3HA protein was added to 336 μg non-fluorescent 3HA protein (30% fluorescent 3HA by mass) and used to create nanoparticles as described above.

3.2.14 Immunization and Biodistribution

All animal studies were approved by the Emory University IACUC under protocol number 2001659 and the Georgia State University IACUC under protocol number A16024. Mice to be given fluorescent proteins and nanoparticles were fed a low-fluorescence diet for 2 weeks prior to immunization to reduce background autofluorescence (LabDiet, St. Louis, MO) [9], and treated with a depilatory cream (Nair) around the injection site one day before immunization.

Groups of five, 6-8 week-old female Balb/c mice were injected with 10 μg of fluorescent or non-fluorescent 3HA nanoparticles or soluble protein, or PBS as a control. Mice injected with non-fluorescent protein and protein nanoparticles were sacrificed after 10 days for spleen and draining lymph node (dLN) germinal center B cell staining. Mice given fluorescent protein and protein nanoparticles were used for antigen biodistribution studies.

For *in vivo* imaging, mice were lightly anesthetized with 2 L/min of 5% isoflurane in medical grade oxygen. Once mice were no longer ambulatory, they were transferred to a Perkin Elmer IVIS Spectrum imaging system (Caliper Life Sciences, Perkin Elmer, Waltham, MA) and kept under anesthesia at 1 L/min of 5% isoflurane in medical grade oxygen. Mice were imaged laterally on the side of injection and dorsally at 0 hours, 6 hours, 24 hours, and days 2, 4, 6, 7 and 8. On day 4, two mice from each group were sacrificed for *ex vivo* draining lymph node and spleen imaging, and on day 8, *ex vivo* imaging was performed on the remaining 3 mice. Fluorescence was quantified with LivingImage software (Perkin Elmer), using the standard size circular quantification tool to capture the fluorescence present between the knee and the upper edge of the quadriceps.

3.2.15 Ex vivo Cell Staining

Cells were harvested from homogenized organs and washed with PBS. Fc receptors were blocked by TruStain fcX (Biolegend) for 10 minutes on ice. Cells were then incubated with PE-conjugated anti-mouse CD95 (clone SA367H8) or FITC-conjugated anti-mouse GL-7 (clone GL7) antibodies for 30 minutes on ice (Biolegend). After two washes, cells were fixed with 1% paraformaldehyde and analyzed with a BD FACSAria flow cytometer (BD Biosciences, San Jose, CA). Data were analyzed with FlowJo software (FlowJo LLC, Ashland, OR).

3.2.16 Statistics

Significance was assessed by a one-way ANOVA or Student's unpaired t-test at a significance level of $p<0.05$. All data shown is representative of at least three independent measurements unless indicated otherwise.

3.3 Results

3.3.1 OVA Protein Nanoparticle Synthesis and Characterization

Ovalbumin protein nanoparticles were made by a modified desolvation procedure [10]. Small- (~270 nm diameter) and medium-sized (~350 nm) nanoparticles were made by desolvation of ovalbumin at 1 mL/min. Increasing the rate of ethanol addition created large (~560 nm diameter) protein nanoparticles. Synthesis parameters are summarized in Table 2. Crosslinking nanoparticles in the desolvation media led to medium and large protein nanoparticles, while crosslinking in PBS created small nanoparticles (Figure 14). Zeta potential was unaffected by nanoparticle size (Figure 15). A summary of size, zeta potential and process yield data can be found in Table 3.

Table 2. Protocol details for creating OVA protein nanoparticles of different sizes. Coat solution was 6.2 mg/mL OVA in PBS.

Step	Small	Medium	Large
Ethanol addition	1 mL/min	1 mL/min	7 mL/min
Centrifugation	7000 g for 5 mins followed by resuspension in PBS	none	none
Crosslinking	Aqueous, 0.82 mM DTSSP, stirring for 1 hour	In 80% ethanol, 0.82 mM DTSSP, stirring for 1 hour	In 80% ethanol, 0.82 mM DTSSP, stirring for 1 hour
Centrifugation	18,000 g for 32 mins	7000 g for 5 minutes	7000 g for 5 minutes
Resuspension	Sonication in 1 mL PBS or coat solution	Sonication in 1 mL PBS or coat solution	Sonication in 1 mL PBS or coat solution
Coating	Two hours at 4°C	Two hours at 4°C	Two hours at 4°C
Second Centrifugation	18,000 g for 32 mins	18,000 g for 32 mins	7,600 g for 5 mins
Second Crosslinking	Aqueous 6.2 mM, stirring for 2 hours	Aqueous 6.2 mM, stirring for 2 hours	Aqueous 6.2 mM, stirring for 2 hours
Quenching	50 mM Tris base, stirring 15 mins.	50 mM Tris base, stirring 15 mins.	50 mM Tris base, stirring 15 mins.
Third Centrifugation after coating and second crosslinking	18,000 g for 32 mins	18,000 g for 32 mins	7,600 g for 5 mins
Resuspension	Sonication in 0.5 mL PBS	Sonication in 0.5 mL PBS	Sonication in 0.5 mL PBS

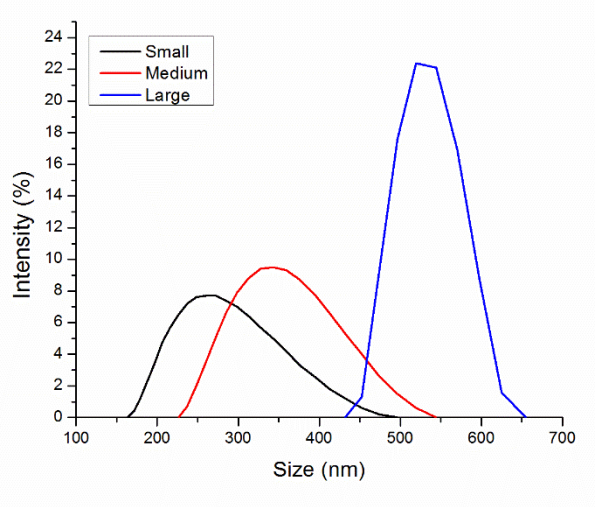

Figure 14. Representative size distributions of OVA protein nanoparticles of different sizes.

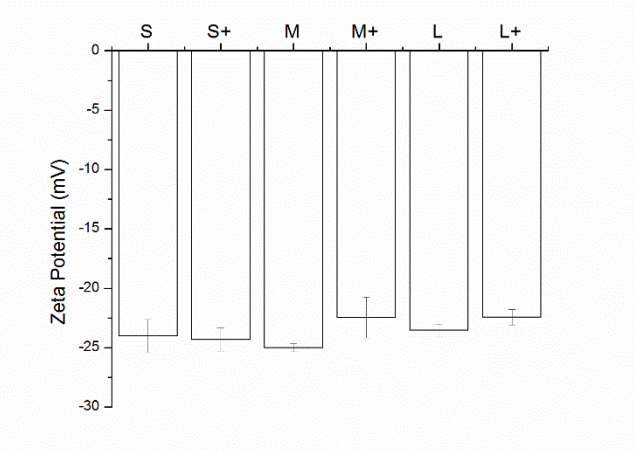

Figure 15. Zeta potential of all protein nanoparticle types measured in 1x PBS, average of three independent replicates.

Table 3. Size, polydispersity (PdI), zeta potential, and yield of protein nanoparticles of different sizes and coatings. Yield was defined as final mass over initial desolvated mass. Since extra mass was adsorbed through the coating step, yield for those particles was higher, and it was possible to exceed 100% yield.

Particle Type	Average Diameter	Average PdI	Zeta Potential (mV)	Yield (%)
Small	277 nm	0.113	-21.7 ± 3.0	79.7 ± 6.0
Small Coated	271 nm	0.094	-21.5 ± 3.5	93.5 ± 7.5
Medium	365 nm	0.116	-21.8 ± 3.5	90.1 ± 3.7
Medium Coated	357 nm	0.135	-20.5 ± 3.0	99.4 ± 21
Large	567 nm	0.055	-22.1 ± 2.7	81.5 ± 3.8
Large Coated	559 nm	0.050	-21.4 ± 2.0	100.3 ± 11

While addition of ethanol to soluble protein is necessary for the desolvation process, the resulting solvent environment can lead to denaturation of some proteins. Given the importance of antigen conformation on the particle surface to trigger pro-immunogenic surface receptor-mediated pathways [11], we added a coating step after particle synthesis. Nanoparticles were resuspended in a solution of soluble OVA in PBS to adsorb antigen to the nanoparticle surface in the absence of desolvent. Successful coating was confirmed by

flow cytometry (Figure 16, left). ELISA with an anti-OVA antibody demonstrated increased antibody binding on the nanoparticle surface after coating (Figure 16, right). Coating the nanoparticles had no effect on particle size or zeta potential (Figure 15, Table 3). Scanning electron micrographs of dried protein nanoparticles demonstrate a roughly spherical morphology and appear to have size distributions smaller than those obtained by DLS in the hydrated state (Figure 17).

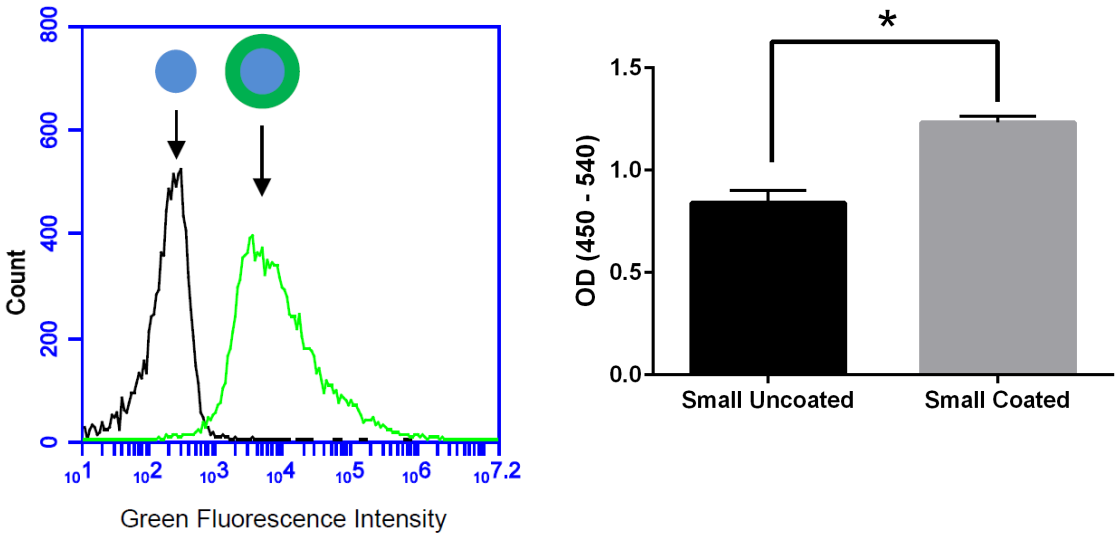

Figure 16. (Left) Fluorescent OVA-coated protein nanoparticles (right trace) had greater fluorescence than uncoated protein nanoparticles (left) as measured by flow cytometry. (Right) Anti-ovalbumin antibody binding was significantly enhanced (*, $p < 0.05$) upon protein nanoparticle coating with OVA.

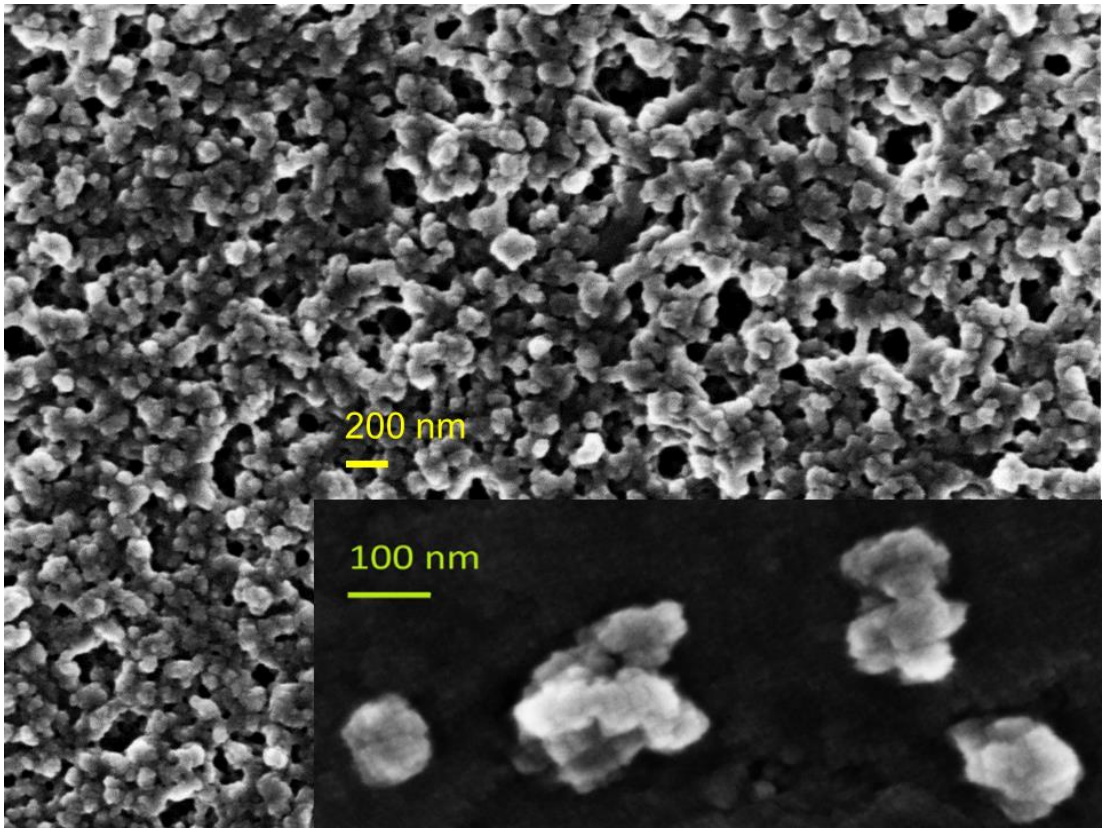

Figure 17. Scanning electron micrographs showing air-dried protein nanoparticles.

3.3.2 Protein Nanoparticle Uptake in Dendritic Cells

Using fluorescent protein nanoparticles and soluble OVA, we tracked antigen uptake in the JAWS II dendritic cell line by flow cytometry. Given the same dose of antigen, cells took up approximately 5-8 times more antigen as protein nanoparticles than the soluble form (Figure 19). Internalization of nanoparticles was confirmed by confocal microscopy (Figure 18). Protein nanoparticle enhancement of antigen uptake relative to soluble protein was greater than any uptake differences among protein nanoparticles of different sizes and coatings (Figure 19).

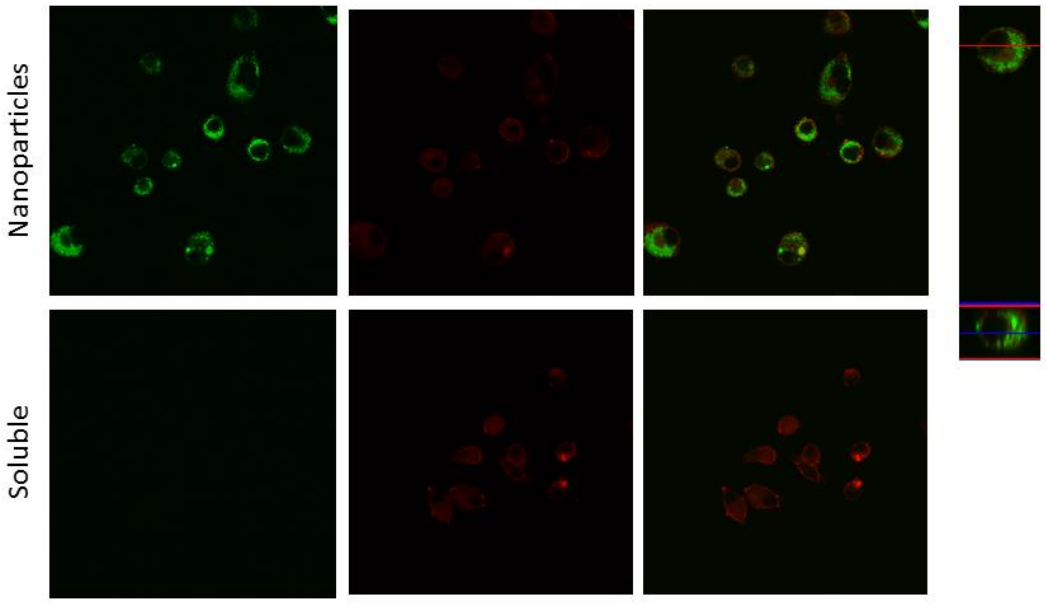

Figure 18. Confocal microscopy was used to image JAWS II dendritic cells with OVA nanoparticles. (First column) Green-fluorescent OVA protein nanoparticles (first row) or soluble OVA protein (second row) were incubated with JAWS II dendritic cells, and the actin cytoskeleton (red, second column) was stained by rhodamine-phalloidin. The merged image (third column) shows antigen associating with dendritic cells, and the z-stack (fourth column), indicates position of antigen with respect to the cell membrane.

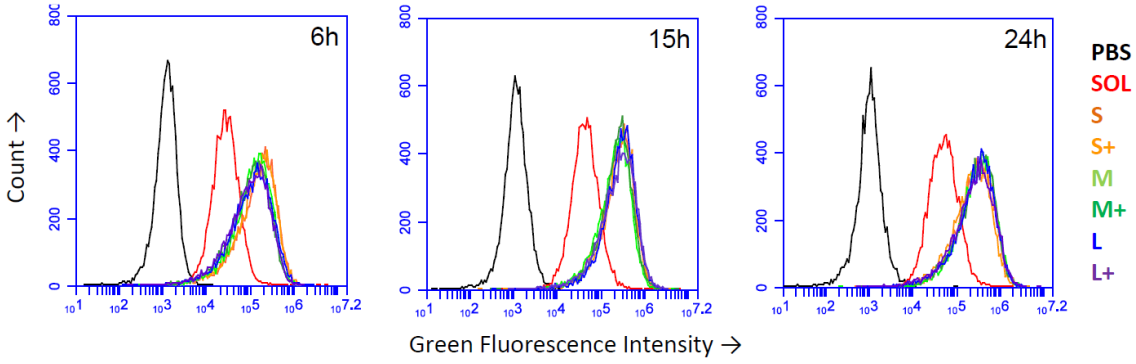

Figure 19. Uptake of OVA protein nanoparticles by JAWS II DCs as measured by flow cytometry after 6 hours, 15 hours, and 24 hours. PBS = PBS-treated cells, SOL = Soluble OVA, S,M,L = Small, Medium, Large, respectively, + = Coated nanoparticles. Traces were consistent across two independent replicates.

3.3.3 OVA Nanoparticles Experience Attenuated Acidification

Upon uptake, endosomal pH was assessed with ratiometric fluorescence[12]. AlexaFluor 647- (a pH-insensitive red fluorophore) and FITC- (a pH-sensitive green fluorophore) conjugated OVA were incorporated into nanoparticles. A standard curve correlating pH to fluorescence ratio was generated by exposing the nanoparticles to pH-adjusted PBS in the presence and absence of cells (Figure 20). While soluble protein was exposed to acidic conditions, all protein nanoparticles experienced attenuated acidification in comparison (Figure 21). No significant differences in pH were observed among protein nanoparticles of different sizes or coatings.

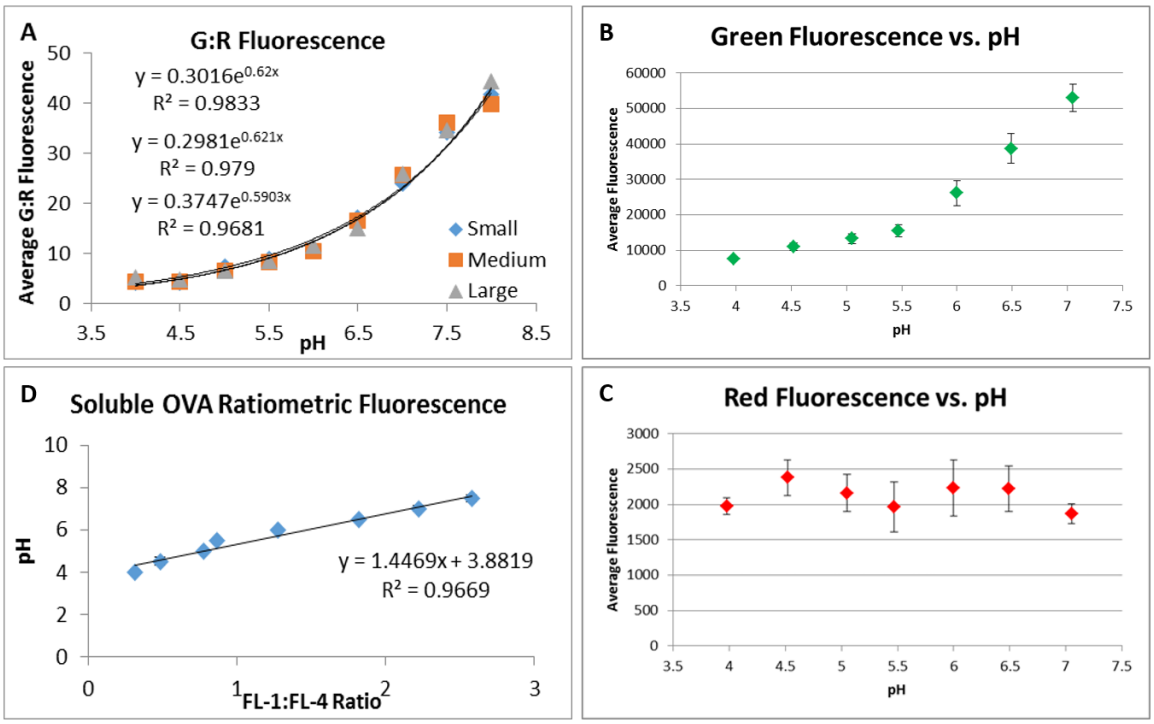

Figure 20. Standard curves of ratiometric fluorescence vs. pH were made from DCs incubated with protein nanoparticles and buffered to various pHs (A). Green fluorescence decreases with pH (B) while red fluorescence does not (C). Standard curve for soluble OVA was measured in DCs by flow cytometry (D).

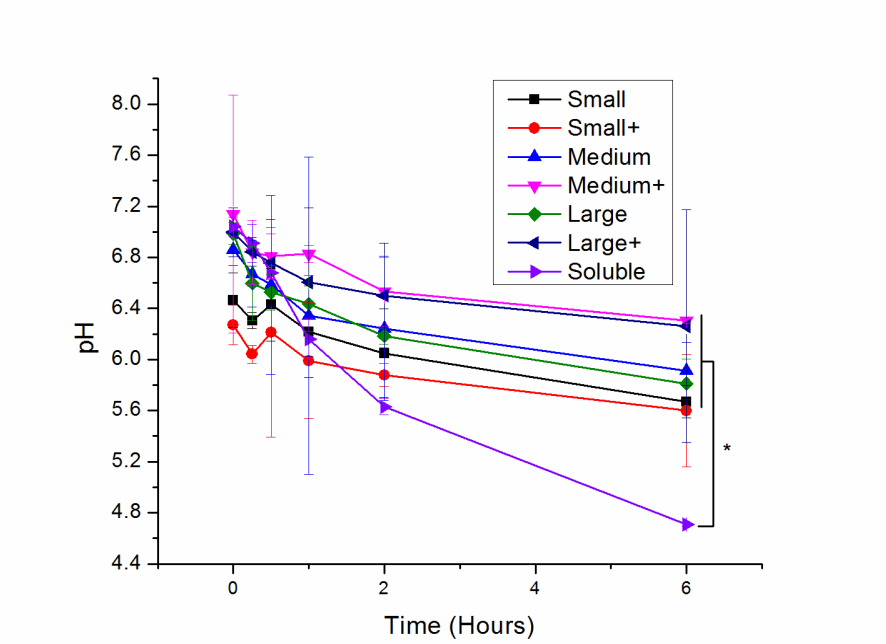

Figure 21. Log-mean pH of red/green protein nanoparticles upon incubation with DCs for various times following a two-hour pulse of nanoparticles. Differences in log-mean pH were significant ($p < 0.05$) between soluble OVA and all nanoparticles except small coated (red circles). Each point is shows an average and standard deviation of three independent replicates (n = 3).

3.3.4 Differences in Uptake Pathways

Uptake inhibitors were used to assess protein nanoparticle uptake routes in JAWS II DCs. Soluble ovalbumin is internalized via clathrin-mediated endocytosis [13], and nanoparticles on the order of 500 nm and larger are internalized primarily through phagocytosis [14], so inhibitors of these two pathways were used to examine uptake route. Chlorpromazine [15] and cytochalasin D [16] were used to inhibit clathrin-mediated uptake and phagocytosis, respectively. Concentration optimization was based on maximizing positive control uptake inhibition and minimizing cytotoxicity. Positive controls were chosen based on evidence for exclusive or predominant uptake by a particular pathway –

transferrin for clathrin-mediated uptake, and 3 µm polystyrene beads for phagocytosis [17, 18]. Uptake inhibition fraction was calculated by the following formula:

$$Uptake\ Inhibition = 1 - \frac{F_{inhib} - F_{auto}}{F_{uninhib} - F_{auto}} \quad (1)$$

Equation 1. Formula used for calculating uptake inhibition of fluorescent OVA or OVA nanoparticles.

Where F_{inhib} and $F_{uninhib}$ are the median fluorescence intensities (MFI) of 10,000 cells in the presence or absence of an uptake inhibitor, respectively, and F_{auto} is the median autofluorescence intensity of 10,000 cells. An uptake inhibition of 1 denotes complete inhibition, while an uptake inhibition of 0 denotes no inhibition. Figure 22 shows uptake inhibition for soluble OVA and OVA nanoparticles. Both soluble OVA and OVA protein nanoparticle uptake were strongly inhibited by chlorpromazine, and differences in inhibition were not significant ($p > 0.05$). Cytochalasin D strongly inhibited soluble OVA uptake, but inhibited OVA nanoparticle uptake to a significantly lesser degree ($p < 0.05$). No significant differences in uptake inhibition ($p > 0.05$) were observed among protein nanoparticle types.

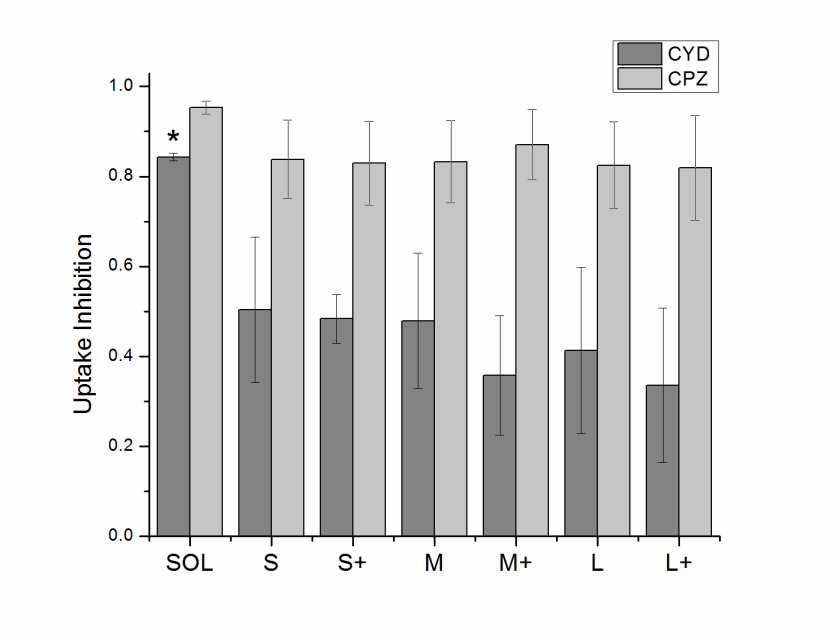

Figure 22. Uptake inhibition of fluorescent protein nanoparticles was determined by flow cytometry and normalized by Equation 2. Cytochalasin D = CYD, Chlorpromazine = CPZ. Soluble OVA uptake was inhibited by CYD to a significantly greater degree than any protein nanoparticles were (*, $p < 0.05$). CPZ inhibited uptake of nanoparticulate and soluble OVA to a similar degree. Bars show average and standard deviation of three independent replicates (n = 3).

3.3.5 OVA Nanoparticles Trigger DC Maturation and Fc Receptor Upregulation

DC upregulation of the maturation marker CD86 was assessed by flow cytometry after stimulation with protein nanoparticles (Figure 23). Isotype controls were used to differentiate between upregulation of CD86 and Fc receptors upon stimulation. Protein nanoparticles trigger upregulation of CD86, with small, uncoated protein nanoparticles causing the greatest upregulation (Figure 23). However, OVA protein nanoparticles also induce upregulation of Fc receptors, which is not observed in response to soluble OVA or the lipopolysaccharide positive control.

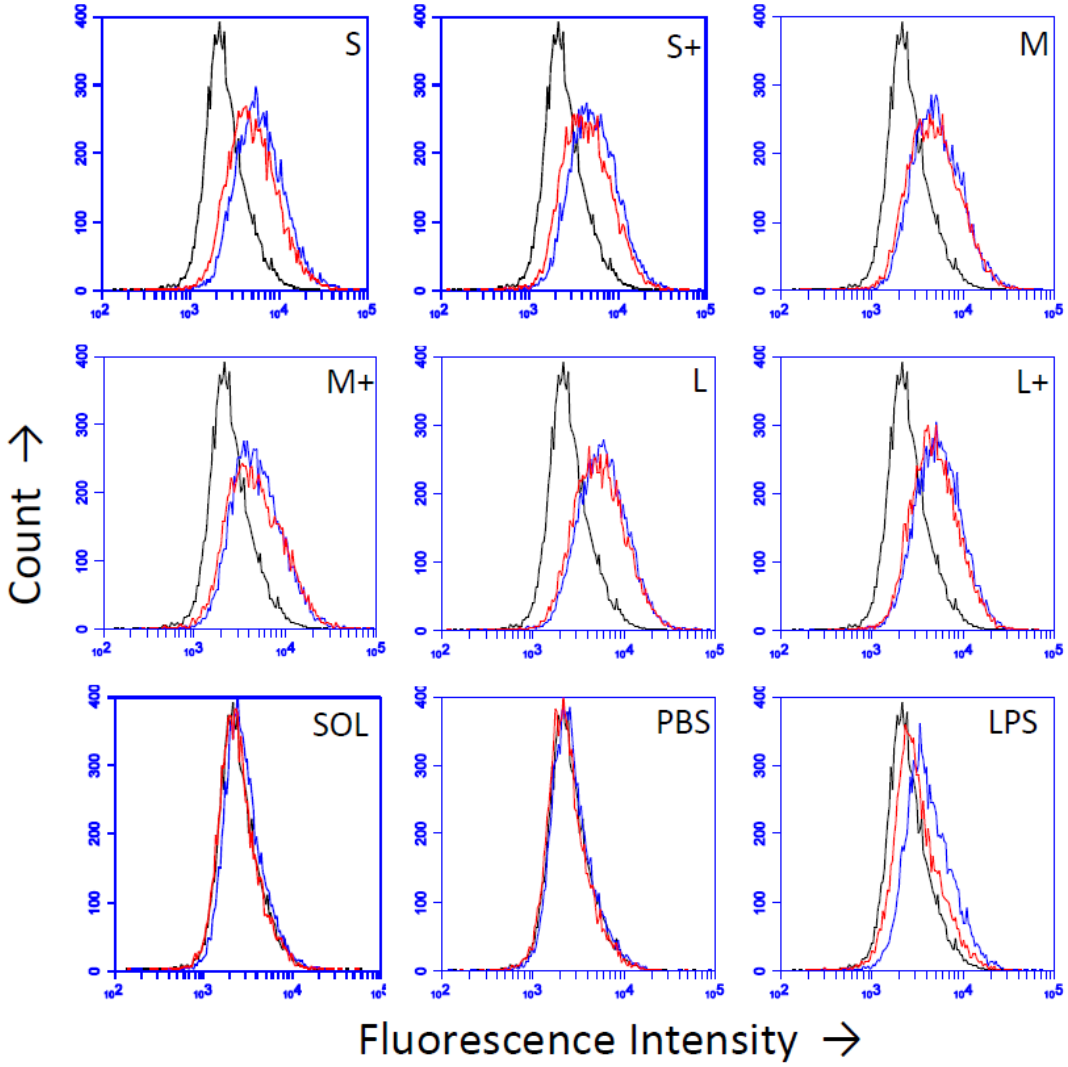

Figure 23. DC CD86 upregulation 24 hours post-protein nanoparticle treatment was assessed by flow cytometry. Black = unstained control, Red = isotype control, Blue = CD86. Traces are representative of three independent replicates.

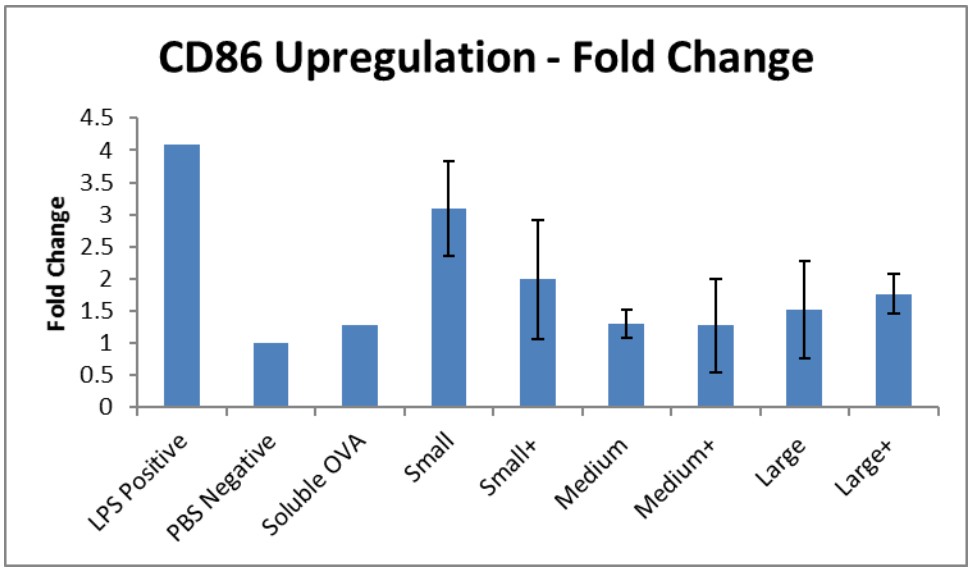

Figure 24. DC CD86 upregulation 24 hours post-nanoparticle treatment, quantified as a fold-increase in (CD86 - Isotype) expression normalized to the PBS control group (CD86 - Isotype) expression. Error bars represent standard deviations of 3 independent pairs of CD86/Isotype measurements.

3.3.6 Inflammatory Cytokine Production is Nanoparticle Size- and Coating-Dependent

Production of the pro-inflammatory cytokines TNF-α in JAWS dendritic cells and IL-1β in BMDCs was examined after protein nanoparticle and soluble OVA stimulation. IL-1β production was observed in response to soluble OVA and protein nanoparticles, but only small and medium coated protein nanoparticles induced greater upregulation than soluble OVA (Figure 26). Large nanoparticles did not trigger an enhanced IL-1β response regardless of coating. Conversely, TNF-α production in response to protein nanoparticles was lower than that of soluble OVA (Figure 25). Coating protein nanoparticles with additional OVA led to increases in the DC TNF-α responses to medium and large, but not small, protein nanoparticles. Although medium coated nanoparticles triggered the highest levels of TNF-α, they did not reach the levels of TNF-α induced by soluble OVA.

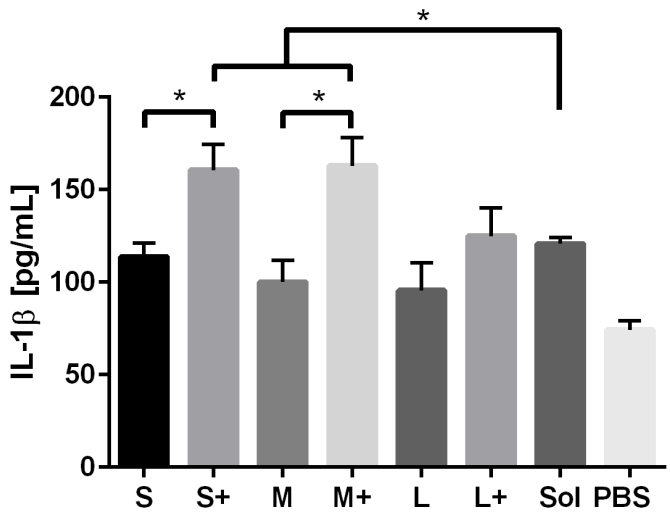

Figure 26. IL-1β production in response to protein nanoparticles was assessed by ELISA. Sol = Soluble OVA treatment, PBS = Negative control. Standard deviations are of three independent replicates.

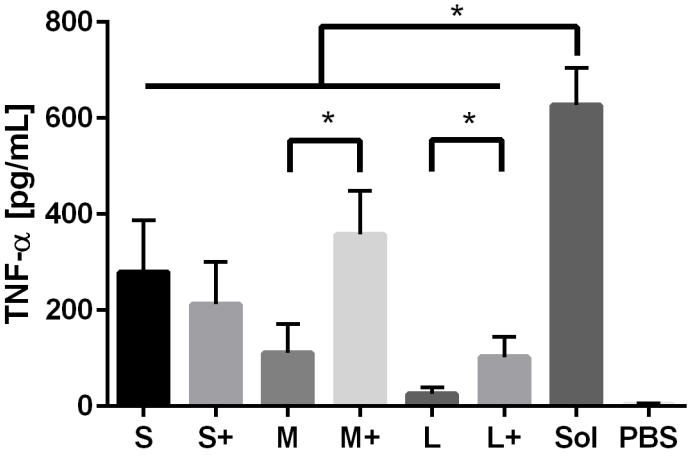

Figure 25. TNF-α production in response to protein nanoparticles was assessed by ELISA. Sol = Soluble OVA treatment, PBS = Negative control. Averages and standard deviations are of three batches of protein nanoparticles, each replicated three times (n = 9).

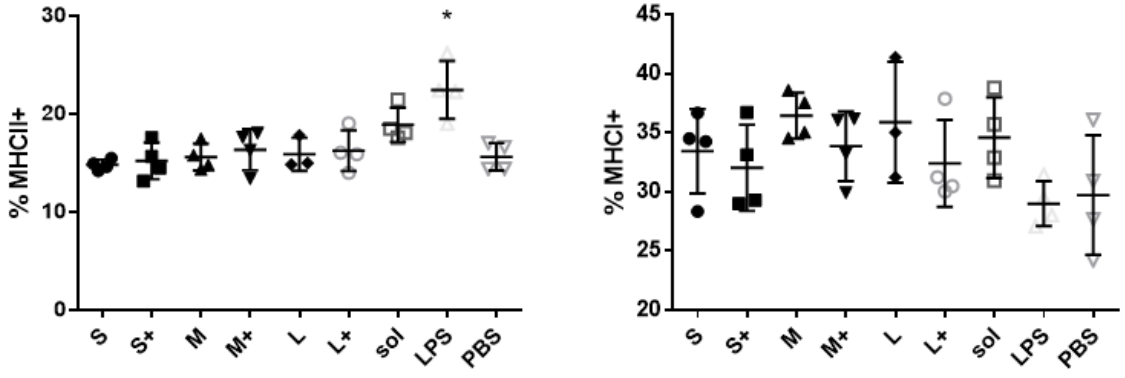

Figure 27. MHC II (left) and MHCI (right) upregulation by BMDCs in response to OVA protein nanoparticles, soluble OVA (sol), soluble OVA + 1 µg/mL LPS (LPS), or PBS control. Data is represented as % of cells that are MHC "positive", or having a fluorescence intensity above a cutoff threshold. Each data point was derived from 10,000 cells analyzed.

3.3.7 Protein Nanoparticles do not Enhance MHC I and MHC II Presentation

Upregulation of MHC II or MHC I-SIINFEKL was assessed by flow cytometry, and the percentages of cells expressing high levels of MHC II or MHC I-SIINFEKL are reported in Figure 27. No significant differences in MHC I-SIINFEKL expression were observed across any groups (right). LPS-treated BMDCs expressed significantly higher levels of MHC II than OVA protein nanoparticle types and PBS (left). No significant differences between protein nanoparticles, soluble OVA, and PBS were observed. Our observations of humoral responses generated to protein nanoparticles in previous *in vivo* studies appears contradictory to the lack of MHC II presentation observed here, although the display of MHC II on LPS-stimulated BMDCs could suggest that different timescales of MHC II presentation are relevant for different types of adjuvants.

3.3.8 3HA Nanoparticles Enhance Germinal Center B Cell Populations

Ten days after immunization, mice given 3HA nanoparticles, 3HA soluble protein, or PBS were sacrificed. Their draining lymph nodes and spleens were homogenized and stained for CD95 and GL7, markers of active germinal center B cells [19, 20]. Mice given nanoparticles showed elevated numbers of germinal center B cells as compared to mice immunized with soluble protein or PBS (Figure 28). Germinal center B cell responses in the spleen showed significantly higher numbers in mice treated with nanoparticles in comparison to PBS-immunized mice (Figure 28).

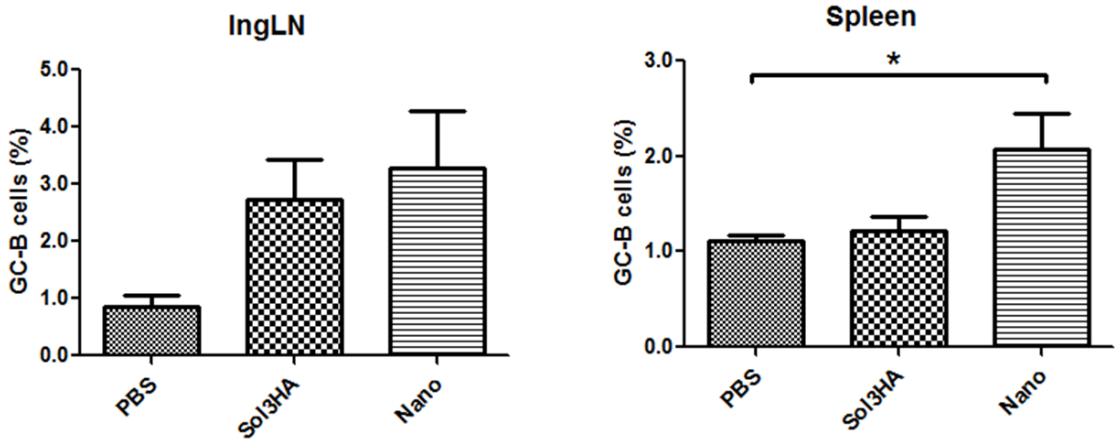

Figure 28. Cells from draining lymph nodes (IngLN) and spleens were stained for CD95$^+$/GL7$^+$ B cells (GC-B cells). Bars represent percentages of positive cells, error bars represent standard deviation of 5 mouse organs. (Courtesy of Dr. Jong Rok Kim)

3.3.9 Nanoparticles and Soluble Protein Drain the Injection Site at Similar Rates

Fluorescent 3HA nanoparticles or soluble protein were injected intra-muscularly into mice and fluorescence distribution monitored over 8 days. Figure 29 shows representative fluorescent images of mice taken at Day 0 and Day 4, with the green circle showing representative areas used to quantify injection site (muscle) fluorescence across images. Over the first 24 hours, soluble protein showed a stronger loss in fluorescence than nanoparticles did (Figure 30, Figure 32). Soluble and nanoparticle injection site fluorescence decay between days 1 and 8 followed roughly the same rate (Figure 30).

3.3.10 Nanoparticles are Retained in the Spleen Better than Soluble Protein

Two mice were sacrificed on day 4 and three mice on day 8 for *ex vivo* lymphatic organ imaging. No fluorescence was detected in the spleen or lymph nodes on either day (Figure 31). Nanoparticle fluorescence in the spleen was elevated on Day 8 in comparison to soluble protein, and was significantly more fluorescent the spleens of mice immunized with PBS (Figure 31, Figure 33).

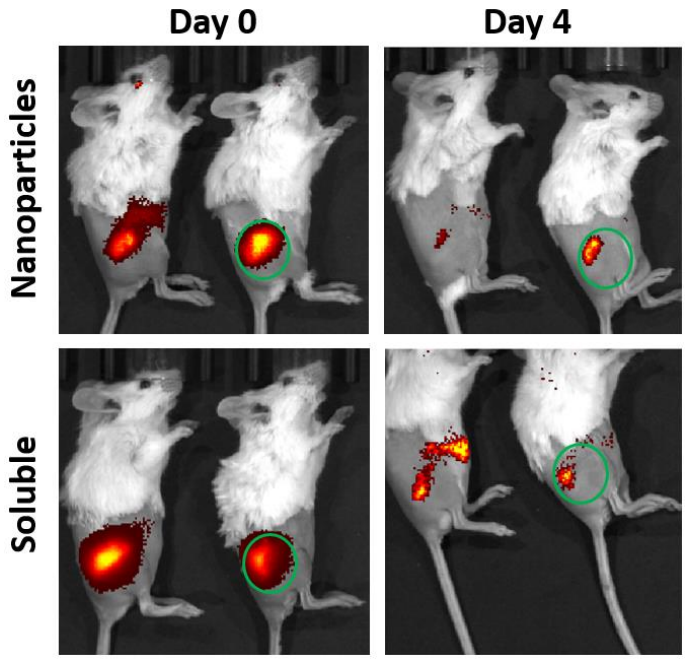

Figure 29. 3HA nanoparticles and soluble fluorescent 3HA visualized immediately after injection and 4 days after injection. The green circle in the figures show representative areas that were used for fluorescence quantification.

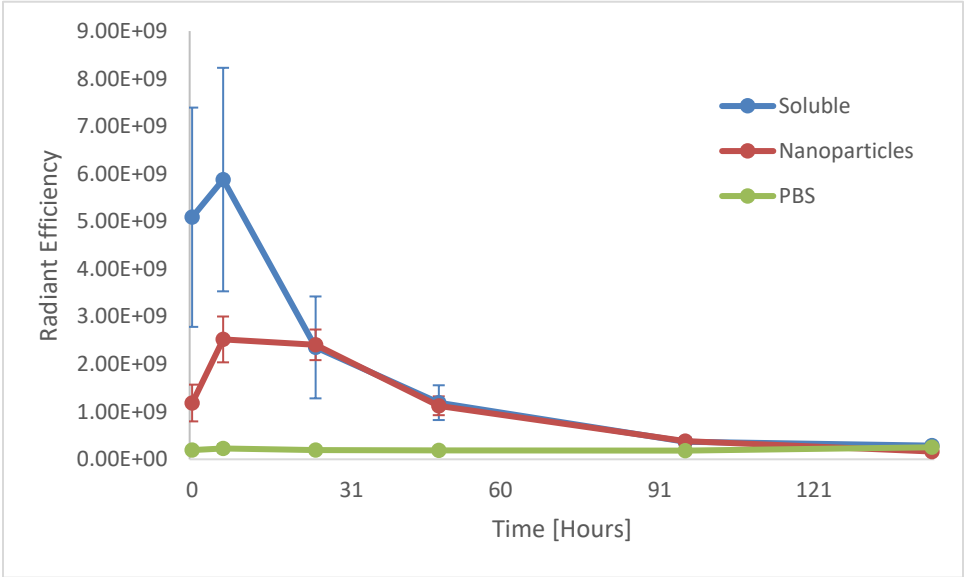

Figure 30. Quantification of fluorescence at injection site. Lateral images of mice injected with fluorescent soluble 3HA, 3HA nanoparticles, or PBS had their right leg fluorescent radiant efficiency quantified with the LivingImage software, and the fluorescence was tracked over the course of 6 days. Error bars represent the standard deviation of five mice.

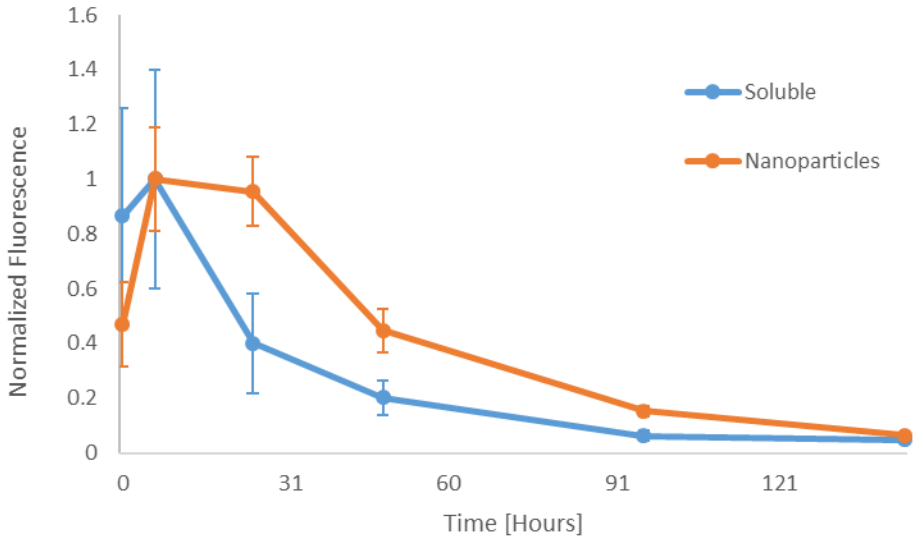

Figure 32. Quantification of fluorescence in Figure 30, normalized to the highest observed at 6 hours. Error bars represent the coefficient of variance (SD/σ) normalized by the average fluorescence at each point.

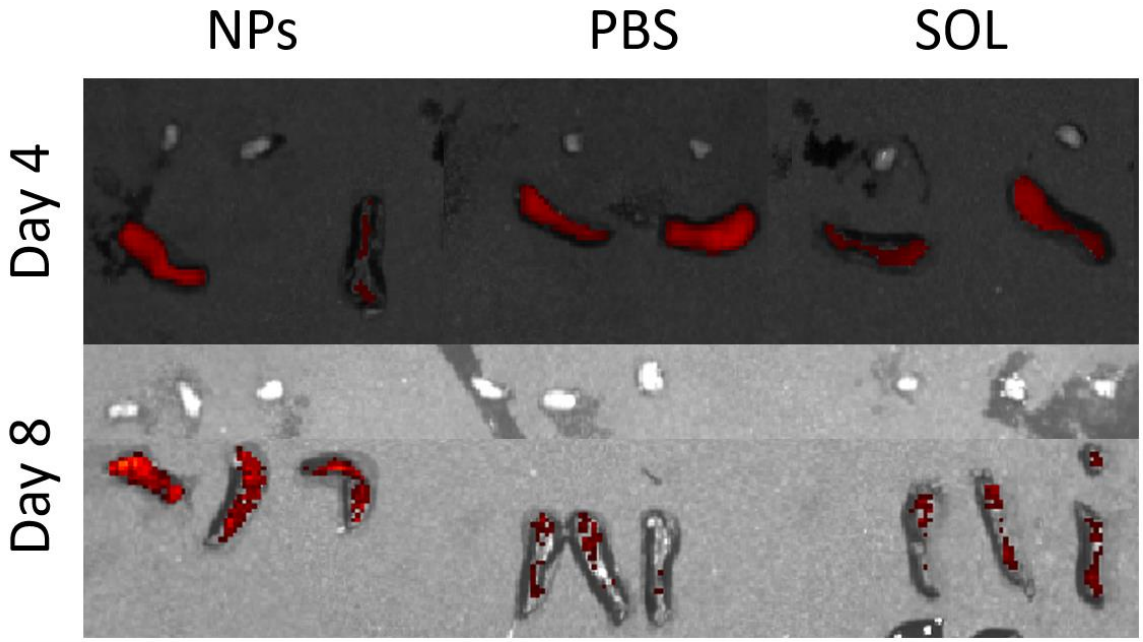

Figure 31. Draining inguinal lymph nodes (top row) and spleens (bottom row) were taken from sacrificed mice at days 4 and 8.

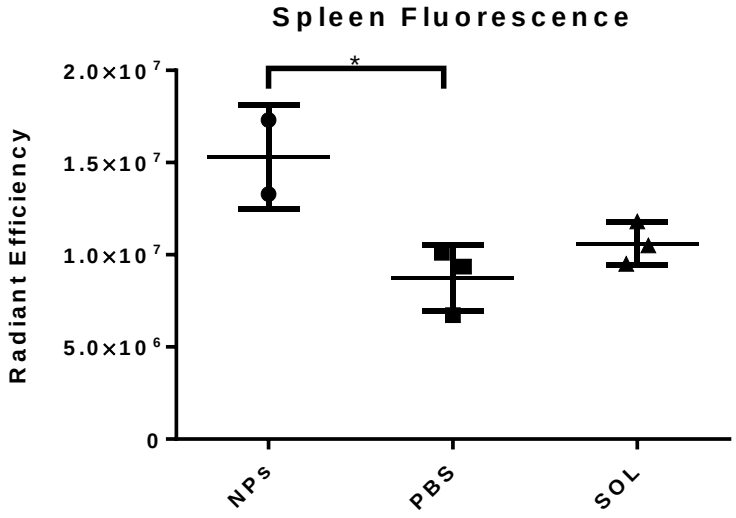

Figure 33. Spleens from Day 8 (bottom row of Figure 31) had their fluorescence quantified by the LivingImage software. One spleen from the NP group was excluded from quantification, as its bent shape obscured part of the fluorescence. Error bars represent standard deviation among the groups. * = $p < 0.05$

3.4 Discussion

Current nanoparticle vaccine research seeks to leverage the encapsulating biomaterial properties to enhance immunogenic responses to component antigens. Protein nanoparticles, made entirely from crosslinked antigen, demonstrate that altering the presentation of protein antigens from a soluble to a nanoparticulate form is sufficient for enhancing vaccine adjuvancy. Our prior work showed that protein nanoparticles made from influenza proteins enhanced antigen immunogenicity and immune protection [1]. Our hypothesis that differences in dendritic cell processing of nanoparticulate and soluble antigen led to the different *in vivo* immune responses motivated the present studies. We examined the differences between soluble OVA and OVA protein nanoparticles and the role of two fundamental protein nanoparticle properties, size and coating, in enhancing DC

responses, as well as the *in vivo* differences in biodistribution and GC-B cell proliferation in response to nanoparticulate and soluble 3HA.

3.4.1 Initial Protein Nanoparticle Uptake and Processing is Size- and Coating-Independent

Initial DC uptake and processing was similar among OVA protein nanoparticles of different sizes and coatings. Protein nanoparticles greatly enhanced antigen uptake over soluble antigen (Figure 19), which has been seen for other types of nanoparticles with other cell types as well [10, 21]. However, protein nanoparticle size and coating did not significantly affect antigen internalization in the size range tested. While some studies found a negative correlation between particle size and uptake [12, 22], the size range over which uptake differences were observed spanned 50 nm to 3 μm. Still other work saw no influence of size on uptake within this wide size range [23], emphasizing the importance of nanoparticle material on uptake trends.

Chlorpromazine inhibited uptake of soluble OVA and protein nanoparticles by approximately 90%, indicating clathrin-mediated uptake of both soluble and protein nanoparticle forms of OVA. Since soluble OVA is known to undergo clathrin-mediated uptake through the mannose receptor [13], the mannose receptor could be involved in OVA protein nanoparticle uptake as well. The comparable uptake of coated and uncoated protein nanoparticles is consistent with mannose receptor-mediated uptake, since glyco-antigens present in OVA would be accessible on either the coated or uncoated protein nanoparticles. Similar to our findings of coating-independent degree of uptake, a study by Thomann-

Harwood et al. found coating alginate nanoparticles with mannan, a polysaccharide that shares a receptor with OVA, had no effect on particle uptake [4].

Treatment of DCs with cytochalasin D reduced protein nanoparticle uptake by roughly 50%, but reduced soluble OVA uptake by more than 80%. Given the strong inhibition of cytochalasin D on soluble OVA uptake, it was surprising to see protein nanoparticles still taken up despite cytochalasin D treatment. This phenomenon could be explained by the role of actin in clathrin-mediated endocytosis. Actin depolymerization with cytochalasin D treatment is a common strategy for inhibiting phagocytosis [16], but cytochalasin D cannot completely depolymerize F-actin associated with clathrin-coated structures[24]. Clathrin-coated vesicle formation from the plasma membrane requires actin polymerization proportional to the maximum circumference of the object being internalized [24]. By comparing antigen volume to circumference ratios for spherical soluble proteins and protein nanoparticles, we find that nanoparticle uptake requires much less actin polymerization than soluble antigen uptake for the same amount of antigen (Equation 2).

$$\frac{\frac{V_{PNP}}{C_{PNP}}}{\frac{V_{sol}}{C_{sol}}} = \frac{r_{PNP}^2}{r_{sol}^2} = \frac{150\ nm^2}{5\ nm^2} = 900 \qquad (2)$$

Equation 2. Volume to circumference ratios of nanoparticles are much greater than those of soluble proteins, suggesting nanoparticles deliver more antigen to DCs than soluble protein does for a given amount of actin polymerization.

Given partial inhibition of clathrin-mediated uptake by cytochalasin D, the preceding observation could explain efficient inhibition of soluble OVA uptake but less efficient inhibition of OVA protein nanoparticle uptake. As with other experiments using endocytosis inhibitors, we cannot discount the impact of off-target effects, including potential compensatory upregulation of other endocytic mechanisms in response to cytochalasin D or chlorpromazine treatment.

Upon antigen internalization, DCs acidified soluble OVA to a significantly greater extent than OVA protein nanoparticles. Although uptake inhibition data suggest a common uptake mechanism for soluble OVA and OVA protein nanoparticles, the attenuated acidification of protein nanoparticles as compared to soluble OVA suggests different internal routing for protein nanoparticles and soluble antigen. Our data is also consistent with lysosomal colocalization studies that show antigen in nanoparticle cores can achieve cytosolic delivery, while soluble or nanoparticle-adsorbed antigen cannot [25], although confocal microscopy studies assessing Lysotracker colocalization with fluorescent protein nanoparticles would be needed to confirm this hypothesis. The pH 4.7 experienced by soluble OVA is characteristic of endosomal fusion with lysosomes, a process promoting proteolytic antigen degradation [26]. Attenuated acidification is known to protect antigens from rapid degradation and lead to enhanced cross-presentation of MHC Class I-restricted antigen peptides [12, 27]. Cross presentation of exogenous antigen on MHC I by dendritic cells is necessary for $CD8^+$ T cell responses, which are essential for providing immunity against intracellular bacterial and viral infections and cancerous host cells [28]. Our data showing attenuated protein nanoparticle acidification allows the possibility of endosomal

escape of some internalized protein nanoparticles, a phenomenon that would be consistent with the elevated IL-1β levels observed in response to protein nanoparticle treatment [29].

3.4.2 Inflammatory Cytokine Secretion is Size- and Coating-Dependent

IL-1β is known to originate from activation of the inflammasome, a heterotrimeric enzyme complex assembled in response to internalization of certain types of particulate antigens [30]. IL-1β-production from inflammasome activation allows for the rapid cleavage of pro-inflammatory cytokines into their active form, triggering a local, innate immune response [5]. The NLRP3 inflammasome is the only one that does not have a specific ligand associated with it [31], and is implicated in nanoparticle-mediated inflammasome activation [30]. Not all nanoparticles can trigger inflammasome activation [30, 31]. Alum [32], silica [29], LPS-coated PLGA [33] and textured polymeric [34] particles have all been shown to trigger inflammasome activation, while uncoated PLGA particles [33] and lipid cubosomes [30] cannot. Recently, soluble ovalbumin was found to activate the inflammasome in a murine model [35], and our stimulation of BMDCs confirms this. Additionally, we see enhanced production of IL-1β in response to small and medium coated protein nanoparticles over large nanoparticles and soluble OVA. This suggests protein nanoparticle activation of the inflammasome is enhanced by small size and repeated surface antigen display, consistent with a viral-mimetic design strategy [36]. Our findings also demonstrate IL-1β production by BMDCs in the absence of pretreatment with LPS or other stimuli, a step commonly used for *in vitro* inflammasome activation, but known to bias the resulting inflammatory response [31].

TNF-α enhances local inflammatory responses through activation of the NF-κB pathway in multiple cell types [37]. In addition, it directs DCs to begin maturation and migration to lymph nodes[5]. Given the strong IL-1β responses observed, it was surprising to see DC TNF-α responses to protein nanoparticles lower than soluble OVA. The patterns for TNF-α and IL-1β production are distinct from one another, suggesting different mechanisms of activation despite an overlap in signaling pathways and downstream targets [38, 39]. Studies suggest while both molecules are pro-inflammatory cytokines, only TNF-α can act as a chemokine for recruiting innate immune cells to the site of inflammation, which could explain the lower baseline observed for TNF-α secretion than that of IL-1β [39].Given soluble OVA's inherent inflammasome-stimulating capabilities, it is possible that epitopes responsible for inflammasome activation also trigger TNF-α production. This would be consistent with our results showing enhanced TNF-α production in response to protein nanoparticle coating for medium and large particles, but does not explain why coating small OVA protein nanoparticles does not enhance TNF-α production. Furthermore, our findings that small coated 3HA nanoparticles trigger more TNF-α than uncoated 3HA nanoparticles also suggest an antigen-dependence to protein nanoparticle-induced TNF-α (Figure 3). Overall, the discrepancy in TNF-α responses between OVA and 3HA nanoparticles and soluble protein also supports the claim that TNF-α signaling is not characteristic of all types of nanoparticle-mediated adjuvancy [40]. Although TNF-α is known to enhance monocyte and neutrophil extravasation at the site of inflammation [5], its role in promoting immunity following vaccination remains to be fully elucidated.

DC responses to coated protein nanoparticles may be component-antigen dependent. Given the lack of pathogen-associated molecular patterns (PAMPs) or DC-

specific epitopes on ovalbumin, however, the enhanced inflammatory responses seen to coated OVA nanoparticles may be due to proteins other than OVA. Serum protein adsorption to nanoparticles *in vitro* and *in vivo* is ubiquitous and dependent on nanoparticle surface properties [41]. We found OVA-coated OVA protein nanoparticles bind less BSA, a representative serum protein, than uncoated OVA protein nanoparticles do (Figure 34). The protein corona on nanoparticles has been shown to remain attached during cellular uptake[42], and the uptake of non-immunogenic serum proteins on the protein nanoparticles may explain the attenuated DC inflammation observed. *In vivo*, the protein corona may have immunostimulatory effects if complement or immunoglobulin is adsorbed, and engineering vaccine nanomaterials to preferentially adsorb these proteins is an active area of research [43].

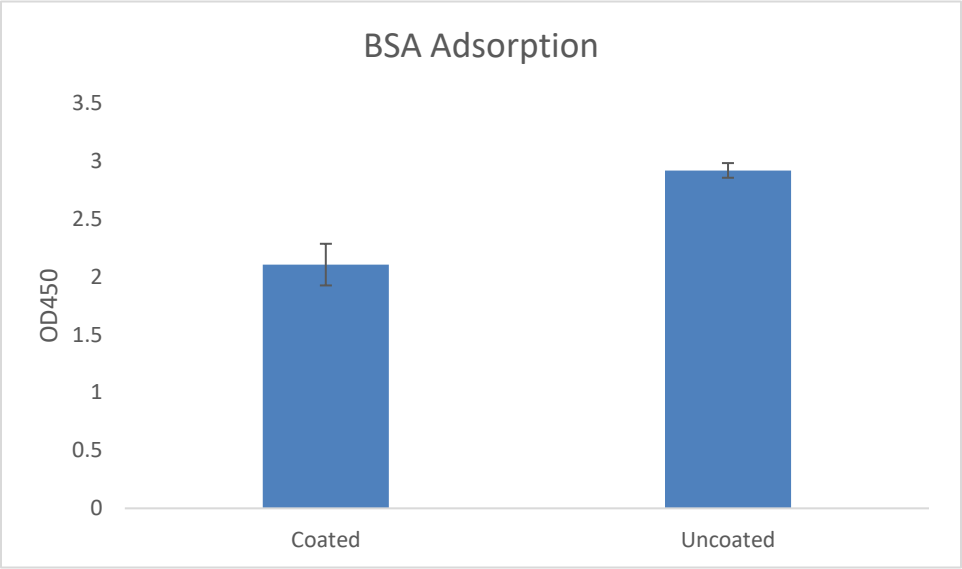

Figure 34. Small coated and uncoated OVA nanoparticles were incubated in 10 mg/mL BSA for 2 hours, collected by centrifugation, and crosslinked as described in Table S1. Nanoparticles were then assessed for BSA presence via ELISA. Uncoated OVA nanoparticles adsorbed significantly more BSA than OVA-coated OVA nanoparticles did (p = 0.02, n = 2 per group).

While coating protein nanoparticles generally enhances DC inflammatory responses, we see deviations from this trend at small sizes for TNF-α. In general, cytokine responses are enhanced in response to coated and smaller-sized protein nanoparticles, although the enhancement in response to coating is greater than that of decreasing size. Therefore, we believe particle size plays a lesser role in inflammatory cytokine production than particle coating.

3.4.3 DC Maturation

All protein nanoparticle types led to slight CD86 upregulation, indicative of DC maturation, a process necessary for successful antigen presentation. DC maturation markers, including CD86 as well as CD80 and CD40, have been upregulated in response to other types of nanoparticles [23]; and while small and small coated protein nanoparticles qualitatively appeared to upregulate CD86 the most compared to soluble (Figure 23), large distributions of maturation marker expression make quantitative comparisons of upregulation difficult. Although protective humoral and cell-mediated immune responses have been observed in response to M2e and hemagglutinin protein nanoparticles (Figure 7) [1, 2], we were unable to observe significant MHC II upregulation in BMDCs after 24 hours of protein nanoparticle stimulation (Figure 27). This discrepancy, coupled with the observed upregulation of MHC II in response to soluble OVA + LPS, suggests that different adjuvants trigger different rates of MHC II upregulation and antigen presentation. Increases in isotype control fluorescence indicate Fc receptor upregulation in response to protein nanoparticle stimulation of DCs, but not in response to soluble OVA or to the positive control LPS. To our knowledge, this is the first time FcR upregulation has been observed in response to nanoparticle stimulation. While FcR-targeted nanoparticle

vaccines are being studied [44], further investigation into the upregulation phenomenon is required to determine if there is a synergistic effect between nanoparticle- and opsonization-mediated adjuvancy.

3.4.4 Biodistribution and the Importance of Germinal Centers

In vivo, the ability of hemagglutinin protein nanoparticles to induce germinal center formation is crucial for providing protective immunity, and corroborates the *in vitro* correlates of inflammation and maturation we observed with DCs. The ability of nanoparticle vaccines such as liposomes, polymeric particles, and micelles to induce germinal center formation has been previously documented [45-47]. Though some groups have found soluble antigen is unable to trigger germinal center formation [45], we cannot exclude that possibility with soluble 3HA, as elevated levels of LN GC-B cells were still detected in comparison to PBS.

The elevated numbers of GC-B cells found in the spleens of mice immunized with nanoparticles correlates with the significant level of antigen retention found in the spleen as well (Figure 28, Figure 33). While literature suggests spleen-resident follicular dendritic cells are associated with this antigen and responsible for the germinal center response[5], flow cytometry or immunohistochemical staining would be needed to confirm this hypothesis. Overall, the higher retention of nanoparticulate over soluble antigen in the spleens of immunized mice, coupled with increased germinal center B cells in nanoparticle-

immunized mice allude to splenic antigen retention as a key component of the mechanism linking nanoparticulate antigen to enhanced immune responses.

Injection site drainage rates were similar between nanoparticle and soluble 3HA between 1 and 8 days. Although an initial loss of soluble 3HA was observed over the first 24 hours, the amount of antigen persisting at the injection site was the same afterwards, suggesting uneven starting doses of antigen. Although antigen persistence at the injection site has traditionally been a goal of controlled-release vaccine therapeutics [48, 49], recent studies suggest that extended persistence of antigen at an injection site can lead to T cell dysfunction or deletion [50]. The clearance of our nanoparticles from the site of injection is a promising sign that our vaccine will not trigger adverse consequences associated with persistence, and precludes injection site retention from being a mechanism of protein nanoparticle adjuvancy.

3.5 Conclusion

In this chapter, we have examined differences in dendritic cell responses to OVA protein nanoparticles of different sizes and coatings, as well as *in vivo* biodistribution and germinal center formation in response to 3HA protein nanoparticles. Our *in vitro* data show that protein nanoparticles enhance antigen uptake in DCs, yet enhanced antigen delivery alone does not lead to an across-the-board increase in DC inflammation. The observation that protein nanoparticles experience attenuated endosomal acidification in comparison to soluble antigen supports the hypothesis of protein nanoparticles enhancing antigen cross-presentation, which was also supported by the successful immunization of mice with M2e peptide protein nanoparticles [1]. Our incorporation of the full-length proteins OVA and

hemagglutinin [2] into protein nanoparticles suggests that multiple types of protein antigens can be incorporated into immunogenic protein nanoparticles. While readouts of protein nanoparticle uptake, uptake mechanism, and intracellular pH are independent of nanoparticle type, markers of inflammation are dependent on size and coating. Protein nanoparticles between 270-350 nm in diameter trigger greater inflammatory responses than 560 nm particles, highlighting the importance of small sizes in protein nanoparticle design. Our data suggest a separation of initial antigen uptake and processing from downstream inflammatory outputs. On a fundamental level, this would imply that size- and coating-mediated nanoparticle adjuvancy does not occur at the point of internalization. Consequently, nanoparticle size can play a complementary role to membrane receptor-mediated adjuvants (i.e. TLR ligands) on the nanoparticle surface for optimal DC responses. In examining these responses, the observed decoupling of TNF-α and IL-1β production in response to soluble or nanoparticulate OVA underscores the importance of identifying *in vitro* inflammatory correlates to successful *in vivo* immunization. The observed IL-1β responses also implicate activation of the inflammasome in response to protein nanoparticles, supporting other work showing non-crystalline adjuvant nanoparticles can activate the inflammasome [33].

Our *in vivo* data implicate splenic antigen retention and germinal center formation in the mechanism of protein nanoparticle adjuvancy. Taken together, these results suggest that coatings on vaccine nanoparticles should be directed toward activating specific responses rather than only enhancing cellular uptake, and that adjuvant receptor targets on spleen-resident immune cells are of particular importance. We explore this idea further

with immunoglobulin-mediated adjuvancy and Fc-receptor targeting of protein nanoparticles in Chapter 5.

REFERENCES

[1] L. Wang, A. Hess, T.Z. Chang, Y.C. Wang, J.A. Champion, R.W. Compans, B.Z. Wang, Nanoclusters self-assembled from conformation-stabilized influenza M2e as broadly cross-protective influenza vaccines, Nanomed-Nanotechnol 10(2) (2014) 473-482.

[2] T.Z.C. Li Wang, Yuan He, Jong R. Kim, Shelly Wang, Teena Mohan, Zachary Berman, Mark S. Tompkins, Ralph A. Tripp, Richard W. Compans, Julie A. Champion, Bao-Zhong Wang, Coated protein nanoclusters from recombinant trimeric H7N9 HA are highly immunogenic to induce immune protection and long-lasting humoral immunity, Nanomedicine-Uk Submitted (2016).

[3] T. Fifis, A. Gamvrellis, B. Crimeen-Irwin, G.A. Pietersz, J. Li, P.L. Mottram, I.F.C. McKenzie, M. Plebanski, Size-dependent immunogenicity: Therapeutic and protective properties of nano-vaccines against tumors, J Immunol 173(5) (2004) 3148-3154.

[4] L.J. Thomann-Harwood, P. Kaeuper, N. Rossi, P. Milona, B. Herrmann, K.C. McCullough, Nanogel vaccines targeting dendritic cells: Contributions of the surface decoration and vaccine cargo on cell targeting and activation, J Control Release 166(2) (2013) 95-105.

[5] K. Murphy, P. Travers, M. Walport, C. Janeway, Janeway's immunobiology, Garland Science, New York, 2012.

[6] V. Manolova, A. Flace, M. Bauer, K. Schwarz, P. Saudan, M.F. Bachmann, Nanoparticles target distinct dendritic cell populations according to their size, Eur J Immunol 38(5) (2008) 1404-1413.

[7] S.T. Reddy, A.J. van der Vlies, E. Simeoni, V. Angeli, G.J. Randolph, C.P. O'Neil, L.K. Lee, M.A. Swartz, J.A. Hubbell, Exploiting lymphatic transport and complement activation in nanoparticle vaccines, Nat Biotech 25(10) (2007) 1159-1164.

[8] P. Pradhan, H. Qin, J.A. Leleux, D. Gwak, I. Sakamaki, L.W. Kwak, K. Roy, The effect of combined IL10 siRNA and CpG ODN as pathogenmimicking microparticles on Th1/Th2 cytokine balance in dendritic cells and protective immunity against B cell lymphoma, Biomaterials 35(21) (2014) 5491-5504.

[9] Y. Inoue, K. Izawa, S. Kiryu, A. Tojo, K. Ohtomo, Diet and abdominal autofluorescence detected by in vivo fluorescence imaging of living mice, Mol Imaging 7(1) (2008) 21-27.

[10] L.H. Estrada, S. Chu, J.A. Champion, Protein nanoparticles for intracellular delivery of therapeutic enzymes, J Pharm Sci-Us 103(6) (2014) 1863-71.

[11] C.L. Chu, Y.L. Yu, Y.C. Kung, P.Y. Liao, K.J. Liu, Y.T. Tseng, Y.C. Lin, S.S.Y. Hsieh, P.C.S. Chong, C.Y. Yang, The Immunomodulatory Activity of Meningococcal Lipoprotein Ag473 Depends on the Conformation Made up of the Lipid and Protein Moieties, Plos One 7(7) (2012).

[12] K.K. Tran, H. Shen, The role of phagosomal pH on the size-dependent efficiency of cross-presentation by dendritic cells, Biomaterials 30(7) (2009) 1356-1362.

[13] S.E. Autenrieth, I.B. Autenrieth, Variable antigen uptake due to different expression of the macrophage mannose receptor by dendritic cells in various inbred mouse strains, Immunology 127(4) (2009) 523-529.

[14] S.D. Xiang, A. Scholzen, G. Minigo, C. David, V. Apostolopoulos, P.L. Mottram, M. Plebanski, Pathogen recognition and development of particulate vaccines: Does size matter?, Methods 40(1) (2006) 1-9.

[15] E.M. Plummer, M. Manchester, Endocytic Uptake Pathways Utilized by CPMV Nanoparticles, Mol Pharmaceut 10(1) (2013) 26-32.

[16] L. Thiele, B. Rothen-Rutishauser, S. Jilek, H. Wunderli-Allenspach, H.P. Merkle, E. Walter, Evaluation of particle uptake in human blood monocyte-derived cells in vitro. Does phagocytosis activity of dendritic cells measure up with macrophages?, J Control Release 76(1-2) (2001) 59-71.

[17] B.D. Chithrani, W.C.W. Chan, Elucidating the Mechanism of Cellular Uptake and Removal of Protein-Coated Gold Nanoparticles of Different Sizes and Shapes, Nano Letters 7(6) (2007) 1542-1550.

[18] E.J. Brown, T.H. Steinberg, Phagocytosis, in: A.G. Lee (Ed.), Biomembranes: A Multi-Volume Treatise, JAI1996, pp. 33-63.

[19] C. Lagresle, C. Bella, P.T. Daniel, P.H. Krammer, T. Defrance, Regulation of Germinal Center B-Cell Differentiation - Role of the Human Apo-1/Fas (Cd95) Molecule, J Immunol 154(11) (1995) 5746-5756.

[20] G. Laszlo, K.S. Hathcock, H.B. Dickler, R.J. Hodes, Characterization of a Novel Cell-Surface Molecule Expressed on Subpopulations of Activated T-Cell and B-Cell, J Immunol 150(12) (1993) 5252-5262.

[21] T. Akagi, X. Wang, T. Uto, M. Baba, M. Akashi, Protein direct delivery to dendritic cells using nanoparticles based on amphiphilic poly(amino acid) derivatives, Biomaterials 28(23) (2007) 3427-3436.

[22] C. Foged, B. Brodin, S. Frokjaer, A. Sundblad, Particle size and surface charge affect particle uptake by human dendritic cells in an in vitro model, Int J Pharmaceut 298(2) (2005) 315-322.

[23] B. Koppolu, D.A. Zaharoff, The effect of antigen encapsulation in chitosan particles on uptake, activation and presentation by antigen presenting cells, Biomaterials 34(9) (2013) 2359-2369.

[24] A. Collins, A. Warrington, Kenneth A. Taylor, T. Svitkina, Structural Organization of the Actin Cytoskeleton at Sites of Clathrin-Mediated Endocytosis, Current Biology 21(14) (2011) 1167-1175.

[25] L. Liu, P. Ma, H. Wang, C. Zhang, H. Sun, C. Wang, C. Song, X. Leng, D. Kong, G. Ma, Immune responses to vaccines delivered by encapsulation into and/or adsorption onto cationic lipid-PLGA hybrid nanoparticles, J Control Release 225 (2016) 230-239.

[26] A. Savina, C. Jancic, S. Hugues, P. Guermonprez, P. Vargas, I.C. Moura, A.-M. Lennon-Duménil, M.C. Seabra, G. Raposo, S. Amigorena, NOX2 Controls Phagosomal pH to Regulate Antigen Processing during Crosspresentation by Dendritic Cells, Cell 126(1) (2006) 205-218.

[27] D. Accapezzato, V. Visco, V. Francavilla, C. Molette, T. Donato, M. Paroli, M.U. Mondelli, M. Doria, M.R. Torrisi, V. Barnaba, Chloroquine enhances human CD8(+) T cell responses against soluble antigens in vivo, J Exp Med 202(6) (2005) 817-828.

[28] R. Salerno-Goncalves, M.B. Sztein, Cell-mediated immunity and the challenges for vaccine development, Trends Microbiol 14(12) (2006) 536-542.

[29] V. Hornung, F. Bauernfeind, A. Halle, E.O. Samstad, H. Kono, K.L. Rock, K.A. Fitzgerald, E. Latz, Silica crystals and aluminum salts activate the NALP3 inflammasome through phagosomal destabilization, Nat Immunol 9(8) (2008) 847-856.

[30] S. Neumann, K. Burkert, R. Kemp, T. Rades, P.R. Dunbar, S. Hook, Activation of the NLRP3 inflammasome is not a feature of all particulate vaccine adjuvants, Immunol Cell Biol 92(6) (2014) 535-542.

[31] O. Gross, C.J. Thomas, G. Guarda, J. Tschopp, The inflammasome: an integrated view, Immunol Rev 243(1) (2011) 136-151.

[32] H.F. Li, S.B. Willingham, J.P.Y. Ting, F. Re, Cutting edge: Inflammasome activation by alum and alum's adjuvant effect are mediated by NLRP3, J Immunol 181(1) (2008) 17-21.

[33] S.L. Demento, S.C. Eisenbarth, H.G. Foellmer, C. Platt, M.J. Caplan, W.M. Saltzman, I. Mellman, M. Ledizet, E. Fikrig, R.A. Flavell, T.M. Fahmy, Inflammasome-activating nanoparticles as modular systems for optimizing vaccine efficacy, Vaccine 27(23) (2009) 3013-3021.

[34] C.A. Vaine, M.K. Patel, J.T. Zhu, E. Lee, R.W. Finberg, R.C. Hayward, E.A. Kurt-Jones, Tuning Innate Immune Activation by Surface Texturing of Polymer Microparticles: The Role of Shape in Inflammasome Activation, J Immunol 190(7) (2013) 3525-3532.

[35] M. Ritter, K. Straubinger, S. Schmidt, D.H. Busch, S. Hagner, H. Garn, C.P. da Costa, L.E. Layland, Functional relevance of NLRP3 inflammasome-mediated interleukin (IL)-1 beta during acute allergic airway inflammation, Clin Exp Immunol 178(2) (2014) 212-223.

[36] U. Schroeder, A. Graff, S. Buchmeier, P. Rigler, U. Silvan, D. Tropel, B.M. Jockusch, U. Aebi, P. Burkhard, C.A. Schoenenberger, Peptide Nanoparticles Serve as a Powerful Platform for the Immunogenic Display of Poorly Antigenic Actin Determinants, J Mol Biol 386(5) (2009) 1368-1381.

[37] S. Vallabhapurapu, M. Karin, Regulation and Function of NF-kappa B Transcription Factors in the Immune System, Annu Rev Immunol, Annual Reviews, Palo Alto, 2009, pp. 693-733.

[38] C.A. Dinarello, Interleukin-1, Cytokine and Growth Factor Reviews 8(4) (1997) 253-265.

[39] S. Nistico, N. Paolillo, D. Minella, S. Piccirilli, V. Rispoli, E. Giardina, M. Biancolella, S. Chimenti, G. Novelli, G. Nistico, EFFECTS OF TNF-alpha AND IL-1 beta ON THE ACTIVATION OF GENES RELATED TO INFLAMMATORY, IMMUNE RESPONSES AND CELL DEATH IN IMMORTALIZED HUMAN HaCat KERATINOCYTES, Int. J. Immunopathol. Pharmacol. 23(4) (2010) 1057-1072.

[40] T.D. Karlson, Y.Y. Kong, C.L. Hardy, S.D. Xiang, M. Plebanski, The signalling imprints of nanoparticle uptake by bone marrow derived dendritic cells, Methods 60(3) (2013) 275-283.

[41] M. Lundqvist, J. Stigler, G. Elia, I. Lynch, T. Cedervall, K.A. Dawson, Nanoparticle size and surface properties determine the protein corona with possible implications for biological impacts, P Natl Acad Sci USA 105(38) (2008) 14265-14270.

[42] C.C. Fleischer, C.K. Payne, Nanoparticle-Cell Interactions: Molecular Structure of the Protein Corona and Cellular Outcomes, Accounts Chem Res 47(8) (2014) 2651-2659.

[43] C. Gunawan, M. Lim, C.P. Marquis, R. Amal, Nanoparticle-protein corona complexes govern the biological fates and functions of nanoparticles, J Mater Chem B 2(15) (2014) 2060-2083.

[44] L.J. Cruz, F. Rueda, B. Cordobilla, L. Simon, L. Hosta, F. Albericio, J.C. Domingo, Targeting Nanosystems to Human DCs via Fc Receptor as an Effective Strategy to Deliver Antigen for Immunotherapy, Mol Pharmaceut 8(1) (2011) 104-116.

[45] J.J. Moon, H. Suh, A.V. Li, C.F. Ockenhouse, A. Yadava, D.J. Irvine, Enhancing humoral responses to a malaria antigen with nanoparticle vaccines that expand T-fh cells and promote germinal center induction, P Natl Acad Sci USA 109(4) (2012) 1080-1085.

[46] J.J. Moon, H. Suh, M.E. Polhemus, C.F. Ockenhouse, A. Yadava, D.J. Irvine, Antigen-Displaying Lipid-Enveloped PLGA Nanoparticles as Delivery Agents for a Plasmodium vivax Malaria Vaccine, Plos One 7(2) (2012) 9.

[47] Z. Luo, S. Shi, L. Jin, L. Xu, J. Yu, H. Chen, X. Li, Cationic micelle based vaccine induced potent humoral immune response through enhancing antigen uptake and formation of germinal center, Colloids and Surfaces B: Biointerfaces 135 (2015) 556-564.

[48] J.H. Eldridge, R.M. Gilley, J.K. Staas, Z. Moldoveanu, J.A. Meulbroek, T.R. Tice, Biodegradable Microspheres - Vaccine Delivery System for Oral Immunization, Current Topics in Microbiology and Immunology 146 (1989) 59-66.

[49] J.L. Cleland, Single-administration vaccines: controlled-release technology to mimic repeated immunizations, Trends Biotechnol 17(1) (1999) 25-29.

[50] Y. Hailemichael, Z.M. Dai, N. Jaffarzad, Y. Ye, M.A. Medina, X.F. Huang, S.M. Dorta-Estremera, N.R. Greeley, G. Nitti, W.Y. Peng, C.W. Liu, Y.Y. Lou, Z.Q. Wang, W.C. Ma, B. Rabinovich, K.S. Schluns, R.E. Davis, P. Hwu, W.W. Overwijk, Persistent antigen at vaccination sites induces tumor-specific CD8(+) T cell sequestration, dysfunction and deletion, Nat Med 19(4) (2013) 465-+.

CHAPTER 4. COLD-CHAIN-INDEPENDENT STORAGE OF PROTEIN NANOPARTICLE VACCINES

4.1 Introduction

While the other chapters of this thesis (and a significant fraction of vaccine research) are devoted to the development of new types of immunogenic vaccines, effective distribution of vaccines is a non-trivial problem, and a significant hurdle to eradicating diseases worldwide. The World Health Organization (WHO) estimates around 1.5 million people die each year from vaccine-preventable diseases [1]. Despite advances in vaccine development, vaccine distribution infrastructure remains inadequate in many parts of the world, and it is estimated that up to 40-50% of all vaccine doses are wasted in certain countries [2].

Crucial to current vaccine transport is the idea of the cold-chain – a series of refrigerated enclosures with tight temperature control that allows for stable transport of vaccine from manufacturer to patient. Tight controls on temperature are important for whole pathogen vaccines, as these are particularly prone to stability losses [3]. Membrane-bound pathogens, such as bacteria and certain viruses including influenza, are especially prone to osmotic stress, and changing salt concentrations with evaporating solvent can lead to pathogen shrinkage and destruction [3, 4].

Although recombinant, subunit protein vaccines have been proposed as a means of working around stability issues with unstable whole pathogen vaccines, issues with low immunogenicity and appropriate adjuvant choice have slowed their development as a

viable alternative [3]. Our protein nanoparticles are a means of delivering antigen and an adjuvant in the same delivery vehicle, and are thus an excellent candidate for testing cold-chain-independent vaccine stability.

In the case that storage losses arise, lyophilization, or freeze-drying, has been shown to enhance vaccine stability [5, 6]. Protein nanoparticles in particular have been lyophilized previously, although increases in size due to aggregation and decreases due to particle collapse have been observed [7, 8]. Lyophilized and reconstituted protein nanoparticles made from β-galactosidase retained approximately 84% of enzyme activity, indicating the potential for antigen structure to be preserved in protein nanoparticle vaccines [8].

Although Herrera-Estrada et al. showed enzyme activity in protein nanoparticles was preserved, the study did not examine whether surface protein was denatured, a key element of 3HA nanoparticles, and the most likely region of protein denaturation to occur. The hemagglutination assay measures properly conformed surface protein. In case hemagglutinating activity is lost, the use of stabilizing excipients may be needed. The addition of certain excipient sugars and salts as cryoprotectants during the freeze-drying process has also been shown to stabilize nanoparticles by forming an amorphous glass surrounding the particles, disrupting ice crystal formation [5]. A recent study of an excipient screen for influenza subunit vaccine formulation into a microneedle patch established an arginine/calcium heptagluconate buffer system to be optimal for preserving hemagglutinin structure and hemagglutinating activity for 6 months [9]. Although the microneedles tested were air-dried instead of lyophilized, lyophilization is hypothesized to be a gentler process on proteins, due to the instantaneous immobilization of proteins during

flash freezing and the damaging effects of increasing ion concentration in an evaporating liquid [10].

We hypothesize that our crosslinked protein nanoparticles stored at room temperature and at 37°C will immunize mice equally well as nanoparticles made from fresh protein. We will use trimerized hemagglutinin (3HA) nanoparticles, described earlier in Chapter 2, for these stability experiments due to an easy *in vitro* readout of protein structure preservation. The hemagglutination assay is a simple *in vitro* test for the preservation of the biological activity of hemagglutinin, and will be used to test whether extended warm temperature storage results in activity loss.

4.2 Materials and Methods

4.2.1 Nanoparticle Synthesis and Characterization

3HA nanoparticles were synthesized and characterized as described in Chapter 2 [11]. Briefly, ethanol was added to a 1.6 mg/mL 3HA solution at a rate of 1 mL/min under constant stirring at 600 rpm in a 400 μL +100 μL volume ratio of ethanol to protein solution. The particles were collected by centrifugation, and resuspended in sterile PBS with sonication. 800 μg soluble 3HA protein was added at a final concentration of 1.6 mg/mL to 480 μg desolvated 3HA nanoclusters and an amine crosslinking reaction was performed using 3 mM 3,3´-Dithiobis[sulfosuccinimidylpropionate (DTSSP, Thermo Scientific, Waltham, MA) for 12 hours while stirring to coat the nanoparticles. Coated nanoclusters were collected by centrifugation, and protein concentration was measured by a BCA assay according to the manufacturer's instructions (Thermo Scientific) to estimate the total protein content in nanoparticles. Dynamic light scattering (DLS) was performed

in PBS with a Malvern Zetasizer Nano ZS (Malvern Instruments, Westborough, MA) to assess nanoparticle size distributions.

Hemagglutinating capability of 3HA nanoparticles was tested as previously described in Chapter 2 and elsewhere [11]. Briefly, 5 μg of 3HA protein or 3HA protein nanoparticles in 100 μL of phosphate-buffered saline was serially diluted by half across 11 wells of a 96-well plate. 50 μL of 0.5% turkey RBCs were then added to each well, and incubated at room temperature for 1 hour. The hemagglutination titer was read as the last well in the serial dilution that did not form a red button of settled RBCs.

4.2.2 Lyophilization and Extended Storage

Extended wet storage of 3HA nanoparticles was performed in PBS at room temperature or 37°C. Nanoparticles and soluble protein were diluted to 200 μg/mL in six 100 μL aliquots in 2 mL centrifuge tubes. The tubes were sealed with parafilm and incubated for up to 1 month at 37°C, and up to 3 months at room temperature. At each time point, one 100 μL aliquot was used to measure hemagglutination activity of the nanoparticles, while two 300 μL aliquots were stored at room temperature for *in vivo* immunizations.

For lyophilization, solutions of 3HA nanoparticles were resuspended in either arginine/heptagluconate or ammonium acetate excipient buffer solutions. Nanoparticles were centrifuged and resuspended to a concentration of 50 μg/mL in 15% w/v arginine/heptagluconate buffer solution. The arginine/heptagluconate solution was made by adding 3.75 g of arginine and calcium heptagluconate (Sigma) each to 50 mL of deionized water, and adjusting the solution pH to 7.3. For ammonium acetate storage,

nanoparticles were resuspended to a concentration of 200 μg/mL in 150 mM ammonium acetate. Following buffer exchange, solutions of nanoparticles were flash frozen in liquid nitrogen. Frozen nanoparticle solutions were then exposed to 40 mTorr vacuum overnight in a freeze dryer (Millrock Technologies, Kingston, NY). Reconstitution of nanoparticles was performed by adding an identical volume of milliQ-purified water to lyophilized nanoparticles immediately after lyophilization.

4.2.3 Immunization and Sample Collection

All animal work was done in accordance with the IACUC guidelines of Georgia State University, under IACUC approval number A16024. Female, 6 week old Balb/c mice (Charles River, Wilmington, MA) were intra-muscularly immunized with 10 μg aged 3HA nanoparticles, 20 μg aged 3HA nanoparticles, 10 μg freshly prepared 3HA nanoparticles, 10 μg soluble 3HA protein, or PBS as a control. Five mice per group were immunized twice i.m. at a 3-week interval. To compare antibody responses, sera were collected 2 weeks after each immunization by submandibular venipuncture.

4.2.4 Serum IgG Titer

Serum IgG titer was assessed as previously described [11, 12]. Briefly, ELISA plates were coated with 1 μg/mL 3HA protein in PBS and incubated overnight. Plates were blocked with 1% bovine serum albumin (BSA) in PBS for 1 hour. Mouse serum samples were initially diluted 1:100 in 1% BSA, and serial half-dilutions were made in 1% BSA across the 96-well ELISA plate. Serum sample dilutions were incubated for 1 hour, and 1 μg/mL HRP-conjugated goat-anti-mouse IgG (Life Technologies, Grand Island, NY) in 1% BSA was used as a detection antibody. Chromogenic quantification was performed by

the oxidation of tetramethylbenzidine by hydrogen peroxide (R&D Systems, Minneapolis, MN) according to the manufacturer's instructions. Two times the absorbance of naïve group's serum samples was considered the cutoff for measuring the endpoint titer.

4.2.5 Hemagglutination Inhibition Assessment

Serum hemagglutination inhibition (HAI) activity was assessed according to a protocol adapted from the World Health Organization [13]. 10 μL mouse serum was incubated with 30 μL of receptor-destroying enzyme (RDE) (Denka Seiken Co, Tokyo, Japan) at 37°C overnight, followed by 56°C incubation for 30 minutes to inactivate non-specific agglutinating proteins. Inactivated serum was diluted with 60 μL room temperature PBS, and centrifuged at 500xg for 8 minutes to collect treated serum samples. Eight, 25 μL serial half dilutions of 1:10 treated sera were mixed in a round-bottom 96-well plate with 25 μL of 2 μg/mL 3HA protein and incubated at room temperature for 30 minutes. This concentration of 3HA was chosen based on the ability to agglutinate RBCs after 3 serial dilutions, as indicated in the WHO protocol. To this mixture, 50 μL of a 0.5% turkey RBC suspension (Lampire Biologicals, Pipersville, PA) was added, and the wells were incubated for 1 hour to develop. HAI titer was read as the inverse dilution of the last well able to prevent hemagglutination, or in which a red button was formed.

4.2.6 Statistics

IgG titers were assessed by the Kruskal-Wallis one-way analysis of variance for non-parametric samples. Hemagglutination inhibition titers were analysed by comparing the number of wells neutralized to the standard HAI titer of 40 (2 wells) established by the

WHO as protective, using a one-sample t test. P values less than 0.05 were considered significant.

4.3 Results

4.3.1 Lyophilization Results in Hemagglutination Losses

The agglutination activity of freeze-dried 3HA nanoparticles with arginine and calcium heptagluconate as excipients is summarized in Table 4. Nanoparticles in PBS lost significant hemagglutinating activity upon lyophilization and reconstitution. The arginine/heptagluconate buffer alone caused a diffuse red well color characteristic of hemagglutination. This was most likely due to the high salt concentration of the buffer leading to hemolysis, confounding the results of the lyophilization experiment. Since further buffer exchange or processing could lead to nanoparticle losses that would also decrease the hemagglutinating activity, a volatile excipient buffer that would sublimate during the lyophilization process was chosen to perform a follow-up study instead.

Table 4. Hemagglutination activity of lyophilized and reconstituted 3HA nanoparticles. The number of wells agglutinated by lyophilized and reconstituted nanoparticles were identical across three independent replicates.

Sample	# of Wells Agglutinated
Unlyophilized Nanoparticles	9
Nanoparticles lyophilized in PBS	5
Nanoparticles lyophilized in Arginine/Heptagluconate	9
Arginine/Heptagluconate buffer control	9

Table 5. Hemagglutination activity of lyophilized and reconstituted 3HA nanoparticles. The number of wells agglutinated by the nanoparticles were identical across three independent replicates.

Sample	# of Wells Agglutinated
Unlyophilized Nanoparticles	10
Nanoparticles lyophilized in PBS	7
Nanoparticles lyophilized in Ammonium Acetate	3

Ammonium acetate was shown to be a good excipient buffer for retaining hemagglutinating activity in an influenza subunit vaccine microneedle patch [9], and was used for lyophilization of 3HA nanoparticles. However, nanoparticles lyophilized in the volatile excipient buffer ammonium acetate lost even more activity upon reconstitution than nanoparticles lyophilized in PBS (Table 5). Nanoparticle size also increased after lyophilization and reconstitution, and was inversely correlated to hemagglutination activity (Figure 35).

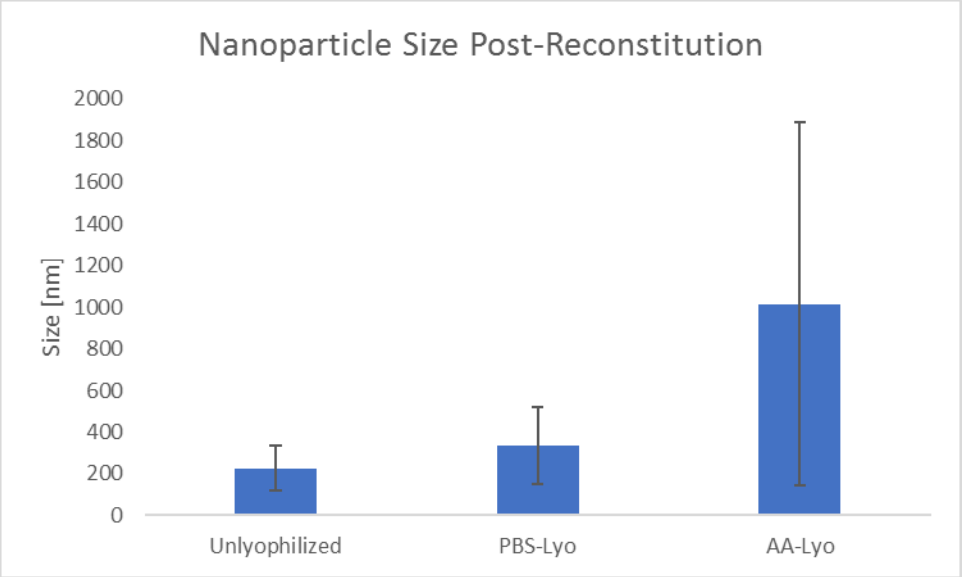

Figure 35. Average 3HA nanoparticle size after lyophilization and reconstitution as determined by DLS. Error bars are representative of the standard deviation of nanoparticle size as determined by polydispersity.

4.3.2 Warm, Wet Storage of Nanoparticles Preserves Hemagglutinating Activity

Liquid formulations of vaccines have several advantages over reconstituted, lyophilized vaccines, including avoiding dosing issues with incorrect reconstitution and potential sterility issues with reconstitution in the field [3]. Nanoparticles stored at 800 µg/mL in PBS at 4°C, room temperature, or 37°C did not lose agglutinating activity after 1 week, but did lose it after one month (Figure 36).

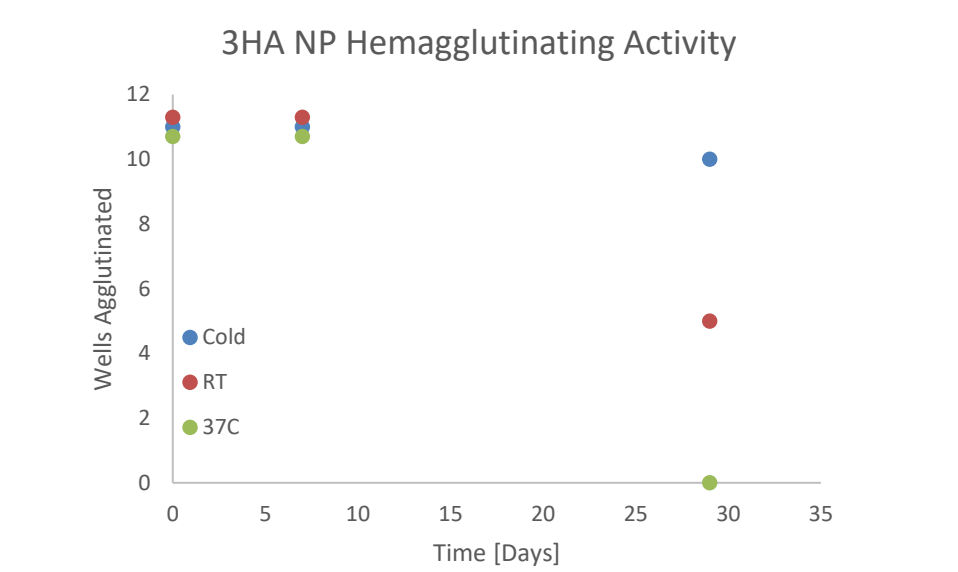

Figure 36. Hemagglutinating activity of nanoparticles stored at 800 µg/mL in PBS at various temperatures for 1 month. Each data point represents the hemagglutinating activity of 1 sample tested.

Nanoparticles diluted to 200 µg/mL in PBS in parafilm-sealed 2 mL centrifuge tubes were stored for approximately 3 months. Nanoparticles stored in PBS at room temperature did not lose agglutinating activity after 112 days, while nanoparticles stored at 37°C retained full hemagglutinating activity for 2 weeks, and lost activity at 1 month (Figure 37). Soluble 3HA in PBS stored at room temperature lost no hemagglutinating activity after 56 days.

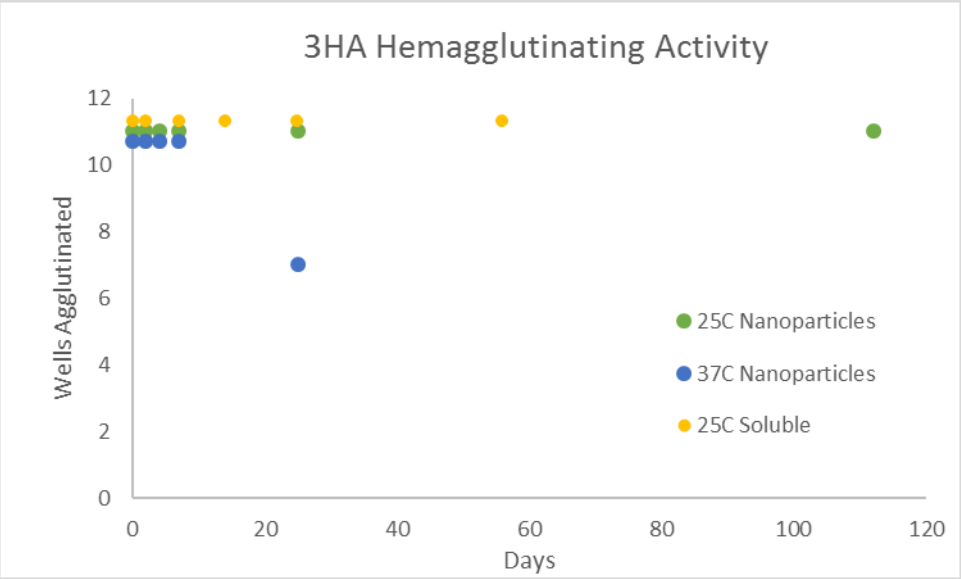

Figure 37. Hemagglutinating activity of 3HA nanoparticles or soluble 3HA protein over the course of approximately 3 months. Each data point represents the hemagglutinating activity of 1 sample tested.

4.3.3 Stored and Fresh Nanoparticles Induce Similar Serum IgG Titers

To compensate for any potential loss in hemagglutinating activity, we immunized mice with a single dose (10 μg) or double dose (20 μg) of nanoparticles stored for 112 days in PBS at room temperature. As controls, mice were immunized with 10 μg freshly-prepared nanoparticles or 10 μg soluble 3HA protein. Serum samples were collected 2 weeks after priming and boosting immunizations and were assessed for anti-3HA IgG titers. No significant differences in IgG titer were observed between the nanoparticles stored at room temperature and freshly made nanoparticles. The double dose of aged nanoparticles induced significantly higher titers compared to soluble protein after the priming immunization, but that significance disappeared after the boost immunization (Figure 38).

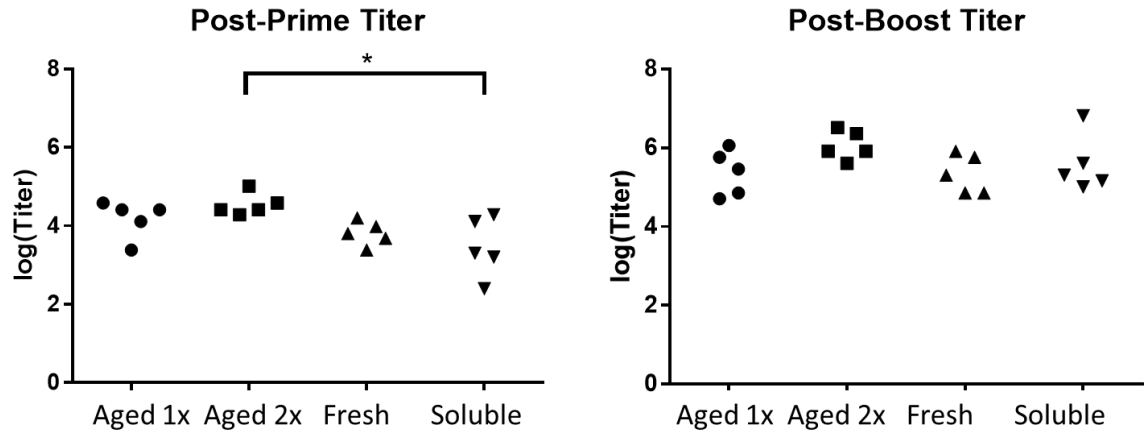

Figure 38. Serum IgG titers from mice 2 weeks after a priming immunization (left) or a boost immunization (right) of 10 µg room temperature-stored 3HA nanoparticles (Aged 1x), 20 µg room temperature-stored 3HA nanoparticles, 10 µg freshly prepared 3HA nanoparticles (fresh) or 10 µg soluble 3HA (soluble). Each point is the IgG titer of one mouse.

4.3.4 Aged Nanoparticles Induce Neutralizing Antibody Responses

Hemagglutination inhibition (HAI) titer is a measurement of the ability of serum antibodies to block hemagglutinin binding to sialic acid residues. This measurement is directly correlated to the ability of an animal's antibodies to block influenza viruses from infecting host cells, and is a means of measuring neutralizing antibody production. The World Health Organization has defined a serum HAI titer of 40 or above to provide good protection against influenza infection [14]. Groups immunized with 10 µg stored and fresh nanoparticles had significantly higher HAI titers than 40, while groups immunized with soluble protein or PBS did not have significantly higher titers than 40 (Figure 39). While the average titer of the 20 µg nanoparticle immunized group did not reach statistical significance ($p = 0.057$), this could be attributed to the low serum sample number in that group.

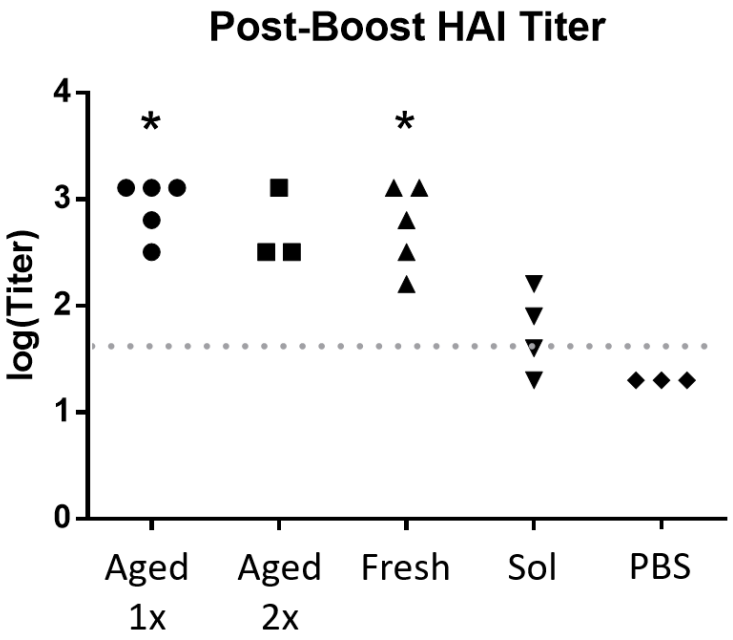

Figure 39. Log of hemagglutination inhibition titer from mice post-boost immunization. Dotted line represents an HAI titer of 40, defined by the WHO to provide protective antibody responses. * represents significantly different average titers from a titer of 40. Each data point represents a serum titer from one mouse.

4.4 Discussion

While 3HA nanoparticles were not stable to lyophilization with or without an ammonium acetate excipient, they could be stored in PBS at room temperature for an extended period of time, making lyophilization and excipients unnecessary. Structural losses upon lyophilization and subsequent reconstitution could have been due to nanoparticle-nanoparticle interactions with each other, as the volatile excipient performed even worse than PBS at preserving hemagglutination and nanoparticle size. Future studies of lyoprotective excipients for protein nanoparticles should examine sugars and polymers that form stabilizing interactions with proteins, and the use of ELISA instead of hemagglutination could provide a more quantitative and solute-independent readout of protein structure preservation.

Nanoparticles were stored at room temperature for 112 days in PBS with no loss in hemagglutinating activity. According to a report by UNICEF and the WHO, approximately 1 month of cold chain is needed for transport of vaccines from a manufacturer in the developed world to a developing region [15]. Storage of protein nanoparticles for almost 3 times this length without additional excipients is especially promising, given that viral and subunit vaccine storage typically requires the addition of polyethylene glycol or sucrose to achieve weeks-long cold chain-independent storage [16, 17].

Nanoparticles stored at 37°C in PBS were able to retain hemagglutinating activity for 2 weeks, but started to lose activity at 1 month. Although we did not immunize mice with nanoparticles stored at 37°C, we hypothesize that a similarly high antibody titer would be achieved based on the correlation between *in vitro* vaccine hemagglutinating activity and *in vivo* immunization efficacy [18]. Two weeks of elevated temperature storage is more than enough time to reach rural health clinics from a distribution center [15], but may not be enough time to store the vaccine there for a prolonged period of time. Surprisingly, soluble 3HA was also able to retain hemagglutinating activity for 56 days. This could be due to the inherent stability of this particular protein, and of recombinant subunit antigens generally [3].

The concentration dependence of hemagglutination loss observed suggests that a major factor in 3HA protein structural loss is nanoparticle-nanoparticle collisions. The observation that nanoparticle size increases after lyophilization and reconstitution would also correlate nanoparticle size increases with a loss in hemagglutination. Excipients to increase stability, wet or lyophilized, should therefore focus on compounds that can bind the 3HA proteins, and shield the nanoparticles from harmful interactions with one another.

Tanaka et al. found that saccharides in sufficient concentration to form a monolayer over proteins stabilized them to lyophilization, and that direct interaction of the protein and the sugar was responsible for the stabilizing effect [19]. Disaccharides such as trehalose (and less commonly sucrose) have been found to be the most effective lyoprotectants [19, 20]. Though these compounds are generally used to protect soluble proteins against denaturation during lyophilization, their mechanism of action suggests that they could protect protein nanoparticles in wet storage as well.

Hemagglutination inhibition data showed that our room temperature-stored nanoparticles were just as effective at inducing neutralizing antibodies as freshly made nanoparticles. The WHO benchmark HAI titer of 40 allows us to compare our vaccine to an accepted standard of immunity, and our data suggests that our nanoparticles stored at room temperature can confer protective immunity. Given the ability of freshly-made 3HA nanoparticles to protect mice against a $10xLD_{50}$ challenge of H7N9 influenza [11], challenge studies should examine whether nanoparticles stored at warm temperatures can also confer protective immunity.

The ability of 3HA nanoparticles to induce better HAI titers than soluble 3HA concurs with current nanoparticle vaccine literature theorizing that multivalent epitope presentation is a mechanism of recombinant antigen nanovaccine adjuvancy [3, 21, 22]. Our previous results in Chapter 3 demonstrating enhanced dendritic cell TNF-α and IL-1β responses to OVA-coated OVA protein nanoparticles also support this hypothesis. Though the hemagglutination assay only works for hemagglutinin and a few other pathogen antigens, the growing consensus on the importance of surface protein conformation suggests that it should be used as a preliminary measure of nanovaccine stability for all

types of antigen-displaying nanoparticle vaccines. Other *in vitro* readouts of protein conformation, such as some ELISAs, should be used as a preliminary assessment of the stability of non-hemagglutinating types of vaccine nanoparticles. Analogous to the HAI assay, competitive inhibition of ELISA coating antigen by anti-sera can also be used as a quantitative measure of neutralizing antibody formation.

4.5 Conclusion

In this chapter, we have shown that 3HA nanoparticles can be stored for up to 112 days at room temperature with no loss in *in vitro* hemagglutinating activity or *in vivo* antibody and neutralizing antibody responses. This exceeds the estimate by the WHO and the United Nations Children's Fund (UNICEF) of the time needed for cold chain-dependent transport of a vaccine from a vaccine manufacturer in the developed world to a developing region off of the grid [15]. The fact that 3HA nanoparticles can remain immunogenic outside of cold-chain storage for more than three times that duration of time is a promising sign that nanoparticle vaccines made from recombinant protein antigens can survive both transport to and storage in the developing world. The 37°C storage time of 2 weeks is sufficient to reach a rural health center in the developing world, but not necessarily enough time to store the vaccine there. Although this timeframe is useful for short-term vaccination drives, achieving extended storage at 37°C beyond 2 weeks will be useful for reaching more people and distributing vaccines that require a prime and boost administration.

The current model of inactivated pathogen vaccine distribution is ready for disruption. Cold-chain-dependent vaccine transport to the developing world relies on large

volumes to bring down costs, a tradeoff that can result in up to 50% of vaccine doses being wasted [23]. As logistics of vaccine transport and storage improve and better healthcare infrastructure improves access to vaccines, recombinant subunit antigen nanoparticle vaccines that can be stored independent of the cold chain can cut down on the amount of vaccines wasted, and play a substantial role in improving global health.

REFERENCES

[1] Immunization Coverage, World Health Organization, 2016, p. http://www.who.int/mediacentre/factsheets/fs378/en/.

[2] M. Zaffran, J. Vandelaer, D. Kristensen, B. Melgaard, P. Yadav, K.O. Antwi-Agyei, H. Lasher, The imperative for stronger vaccine supply and logistics systems, Vaccine 31 (2013) B73-B80.

[3] O.S. Kumru, S.B. Joshi, D.E. Smith, C.R. Middaugh, T. Prusik, D.B. Volkin, Vaccine instability in the cold chain: Mechanisms, analysis and formulation strategies, Biologicals 42(5) (2014) 237-259.

[4] H.J. Choi, J.M. Song, B.J. Bondy, R.W. Compans, S.M. Kang, M.R. Prausnitz, Effect of Osmotic Pressure on the Stability of Whole Inactivated Influenza Vaccine for Coating on Microneedles, Plos One 10(7) (2015).

[5] W. Abdelwahed, G. Degobert, S. Stainmesse, H. Fessi, Freeze-drying of nanoparticles: Formulation, process and storage considerations, Adv Drug Deliver Rev 58(15) (2006) 1688-1713.

[6] J. Rexroad, C.M. Wiethoff, L.S. Jones, C.R. Middaugh, Lyophilization and the Thermostability of Vaccines, Cell Preservation Technology 1(2) (2002) 91-104.

[7] M.G. Anhorn, H.C. Mahler, K. Langer, Freeze drying of human serum albumin (HSA) nanoparticles with different excipients, Int J Pharmaceut 363(1-2) (2008) 162-169.

[8] L.H. Estrada, S. Chu, J.A. Champion, Protein nanoparticles for intracellular delivery of therapeutic enzymes, J Pharm Sci-Us 103(6) (2014) 1863-71.

[9] M.J. Mistilis, M.R. Bommarius As Fau - Prausnitz, M.R. Prausnitz, Development of a Thermostable Microneedle Patch for Influenza Vaccination. LID - 10.1002/jps.24283 [doi], (1520-6017 (Electronic)).

[10] M.J. Pikal, Mechanisms of Protein Stabilization During Freeze-Drying annd Storage: The relative Importance of thermodynamic stabilization and glassy state relaxation dynamics, Freeze-Drying/Lyophilization of Pharmaceutical and Biological Products, Marcel Dekker, New York, 1999, pp. 161-198.

[11] L. Wang, T.Z. Chang, Y. He, J.R. Kim, S. Wang, T. Mohan, Z. Berman, S.M. Tompkins, R.A. Tripp, R.W. Compans, J.A. Champion, B.-Z. Wang, Coated protein nanoclusters from influenza H7N9 HA are highly immunogenic and induce robust protective immunity, Nanomedicine: Nanotechnology, Biology and Medicine 13(1) (2016) 253-262.

[12] L. Wang, A. Hess, T.Z. Chang, Y.C. Wang, J.A. Champion, R.W. Compans, B.Z. Wang, Nanoclusters self-assembled from conformation-stabilized influenza M2e as broadly cross-protective influenza vaccines, Nanomed-Nanotechnol 10(2) (2014) 473-482.

[13] Serological detection of avian influenza A(H7N9) virus infections by modified horse red blood cells: Haemagglutination-Inhibition Assay. 2013 (accessed September 12, 2016.2017).

[14] L.B. Brydak, M. Machala, Humoral immune response to influenza vaccination in patients from high risk groups, Drugs 60(1) (2000) 35-53.

[15] Vaccines: Handled with Care, United Nations Children's Fund (UNICEF) and the World Health Organization (WHO) (2004).

[16] M. Pelliccia, P. Andreozzi, J. Paulose, M. D'Alicarnasso, V. Cagno, M. Donalisio, A. Civra, R.M. Broeckel, N. Haese, P.J. Silva, R.P. Carney, V. Marjomaki, D.N. Streblow, D. Lembo, F. Stellacci, V. Vitelli, S. Krol, Additives for vaccine storage to improve thermal stability of adenoviruses from hours to months, Nat Commun 7 (2016) 7.

[17] A. Flood, M. Estrada, D. McAdams, Y.H. Ji, D.X. Chen, Development of a Freeze-Dried, Heat-Stable Influenza Subunit Vaccine Formulation, Plos One 11(11) (2016) 18.

[18] P. Pushko, T.M. Tumpey, F. Bu, J. Knell, R. Robinson, G. Smith, Influenza virus-like particles comprised of the HA, NA, and M1 proteins of H9N2 influenza virus induce protective immune responses in BALB/c mice, Vaccine 23(50) (2005) 5751-5759.

[19] K. Tanaka, T. Takeda, K. Miyajima, Cryoprotective Effect of Saccharides on Denaturation of Catalase by Freeze-Drying, Chem Pharm Bull 39(5) (1991) 1091-1094.

[20] W. Wang, Lyophilization and development of solid protein pharmaceuticals, Int J Pharmaceut 203(1-2) (2000) 1-60.

[21] M. Kanekiyo, C.J. Wei, H.M. Yassine, P.M. McTamney, J.C. Boyington, J.R.R. Whittle, S.S. Rao, W.P. Kong, L.S. Wang, G.J. Nabel, Self-assembling influenza nanoparticle vaccines elicit broadly neutralizing H1N1 antibodies, Nature 499(7456) (2013) 102-+.

[22] M.F. Bachmann, G.T. Jennings, Vaccine delivery: a matter of size, geometry, kinetics and molecular patterns, Nat Rev Immunol 10(11) (2010) 787-796.

[23] U. WHO, World Bank, State of the World's Vaccines and Immunization, 3rd ed., World Health Organization, Geneva, 2009.

CHAPTER 5. MOLECULAR ADJUVANTS FOR ENHANCING NANOPARTICLE-MEDIATED ADJUVANCY

5.1 Introduction

Particulate vaccine carriers can control release of soluble antigens to the immune system and protect them from degradation [1]. However, nanoparticles have been found to be more than just passive antigen depots, and certain types of particles exhibit their own immunostimulatory effects on antigen presenting cells. The exact nature of this nanoparticulate-mediated adjuvancy is unknown, and many fundamental studies have examined the immunological effects of nanoparticle properties such as size [2], surface charge [3], shape [4], and material [5]. Generalized vaccine particle design principles are difficult to elucidate from these studies, however, due to our incomplete understanding of immunology of vaccination, and specifically the type of immune response needed to successfully vaccinate against a particular pathogen [6].

The molecular adjuvants are another class of immunostimulants. Pathogen-associated molecular patterns (PAMPs) are macromolecules that interact with specific pattern recognition receptors (PRRs) on or inside antigen presenting cells [1, 7]. Receptors that bind bacterially-derived or virally-derived macromolecules are hypothesized to initiate adaptive immune responses geared toward those particular classes of pathogens [7, 8]. Toll-like receptors (TLRs) are a class of membrane-bound PRRs that have been extensively studied for vaccine adjuvant use [9-11]. However, safety concerns over administration of pathogen-derived compounds require thorough investigation [12]. Currently, several

pathogen-derived vaccine adjuvants are undergoing clinical trials, but only two have been approved for use in humans [13].

Flagellin (FliC) is a TLR-5 ligand shown to greatly enhance responses to influenza vaccination [14, 15]. Given the strength of FliC as an adjuvant, vaccines have been proposed with genetic fusion of antigenic peptides with the FliC protein [11, 16], including in our work described in Chapter 2. Nanoparticle vaccines have also been decorated with FliC [17, 18]. At least 6 clinical trials have been completed with FliC-fusion proteins [19]. The propensity of certain FliC-fusion proteins to aggregate, even at 4°C, may decrease their efficacy [11], and the sequence-dependent nature of FliC-fusion protein stability reduces its attractiveness as a platform technology. Nanoparticles with a stable, native FliC coat, or with native FliC admixed can combine the immunostimulatory properties of FliC with those of antigen-containing nanoparticles. The optimal location of antigen and adjuvant in nanoparticle vaccine formulations is still under active research [9, 20], and recent findings suggest that flagellated bacteria in the gut assist in TLR-5-mediated adjuvancy to subcutaneously-administered influenza vaccines [14]. Using TLR ligands as adjuvants, however, poses the risk of safety issues [11] and immune responses against the adjuvant itself [21].

The use of host-derived proteins as vaccine adjuvants may be able to address some of the issues associated with pathogen-derived adjuvants. Antibodies, or immunoglobulins (Ig), coat pathogens during the immune response to an infection, and these proteins may be able to act as *in situ* adjuvants rendering nanoparticles more immunogenic *in vivo*. While antibodies immobilized by affinity interactions on the nanoparticles' surface should remain bound, any soluble Ig in the formulation should be recognized as host protein and

consequently non-immunogenic, and would simply enter the host's circulating repertoire of antibodies. Additionally, the current, widespread good manufacturing practice (GMP) production of humanized antibodies offers a pathway for large-scale production of immunoglobulin-based adjuvants.

The idea of immunoglobulin-mediated adjuvancy has been explored through the use of antibody-bound antigen, or immune complexes, as vaccines [22-25]. IgG2a complexed with soluble OVA was able to enhance specific anti-OVA antibody concentrations and $CD4^+$ T cell responses by over an order of magnitude in comparison to soluble OVA[26]. Although several sources state that immunoglobulins enhance responses against soluble antigen and suppress them when bound to particulates [27], this assertion was based on evidence of anti-Rh factor IgG suppressing immune responses against fetal erythrocytes in pregnant women[28]. Immunosuppressive responses against IgG-opsonized nanoparticulates have not been definitively reported. Moreover, a study comparing the inflammatory properties of soluble and insoluble immune complexes from rheumatoid synovial fluid found that the larger, insoluble immune complexes were more immunostimulatory than the soluble ones [24], supporting the hypothesis that particle size and immunoglobulin opsonization may synergistically enhance immune responses.

The protein corona that forms on nanoparticles in serum *in vivo* consists of many protein types, and biomaterial-serum protein interactions is an active area of research[29]. Engineering biomaterial surfaces to bind antibodies can enhance immunogenicity by targeting the antigen particles to macrophages and dendritic cells via Fc receptors on these antigen-presenting cell types[30]. Follicular dendritic cells in particular can bind to IgG and IgM immune complexes to present to B cells undergoing germinal center reactions, a

process that generates antibodies of higher affinity and of diverse effector functions [7, 31, 32]. Furthermore, antibody-opsonized nano- and microparticles provide a unique platform for activating the complement system, an inflammatory extracellular signaling cascade designed to neutralize infection, trigger local inflammation, and assist in the adaptive immune response [7, 33-35].

In Chapter 2, we found that flagellin need not be associated in a 1:1 ratio with antigen for triggering an effective immune response. In Chapters 2 and 3, we saw the importance of nanoparticle coating in enhancing *in vitro* and *in vivo* responses for 3HA and OVA nanoparticles, respectively. The work in this chapter combines the ideas of these previous chapters – using molecular adjuvant coatings on the surface of nanoparticle vaccines to further enhance their adjuvancy.

Our studies here examine adjuvant nanoparticle coatings of pathogen-derived flagellin (FliC) and host-derived antibodies IgM, IgG1 and IgG2a. Immunoglobulin M is the first antibody isotype made by antibody-producing B cells, and is a stronger activator of the complement system than the more prevalent IgG [36]. It is possible that IgM enhances the adaptive immune response to the antigen to which it is bound. Given its lower affinity and different Fc structure than the more prevalent IgG, IgM likely serves an immunoregulatory function in addition to any neutralizing capabilities it may have. This idea is supported by findings that knockout mice unable to produce secreted IgM have delayed production of affinity-matured antibodies to an antigen challenge, and that delay can be eliminated by the co-immunization of antigen and non-specific IgM [37]. Though IgM has been proposed as a potential vaccine adjuvant due to its interactions with complement, B cells and T cells [38], and IgM has been shown to enhance responses to

soluble protein [39], to the best of our knowledge, IgM has not been tested as part of any subunit vaccine formulation yet [40].

IgG1 and IgG2a are the most and second-most common antibodies found in serum [41]. Many effector functions have been associated with IgG immune complexes, including enhanced T cells responses [26], both up- and down-regulated antibody responses [27] and enhanced dendritic cell cross-presentation of antigen [42]. This may be due in part to the various Fcγ receptors that can bind IgG; at least 6 have been found in mice, and 8 in humans [43]. Since all subtypes of IgG bind to the various Fcγ receptors with varying affinities, it is difficult to draw a correlation between stimulatory and inhibitory receptors and IgG isotype. IgG1 and IgG2a have been correlated, however, as characteristic outputs of T_H2 and T_H1 immune responses, respectively [44]. In testing the IgG1 and IgG2a responses to IgG1- and IgG2a-coated nanoparticles, we assessed whether opsonized protein nanoparticles could participate in immunofeedback cycles to modulate the resulting antibody response.

For these studies, the vaccine nanoparticle core consists of model ovalbumin OVA protein nanoparticles [10, 45]. The FliC/IgM studies comparing OVA, FliC- and IgM-coated OVA nanoparticles examines (1) whether IgM could be used as a host-derived vaccine adjuvant, and (2) whether pathogen-derived adjuvants were more effective bound or unbound from antigen nanoparticles. The studies with IgG1 and IgG2a coated OVA nanoparticles (1) compare the adjuvant capabilities of IgG1 and IgG2a-coated nanoparticles, and (2) whether IgG1 and IgG2a on nanoparticles can influence the IgG1 and IgG2a antibody responses. Overall, this immunization study profiled differences in

host- and pathogen-derived adjuvant responses, and examined the adjuvant capabilities of immunoglobulin-coated nanoparticles.

5.2 Materials and Methods

5.2.1 Materials

Endotoxin-free EndoFit^{TM} ovalbumin was dissolved in sterile phosphate-buffered saline (PBS) for all nanoparticle formulations administered *in vivo*. Ovalbumin and endotoxin-free ovalbumin were purchased from Invivogen (San Diego, CA). Antibodies were purchased from Thermo Fisher Scientific (Rockford, IL) unless stated otherwise.

5.2.2 FliC Expression and Purification

The plasmid pET22b-flic was used to express recombinant FliC from *Salmonella typhimurium*[46]. The plasmid was transformed into *E. coli BL21* for expression. Transformed *E. coli* were grown in 1 L Luria Bertani (LB) broth with 100 μg/mL ampicillin from 10 mL overnight cultures. Expression was induced after approximately 2 hours ($OD_{600} \approx 0.6$) with 0.25 mM isopropyl β-D-1-thiogalactopyranoside (IPTG). Recombinant FliC was expressed over 24 h and purified using native Ni-affinity purification according to the manufacturer's instructions (Ni-NTA agarose, Qiagen, Valencia, CA). Protein concentration was assessed with a BCA assay according to the manufacturer's instructions (Thermo Fisher Scientific), and purity was assessed by SDS-PAGE and Western Blot, stained using a 488-Conjugated Penta-His antibody (Qiagen, Valencia, CA), (Figure 40).

5.2.3 Nanoparticle Synthesis and Characterization

270 nm OVA protein nanoparticle cores and OVA-coated OVA (OVA-OVA) cores were made as previously described[45]. Briefly, 0.4 mL pure ethanol was added at a constant rate to 0.1 mL of 6.2 mg/mL OVA in phosphate-buffered saline (PBS) under constant stirring at 600 rpm. The amine-reactive crosslinker 3,3'-dithiobis[sulfosuccinimidylpropionate] (DTSSP) (ThermoFisher Scientific) was used to stabilize the resulting nanoparticles. The nanoparticles were crosslinked in 0.82 mM DTSSP while stirring at room temperature for one hour, followed by centrifugation to collect the particles and resuspension in PBS by sonication.

OVA nanoparticle cores were coated with FliC by resuspension in 0.9 mg/mL FliC in PBS, and stirred at 600 rpm overnight at 4°C. Coated particles were collected by centrifugation, and resuspended in 5.26 μM DTSSP to stabilize the adsorbed coat. After stirring at 600 rpm for 1 hour at 4°C, the crosslinking reaction was quenched with 50 mM Tris base, and the particles were resuspended by sonication in PBS. A similar method was used to coat OVA cores in 6.2 mg/mL soluble OVA solution to make OVA-OVA nanoparticles.

OVA nanoparticle cores were coated with IgM or IgG by affinity immobilization. 100 μg of OVA nanoparticle cores were mixed with 17.5 μg of anti-OVA mouse IgM (Chondrex, Redmond, WA) in 0.1 mL PBS, and stirred at 4°C for 30 minutes. Binding was quenched by the addition of 24 μg soluble OVA, and the particles were collected by centrifugation and resuspended by sonication in PBS. Mouse anti-OVA IgG1 (Chondrex) or IgG2a (Chondrex and Biolegend) was used to coat OVA nanoparticle cores, OVA

nanoparticle cores made with 10% Alexa Fluor 488-conjugated OVA (Life Technologies, Grand Island, NY), or OVA-OVA cores in a similar manner with 19 μg antibody per 100 μg nanoparticles. For OVA-OVA nanoparticles, antibody density was varied by coating with 19 μg, 5 μg, or 2 μg of IgG antibodies.

To compare affinity- and non-specifically -bound IgG on the nanoparticles, IgG quenched with soluble OVA was used to make quenched IgG-OVA nanoparticles. Briefly, 10 μL of 1μg/mL IgG in PBS was incubated with an equal volume of either 10 mg/mL OVA or BSA in PBS for 2 hours at 4°C. The antibodies were then used to coat OVA cores or OVA-OVA cores by the procedure described above.

Nanoparticle size distribution and zeta potential were assessed by dynamic light scattering (DLS) and electrophoretic light scattering (ELS) respectively with a Malvern Zetasizer Nano ZS (Malvern Instruments, Westborough, MA). Nanoparticle concentration was assessed with a BCA assay according to the manufacturer's instructions (Thermo Scientific). Nanoparticles were resuspended in water, air-dried, and sputter-coated with palladium prior to visualization with a Zeiss Ultra60 FE (Carl Zeiss Microscopy, Cambridge, UK) scanning electron microscope at 5.0 kV.

5.2.4 Antibody Coating Characterization

Antibody coating was confirmed by a modified ELISA procedure. Briefly, 0.2 μg/mL nanoparticles in PBS were incubated on ELISA plates overnight at room temperature. Ig concentration was evaluated using a standard curve of serially-diluted soluble anti-OVA IgM, IgG1, or IgG2a antibodies. Samples were blocked with 1% bovine

serum albumin (BSA) in PBS, and probed with 1 μg/mL of an HRP-conjugated anti-mouse IgM, IgG1 or IgG2a antibody.

Complement activation was assessed by the MicroVue CH50 enzyme immunoassay kit (Quidel, San Diego, CA). Human serum was obtained from two, healthy, consenting donors with the approval of Georgia Institute of Technology IRB #H16083. Approximately 20 mL of blood was collected from each donor, and allowed to clot for 30 minutes at 4°C. Blood was then centrifuged at 2000xG for 10 minutes, and the serum decanted off into sterile centrifuge tubes. Serum was stored at 4°C for up to 2 weeks and at -80°C for extended storage. To activate complement, 15 μg of nanoparticles were added to 14 μL serum, and incubated for 1 hour at 37°C. Terminal complement complex (TCC) formation was assessed according to the kit manufacturer's instructions.

5.2.5 FliC Coating Characterization

FliC activity was characterized by a TLR-5-dependent luciferase activation assay *in vitro*. Hela cells (ATCC, Manassas, VA) were grown in DMEM supplemented with 10% fetal bovine serum (FBS), and cultured in humidified 5% CO_2 at 37°C. Cells were incubated overnight at a density of $2*10^6$ cells/well in a 6-well plate, and transfected the following day with 10 μg pUNO1-hTLR5, 2 μg pGL4.32-[Luc2/Nf-κB/Hygro] (Invivogen, San Diego, CA) and 15 μL Lipofectamine 2000 (Invitrogen, Grand Island, NY) in DMEM with 1% FBS. Transfected cells were plated the following day at a density of $5*10^4$ cells/well in a 96-well plate in DMEM with 1% FBS. 1 μg/mL nanoparticles were suspended in fresh DMEM + 1% FBS and used to stimulate transfected cells for 8 hours. Bright-Glo Luciferase Assay reagent (Promega, Madison, WI) was diluted 1:1 with serum-

free DMEM and used to assess luciferase activity according to the manufacturer's instructions.

5.2.6 Immunization

All animal work was compliant with the NIH Guide for the Care and Use of Laboratory Animals and all protocols and procedures employed were reviewed and approved by the Emory University and Georgia State Institutional Animal Care and Use Committees. Seven-week old female Balb/c mice (Jackson Laboratory, Bar Harbor, ME) were given 50 μL intra-muscular (i.m.) injections into the right hind-leg of 0.2 mg/mL nanoparticle formulations as described in Tables 7 and 8. Injections were repeated 21 days after priming for a boost administration.

5.2.7 Sample Collection

Blood was collected from immunized mice by submandibular venipuncture two weeks after prime and boost immunizations. Blood was allowed to clot at 4°C for at least 30 minutes, and was centrifuged at 2700xG for 5 minutes to collect serum. Serum samples were stored at -20°C for further analysis.

Following euthanasia on day 39, splenocytes were prepared from mouse spleens. Briefly, spleens extracted from mice were homogenized manually with the plunger of a 1 mL syringe and cells collected by centrifugation at 300xG for 5 minutes. Cells collected were resuspended in red blood cell lysis buffer (150 mM NH_4Cl, 10 mM NH_4HCO_3, 1 mM Na_2EDTA, pH 7.4) for 5 minutes at room temperature, quenched with RPMI 1640 media (ATCC, Manassas, VA) and centrifuged for 5 minutes at 2300xG. Splenocytes collected

were resuspended in RPMI 1640 at 4°C and counted by flow cytometry (BD Accuri c6, BD Biosciences, San Jose, CA).

5.2.8 Serum Antibody Assessment

OVA-specific IgG antibody titers were assessed by ELISA, as previously described[10]. Briefly, serial two-fold dilutions of serum were analyzed using a standard ELISA procedure, with 1 μg/mL OVA in PBS as the capture antigen, 1% bovine serum albumin (BSA) in PBS as the blocking solution, and 1 μg/mL HRP-anti-mouse IgG in 1% BSA solution as the detection antibody. Chromogenic quantification was assessed by the oxidation of tetramethylbenzidine by hydrogen peroxide (R&D Systems, Minneapolis, MN) according to the manufacturer's instructions. Two times the absorbance of naïve group's serum samples was the cutoff for measuring the endpoint titer. OVA-specific IgG1 and IgG2a concentrations were also assessed by ELISA, using HRP-conjugated anti-mouse IgG1 and IgG2a, and monoclonal mouse IgG1- or IgG2a-anti-OVA to create a standard curve (Chondrex, Redmond, WA).

5.2.9 Cytokine ELISpot

Splenocytes were seeded at a density of $2.5*10^6$ cells/mL on interferon γ (IFN-γ) and interleukin 4 (IL-4) 96-well ELISpot membranes (R&D Systems, Minneapolis, MN). Splenocytes were stimulated with or without 50 μg/mL endotoxin-free OVA, and incubated at 37°C in humidified air with 5% CO_2 for 36 hours. ELISpot membranes were developed according to the manufacturer's instructions. Wells were imaged using a dissection microscope (Olympus SZX16, Olympus Corporation, Tokyo, Japan), and spots

were counted using ImageQuant TL's colony counting software (GE Healthcare, Pittsburgh, PA).

5.2.10 Splenocyte Flow Cytometry

Splenocytes were seeded at a density of $2.5*10^6$ cells/mL on 96-well plates, and stimulated with or without 50 μg/mL endotoxin-free OVA, and incubated at 37°C in humidified air with 5% CO_2 for 60 hours. Cells were incubated with 1% bovine serum albumin (BSA) in PBS overnight at 4°C, and blocked with TruStain FcX anti-CD16/CD32 (Biolegend, San Diego, CA) at a concentration of 1 $\mu g/10^6$ cells for 1 hour on ice. Alexa-Fluor 488-conjugated anti-CD44 and Alexa-Fluor 647-conjugated anti-CD62L (Biolegend, San Diego, CA) were added to each well at a final concentration of 1 $\mu g/10^6$ cells and 0.25 $\mu g/10^6$ cells, respectively, and incubated on ice for 1 hour. Cells were collected by centrifugation, resuspended in PBS, and analyzed by flow cytometry.

5.2.11 Affinity Maturation

Affinity maturation of anti-OVA serum antibodies was measured using bio-layer interferometry with the ForteBio Octet RED96 system (Pall Corporation, Port Washington, NY). Streptavidin Dip-and-Read Biosensors were used to immobilize 50 μg/mL biotinylated-OVA (Axxora Life Sciences, San Diego, CA). OVA-loaded biosensors were incubated with serum samples diluted 1:50, 1:100, and 1:200 in PBS for 5 minutes, followed by a 5-minute incubation in PBS to measure k_{on} and k_{off} respectively. The resulting binding curves were analyzed using the Octet Data Analysis software package Version 9.0.0.4 to determine K_D values.

5.2.12 BMDC Cell Culture

Bone marrow-derived dendritic cells (BMDCs) were cultured from the femurs and tibias of 12-week old Balb/c mice [47]. Bone marrow progenitor cells were cultured in RPMI 1640 (ATCC, Manassas, VA) supplemented with 10% heat-inactivated FBS, 50 μM β-mercaptoethanol, 1% penicillin-streptomycin, 2mM sodium pyruvate, 1x non-essential amino acids (Thermo Scientific, Grand Island, NY), and 25 ng/mL each of IL-4 and GM-CSF (Peprotech, Rocky Hill, NJ). Cells were matured for one week, and the media was changed on days 2, 4 and 6. On Day 7, cells were harvested by scraping and plated at a density of $2*10^4$ cells/well in 96-well plates for experiments.

5.2.13 BMDC Uptake of Nanoparticles

BMDCs were incubated with IgG1- and IgG2a-coated OVA nanoparticles to examine nanoparticle uptake [47]. For uptake studies, BMDCs were pre-incubated with or without 2 μg/mL anti-CD16/32 TruStain FcX Fc blocker (Biolegend) for 15 minutes at room temperature, and were then incubated with 20 μg/mL fluorescent IgG1- and IgG2a-coated OVA nanoparticles for 3 hours at 37°C. Cells were scraped from the wells, collected by centrifugation, and resuspended in chilled trypan blue to quench external fluorescence. Cells counts and fluorescence was recorded by flow cytometry (BD Accuri).

5.2.14 TNF-α Secretion and CD86 Upregulation

BMDCs were incubated with 20 μg/mL of high, medium, and low density IgG-coated OVA-OVA nanoparticles for 24 hours at 37°C. Supernatants were collected and assayed for TNF-α by ELISA according to the manufacturer's instructions (R&D Systems).

Cells were collected by scraping, and resuspended in 1% BSA in PBS at 4°C overnight to block non-specific blocking. Cells were incubated with 1 μg/mL anti-CD16/32 TruStain FcX (Biolegend) for 1 hour on ice, and stained with 1 μg/mL Alexa Fluor 647-conjugated anti-CD86 (clone GL-1, Biolegend) for 1 hour. Cells were collected by centrifugation, resuspended in PBS, and analyzed by flow cytometry (BD Accuri).

5.2.15 Statistical Analysis

Serum antibody titers were analyzed using the Mann-Whitney U test. Antibody concentrations and T cell counts were analyzed using one-way ANOVA followed by Sidak's multiple comparisons test. Comparisons between two groups were performed using Student's t test, while comparisons between multiple groups was performed by one-way ANOVA followed by Sidak's multiple comparisons test. All statistical analyses were conducted using GraphPad Prism 6 (GraphPad, La Jolla, CA). P values of $p < 0.05$ were considered statistically significant (* = $p < 0.05$, ** = $p < 0.01$). To test our hypotheses for the IgM and FliC studies, statistical comparisons were assessed between G1 and G3, between G2 and G4, and for T cell counts, between G6 and all other groups. Comparisons between these groups that were significant are noted in the figures, while comparisons that were not significant are not shown.

5.3 Results

5.3.1 Flagellin Expression and Purification

Recombinant flagellin was expressed in *E. coli* BL21 and purified by Ni-NTA affinity chromatography. An SDS-PAGE gel shows a single band in the elution indicating purity, and a western blot indicates the 55 kDa band is the flagellin.

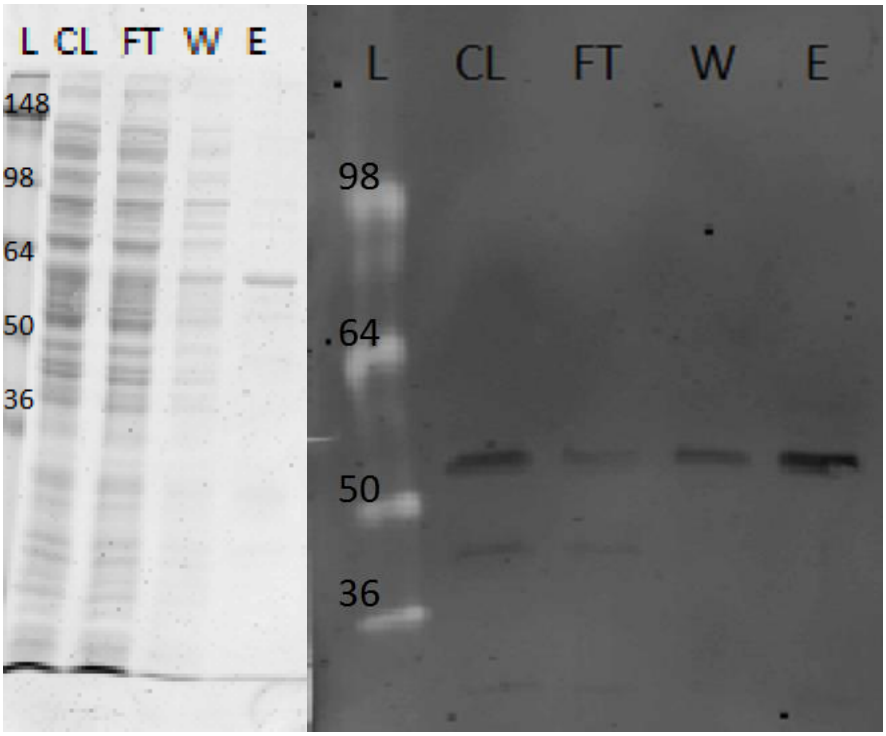

Figure 40. SDS-PAGE (left) and Western blot (right) run after Ni-affinity purification of recombinant FliC. CL = Cleared lysate, FT = Flow-through post-Ni-NTA loading, W = Wash, E = Elution.

5.3.2 Coated Nanoparticle Synthesis and Characterization

Monodisperse, 270 nm OVA nanoparticle cores and OVA-coated OVA nanoparticles (OVA-OVA nanoparticles) were made as previously described in Chapter 3 [45]. Coating the nanoparticles did not significantly alter nanoparticle size (Table 6). IgM-

coating of the nanoparticles without a soluble OVA quenching step resulted in large, 1000 nm particles, suggesting IgM crosslinking of multiple nanoparticles (Figure 41). Coating of FliC and Ig on OVA nanoparticles was assessed by FliC supernatant depletion and by anti-Ig ELISA, respectively. Coverage was reported as an approximate mass adjuvant per mass OVA. SEM images of nanoparticles were consistent with post-processing shrinkage of nanoparticles in comparison to DLS sizes (Figure 42) [47].

Table 6. Physical characterization data of the different nanoparticles synthesized.

1A	Size (nm)	Zeta Potential (mV)	Other Info
OVA-OVA NPs	270 ± 88 nm	-14.4 ± 1.5	Core Yield: 92%
OVA-FliC NPs	255 ± 92 nm	-10.7 ± 0.8	Coating Coverage: 15% mass FliC/mass OVA
OVA-IgM NPs	265 ± 119 nm	-12.0 ± 0.7	Coating Coverage: 0.5% mass IgM/mass OVA
OVA-IgG1 NPs	232 ± 95 nm	-11.0 ±0.95	Coverage: 55% mass IgG1/mass OVA
OVA-IgG2a NPs	245 ± 104 nm	-12.1 ± 0.96	Coverage: 1.75% mass IgG2a/mass OVA

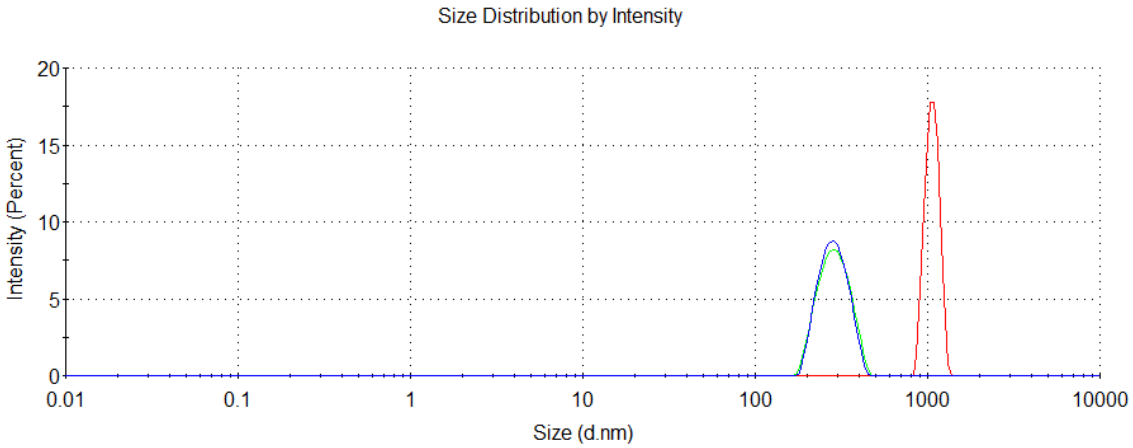

Figure 41. Preliminary coating of OVA nanoparticles (green) with anti-OVA IgM resulted in the formation of microparticles (red), suggesting crosslinking of OVA nanoparticles by the pentameric IgM. Quenching the coating process by addition of soluble OVA following IgM resulted in no change in nanoparticle size (blue).

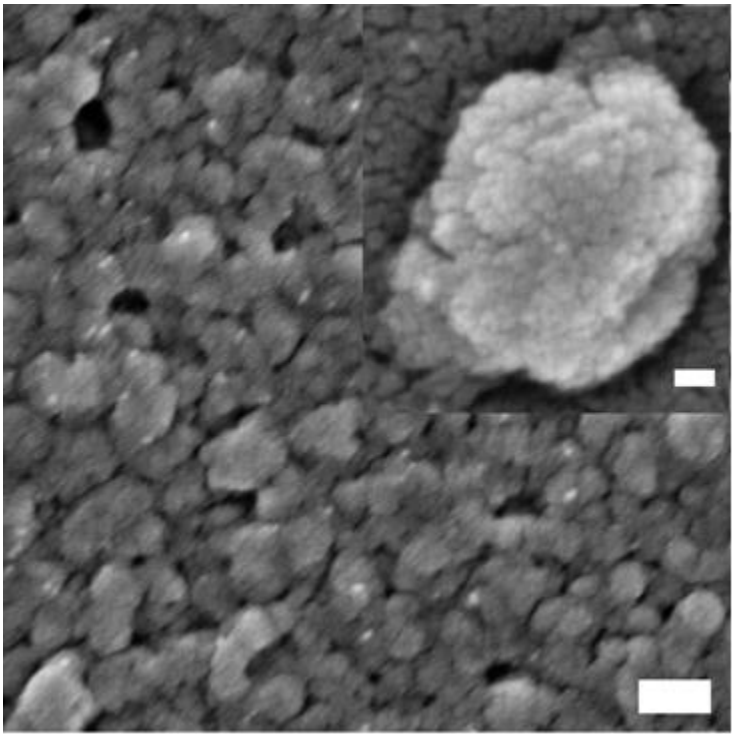

Figure 42. Representative scanning electron micrograph of OVA-coated-OVA nanoparticles. Outer scale bar, 200 nm. Inset scale bar, 30 nm.

5.3.3 Coat Activity

Coat activity was confirmed by testing FliC and Ig functionality. Since FliC is a TLR-5 agonist, FliC-coated nanoparticles were used to activate a TLR-5-dependent luciferase assay. FliC-coated OVA nanoparticles activated TLR-5 signaling, and did not significantly differ in activity compared to soluble FliC admixed with OVA nanoparticles (Figure 43). IgM's ability to activate complement was assessed by incubating IgM-coated nanoparticles with human serum and using ELISA to detect activated complement [34]. Uncoated OVA nanoparticles were found to activate complement, and the IgM coating on these particles did not significantly enhance complement activation (Figure 44A). IgG1 nanoparticles did not significantly enhance complement activation, while IgG2a did (Figure 44B).

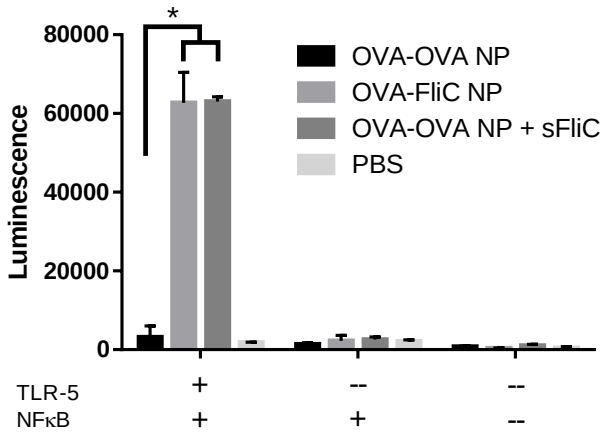

Figure 43. OVA-FliC nanoparticles and OVA-OVA nanoparticles with soluble FliC (sFliC) admixed demonstrated similar levels of TLR-5-dependent NFκB activation in Hela cells as compared to OVA-OVA nanoparticles. Each bar is an average of two technical replicates (n = 2).

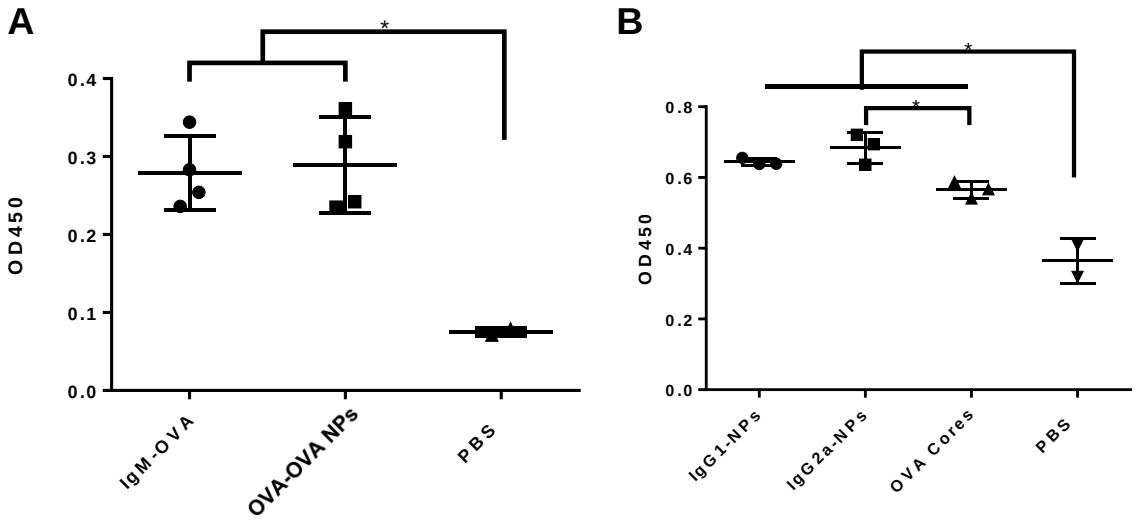

Figure 44. Complement activation as determined by anti-TCC ELISA after mixing nanoparticles with human serum. IgM-coated OVA nanoparticles, IgG1 coated, and uncoated OVA nanoparticles demonstrated similar levels of complement activation. (* = p < 0.05)

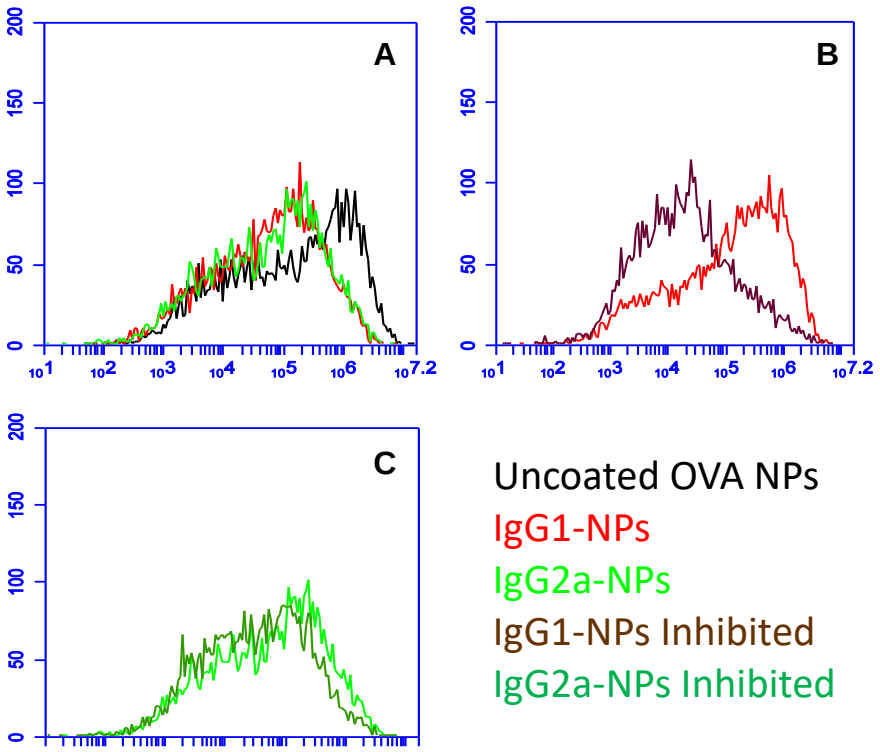

Figure 45. Fluorescent uptake of IgG-coated nanoparticles. (A) Uncoated OVA nanoparticles compared to IgG-coated OVA nanoparticles, (B) IgG1-coated OVA nanoparticles in the presence/absence of Fc blockers,(C) IgG2a-coated OVA nanoparticles in the presence/absence of Fc blockers.

5.3.4 IgG-coated OVA Nanoparticle Uptake

IgG-coated nanoparticles were taken up by BMDCs to a lesser extent than uncoated OVA nanoparticles (Figure 45A). Furthermore, uptake of these nanoparticles was reduced in the presence of an FcγR-blocking antibody, indicating an FcγR-mediated uptake pathway was being utilized by the IgG-coated OVA nanoparticles (Figure 45B, C).

5.3.5 TNF-α Secretion to IgG-Coated OVA Nanoparticles

TNF-α secretion by BMDCs after 24 hours of IgG-coated OVA nanoparticle stimulation was assessed. IgG1-coated nanoparticles induced significantly higher TNF-α responses than uncoated OVA nanoparticles, while IgG2a-coated nanoparticles did not (Figure 46). IgG1 immune complexes (IgG1-IC) induced significantly less TNF-α than IgG1-coated nanoparticles did. IgG2a ICs and IgG2a-coated nanoparticles were not statistically different.

5.3.6 CD86 Upregulation in Response to IgG-Coated OVA Nanoparticles

BMDC upregulation of CD86 after 24 hours of stimulation was also measured. All types of nanoparticles, uncoated and IgG coated, triggered an approximately 5-fold increase in the population of $CD86^+$ cells (Figure 47).

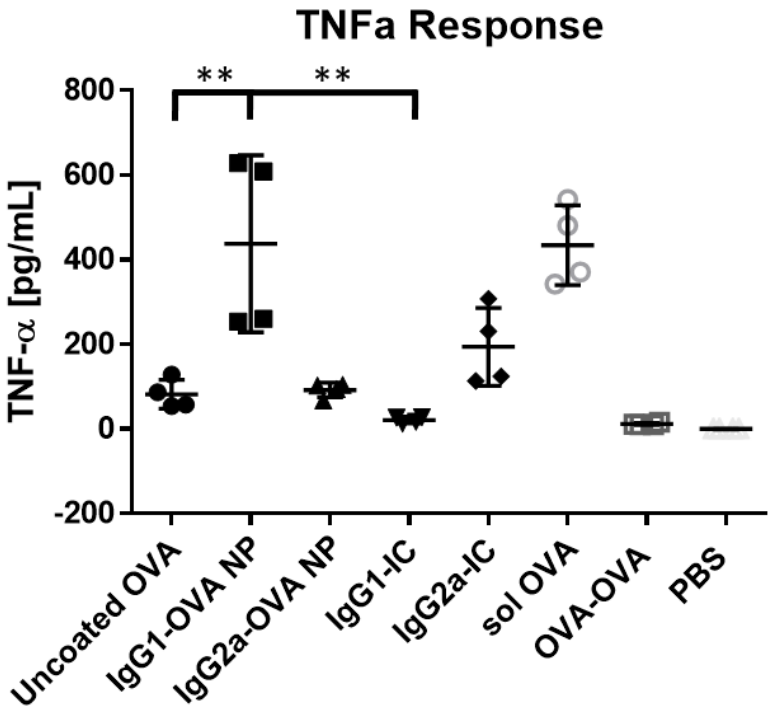

Figure 46. TNF-α secretion by BMDCs after 24 hours of stimulation by IgG1- or IgG2a-coated OVA nanoparticles. IgG1 and IgG2a complexed with soluble antigen (IgG1-IC and IgG2a-IC) were also assessed.

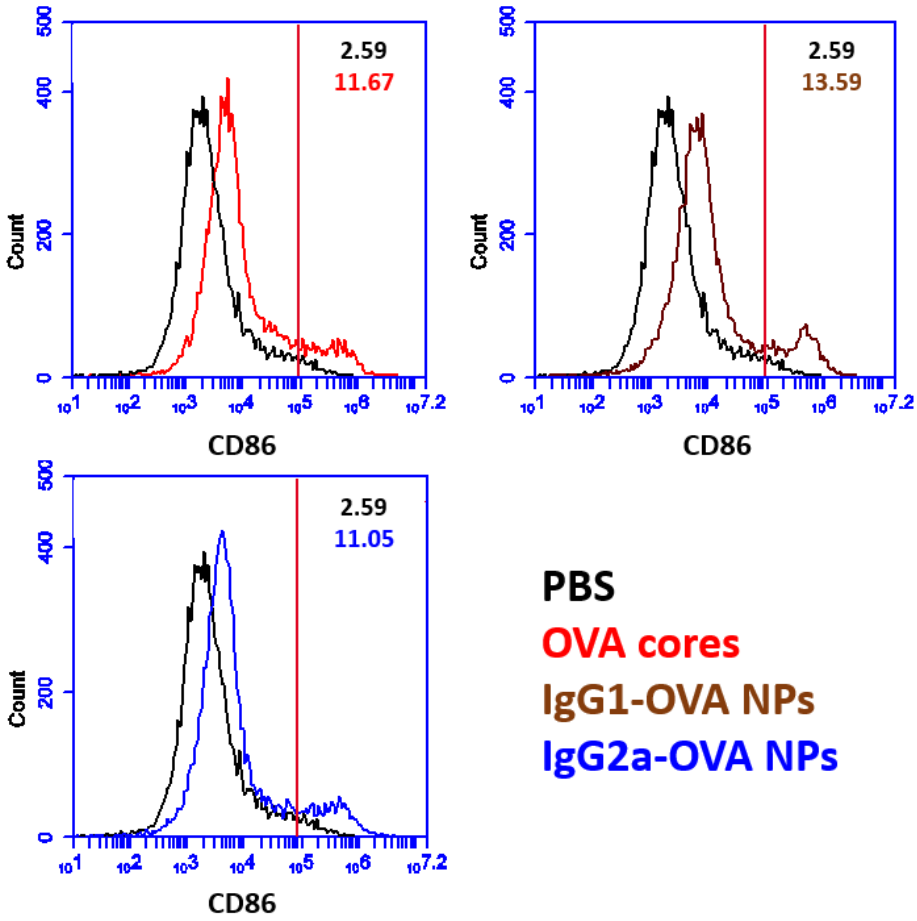

Figure 47. CD86 upregulation in response to BMDC stimulation with OVA core nanoparticles or IgG-coated OVA nanoparticles. Color-coded numbers in the top right of each graph indicate the percentage of the population above the red threshold. Each trace consists of 10,000 cells measured.

5.3.7 Antibody Production

Anti-OVA serum IgG titers were assessed two weeks after priming and boosting (Table 7, Table 8). Following the priming immunization, OVA-IgM nanoparticles (Figure 48, G3) induced non-zero responses in all mice, and induced significantly greater responses than OVA-coated OVA nanoparticles (Figure 48, G1, left). Following a boost immunization of the same formulations, the IgG titers were not significantly different among the groups (Figure 48, right). No significant differences in titer were observed

between OVA-FliC nanoparticles (G2) and OVA nanoparticles admixed with soluble FliC (G4). All groups in the IgG study triggered non-zero antibody responses after the first immunization. No groups had significantly different titers from each other after the prime or boost immunization (Figure 49).

Table 7. Immunization groups and sample collection schedule for the FliC and IgM study. Each group had 5 mice.

	Prime Day 0	Bleed Day 14	Boost Day 21	Bleed Day 36	Sacrifice Day 39
G1: OVA-OVA NPs					
G2: OVA-FliC NPs					
G3: OVA-IgM NPs					
G4: OVA NPs + sFliC					
G5: OVA-FliC and OVA-IgM					
G6: PBS					

Table 8. Immunization groups and sample collection schedule for the IgG study. Each group had 5 mice.

	Prime Day 0	Bleed Day 14	Boost Day 21	Bleed Day 36	Sacrifice Day 39
G7: OVA NPs					
G8: OVA-IgG1 NPs					
G9: OVA-IgG2a NPs					
G10: OVA-IgG1 + OVA IgG2a NPs					
G11: PBS					

FliC/IgM Study Serum Antibody Titers

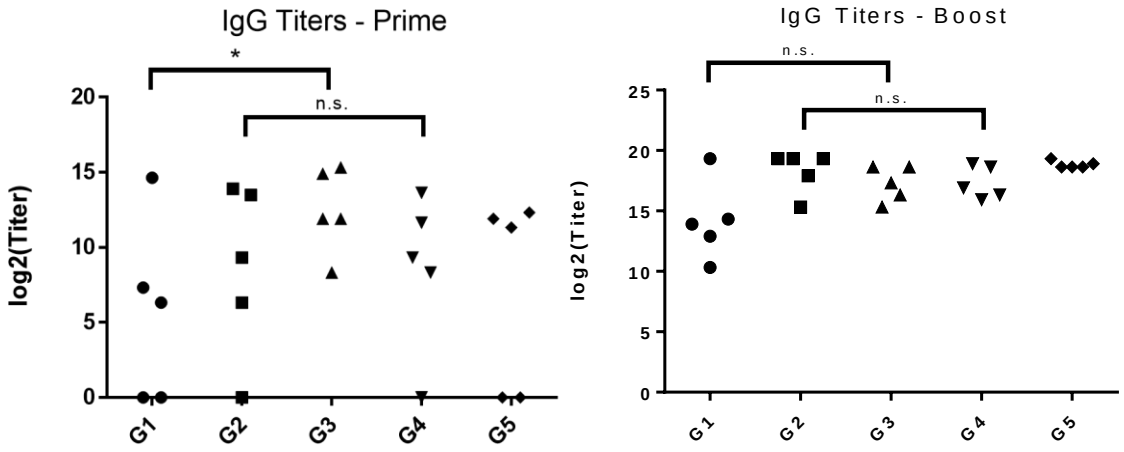

Figure 48. Anti-OVA IgG titers were assessed two weeks after priming (left) and boosting (right) immunizations. Group numbers on the x-axis correspond to the groups in Table 7. Each data point is the average titer of two technical replicates, and titers were assessed for each of the 5 mice per group. (* = p < 0.05)

IgG1/IgG2a Study Serum Antibody Titers

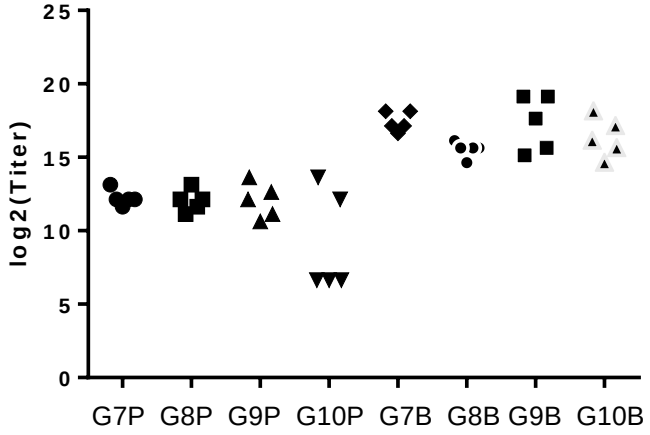

Figure 49. Anti-OVA IgG titers were assessed two weeks after priming (left) and boosting (right) immunizations. Group numbers on the x-axis correspond to the groups in Table 8. Each data point is the average titer of two technical replicates, and titers were assessed for each of the 5 mice per group.

5.3.8 Serum IgG Subtype Responses

Anti-OVA IgG subtype concentrations were also assessed after priming and boosting. OVA-IgM nanoparticles induced significantly higher levels of IgG1 than OVA-OVA nanoparticles did after both priming and boosting (Figure 50A, B, G3). Appreciable IgG2a responses only appeared after the boost immunization in all adjuvanted nanoparticle groups (Figure 50C, D). No significant differences were observed between OVA-FliC nanoparticles and OVA nanoparticles admixed with soluble FliC (Figure 50, G2 and G4).

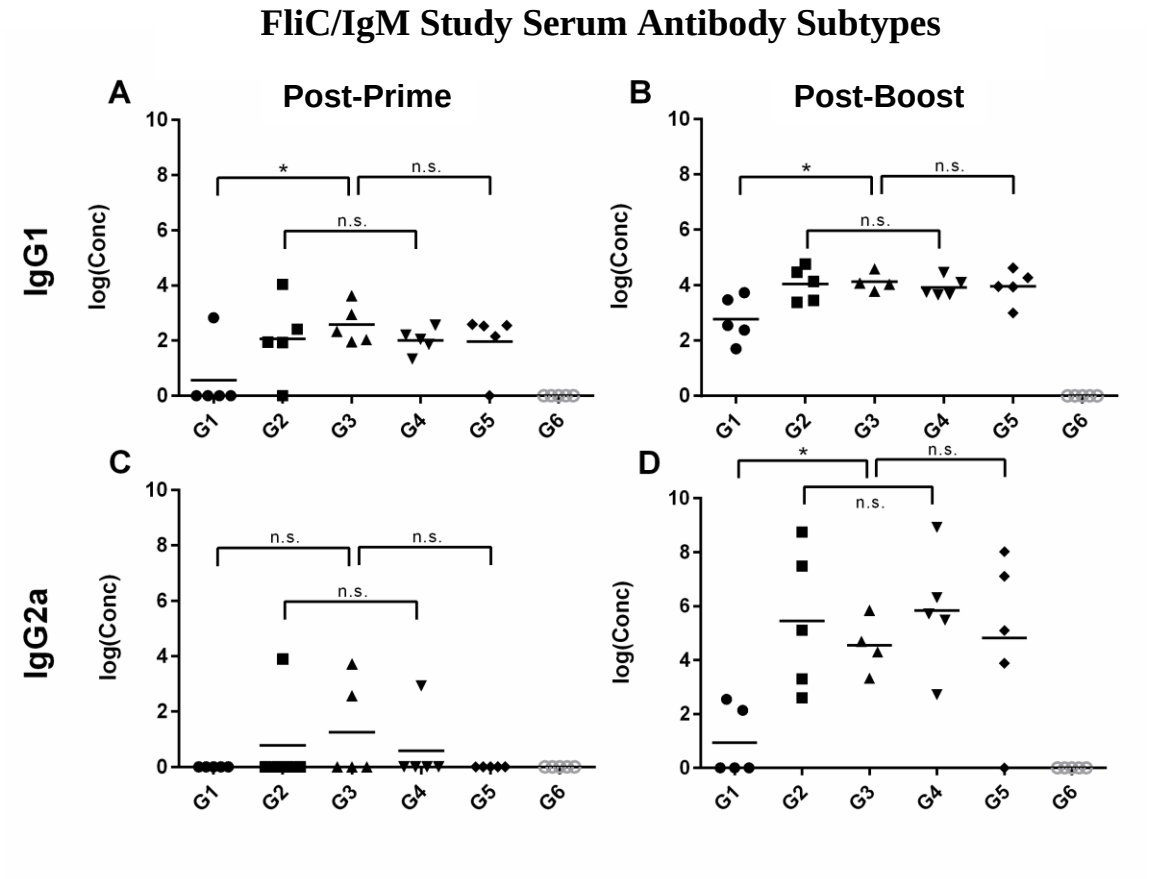

Figure 50. Anti-OVA serum antibody concentrations of IgG1 and IgG2a, as assessed by ELISA from the FliC/IgM study. Each point represents the average concentration as determined by two technical replicates. (* = $p < 0.05$)

IgG subtype differences were also characterized in response to IgG nanoparticles. No significant differences were observed in IgG1 production after a prime or boost administration of IgG-coated nanoparticles (Figure 51A, B). While IgG2a responses post-prime were minimal (Figure 51C), IgG2a responses post-boost were significantly reduced in response to co-administered Ig1-coated and IgG2a-coated nanoparticles, as compared to uncoated and IgG2a-coated nanoparticles (Figure 51D). Uncoated OVA nanoparticles also induced significantly greater IgG2a responses post-boost than IgG1 nanoparticles did.

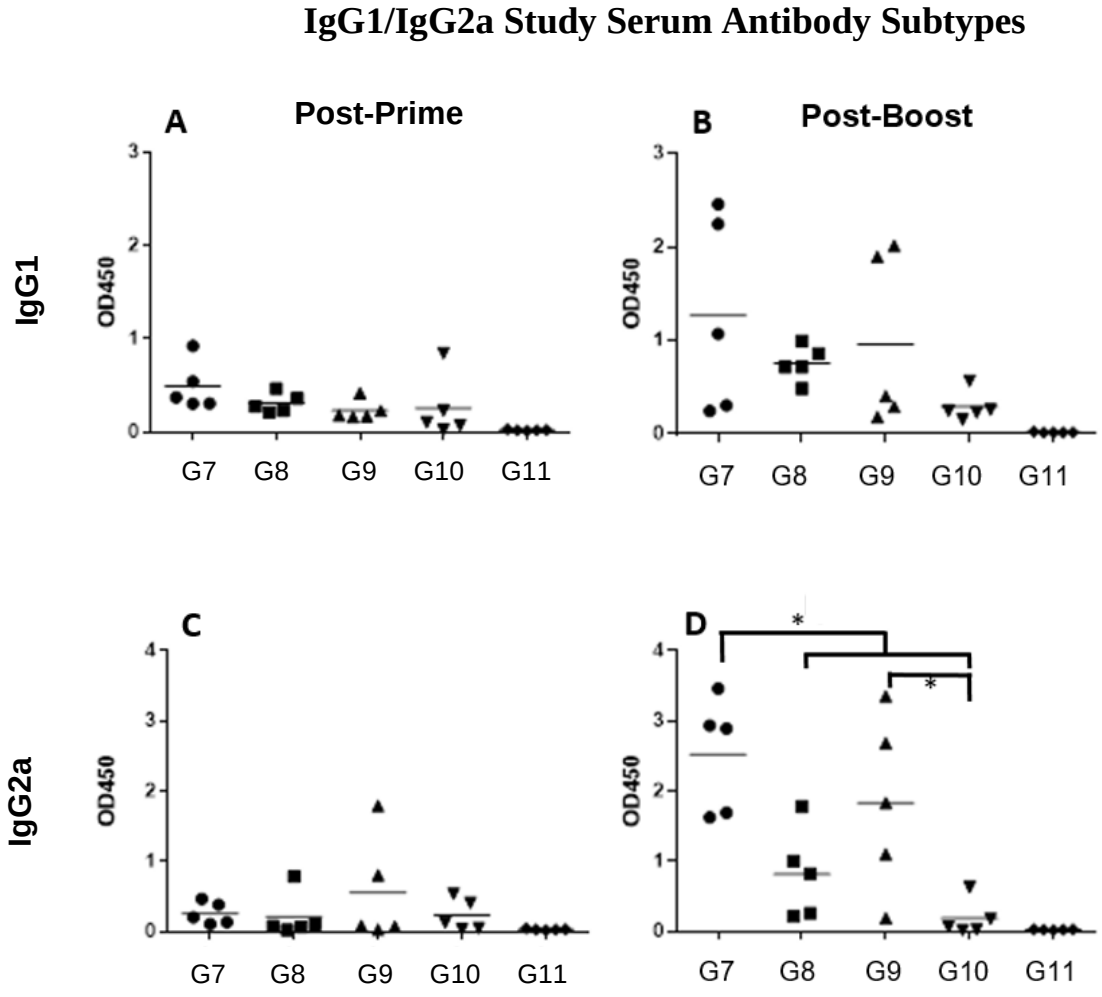

Figure 51. Anti-OVA serum antibody concentrations of IgG1 and IgG2a, as assessed by ELISA from the IgG study. Each point represents the average OD450 as determined by two technical replicates.

5.3.9 T Cell Cytokines

ELISpot was used to examine the ability of OVA-stimulated splenocytes from immunized mice in the FliC/IgM study to produce IFN-γ and IL-4. Both OVA-IgM (Figure 52, G3) and OVA-FliC + OVA-IgM (G5) immunized mice produced significant amounts of IFN-γ-secreting splenocytes. OVA+sFliC (G4) and OVA-FliC + OVA-IgM (G5) immunized mice produced significant amounts of IL-4 (Figure 52, right).

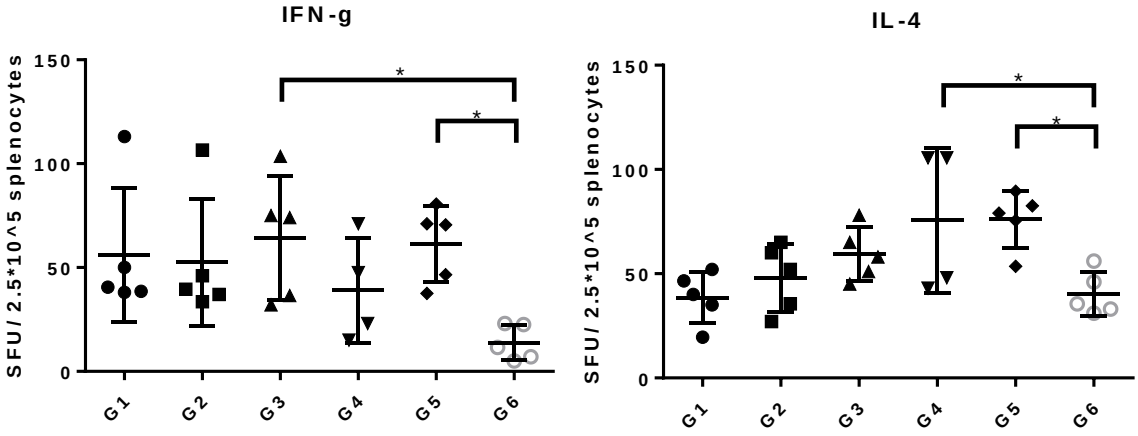

Figure 52. IFN-γ (left) and IL-4 (right) -secreting T-cell counts in $2.5*10^5$ splenocytes post-stimulation with 50 µg/mL OVA. Each data point is an average of two technical replicate counts. (* = $p < 0.05$)

5.3.10 Memory T Cell Expansion

OVA-stimulated and unstimulated splenocytes were stained for CD44 and CD62L and assessed by flow cytometry to profile memory T cell activation. $CD44^+/CD62L^+$ double-positive T cells are indicative of central memory T cells, while $CD44^+/CD62L^-$ single-positive cells are indicative of effector memory phenotypes[48]. Normalizing the number of stimulated, positive cells by the number of unstimulated, positive cells allowed us to report a fold change in the number of positive cells. We found that OVA-IgM

nanoparticles (Figure 54, left, G3) induced a significant upregulation of central memory T cells, and no particle types induced appreciable upregulation of effector memory T cells (Figure 54, right). None of the nanoparticle types induced significant upregulation of either type of memory T cell in the IgG study (Figure 53).

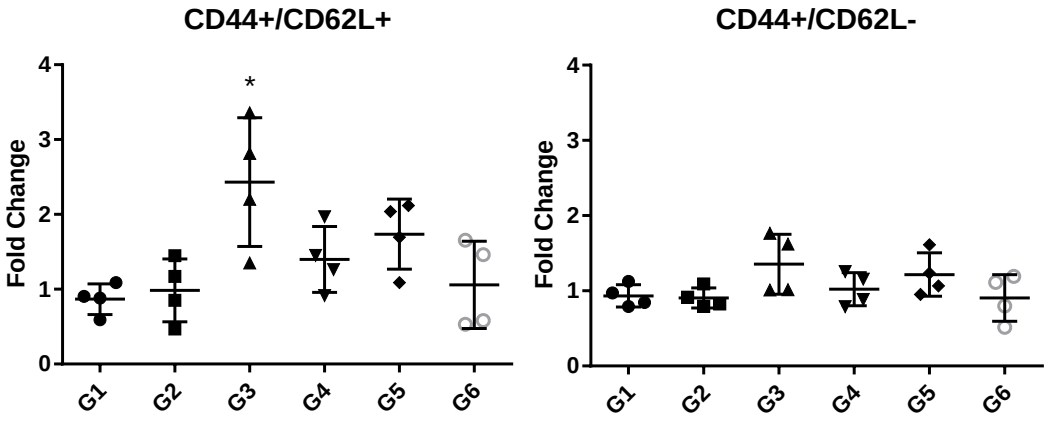

Figure 54. Memory T cell expansion from the FliC/IgM study. Fold change of $CD44^+/CD62L^+$ (left) and $CD44^+/CD62L^-$ (right) splenocytes after stimulation with 50 µg/mL OVA. Each data point is the ratio of the average number of positive cells in a stimulated vs an unstimulated sample of splenocytes. Each average was derived from two technical replicate samples of 10,000 cells each. Example gating is shown in (Figure 55). (* = $p < 0.05$ in comparison to G6)

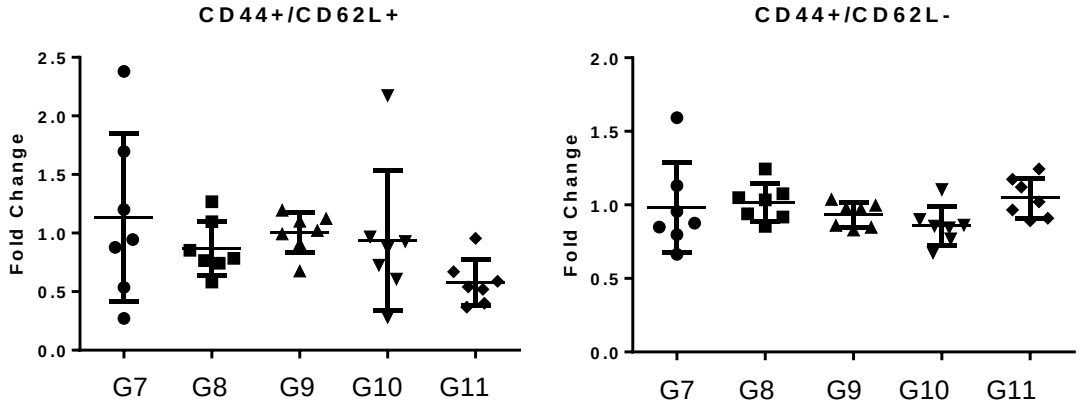

Figure 53. Memory T cell expansion from the IgG study. Fold change of $CD44^+/CD62L^+$ (left) and $CD44^+/CD62L^-$ (right) splenocytes after stimulation with 50 µg/mL OVA. Each data point is the ratio of the average number of positive cells in a stimulated vs an unstimulated sample of splenocytes. Each average was derived from two technical replicate samples of 10,000 cells each. Example gating is shown in (Figure 55).

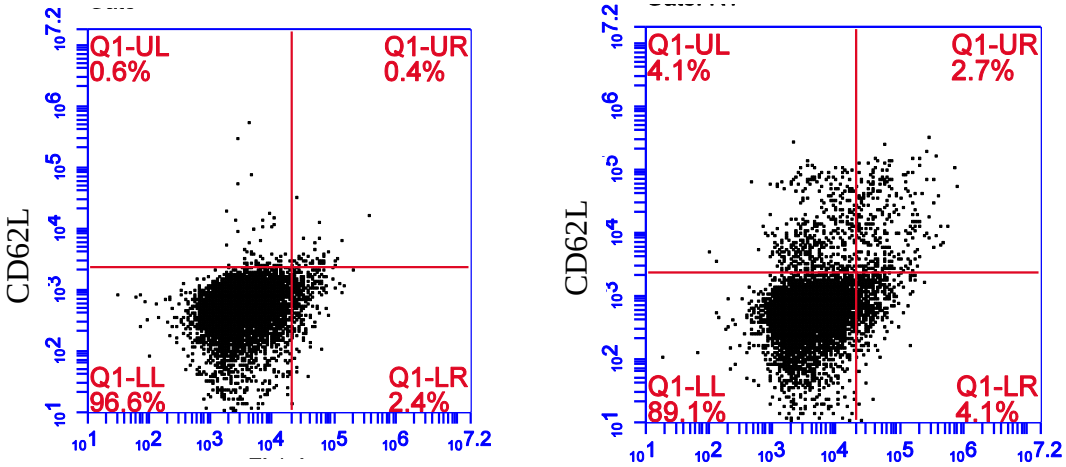

Splenocytes from PBS control mice(G6)

Splenocytes from IgM-NP-immunized mice

Figure 55. Example gating used on splenocytes from immunized mice. Numbers of cells considered double-positive in calculations for Figure 54 and Figure 53 were counted from the upper right quadrant of all samples.

5.3.11 Affinity Maturation

Anti-OVA antibody affinity in sera from the FliC/IgM study was measured with the Octet RED system. Average log(K_D) values for post-prime and post-boost sera were compared to test for affinity maturation. Significant affinity maturation was found in mice immunized with OVA-OVA nanoparticles (Figure 56, G1) and OVA-FliC (G2) nanoparticles ($p < 0.01$) but not in mice immunized with OVA-IgM nanoparticles (G3), OVA-OVA + sFliC (G4), or OVA-IgM+ OVA-FliC (G5).

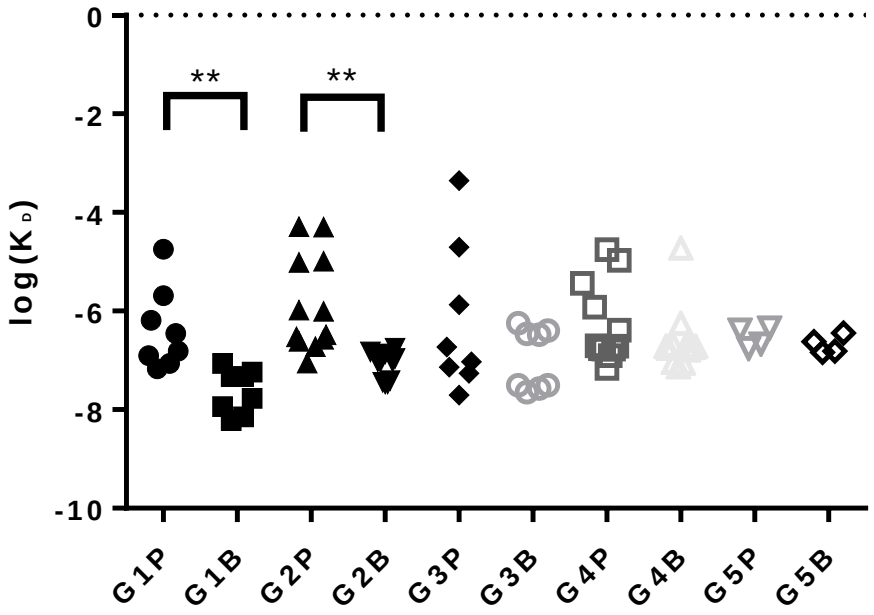

Figure 56. Affinity maturation as assessed by bio-layer interferometry. Each point consists of a K_D value derived from a single association-dissociation run on the Octet RED96. Each column contains K_D values obtained from sera from a particular group post-prime (G#P) or post-boost (G#B). Replication was assessed over 3 dilutions of 4 different serum samples (n = 12). Group 5 was assessed at only two dilutions of two serum samples (n = 4).

5.3.12 Varying IgG Density on OVA-OVA Nanoparticles

The low density of IgG2a coated on OVA nanoparticles in comparison to IgG1 (Table 6) motivated us to examine coating OVA-OVA nanoparticles as a way of increasing antibody density, instead of "bare" desolvated OVA nanoparticles. An additional layer of OVA on the nanoparticles' surface increases epitope availability as determined by polyclonal antibody binding (Figure 16, right), and should therefore enhance monoclonal antibody binding as well. We also looked at coating different amounts of IgG on OVA-OVA nanoparticles to test whether IgG density had an effect on BMDC activation. Coating with 19 μg and 5 μg of antibody revealed no significant difference in surface IgG, but coating with 2μg of IgG resulted in significantly less surface antibody (Figure 57).

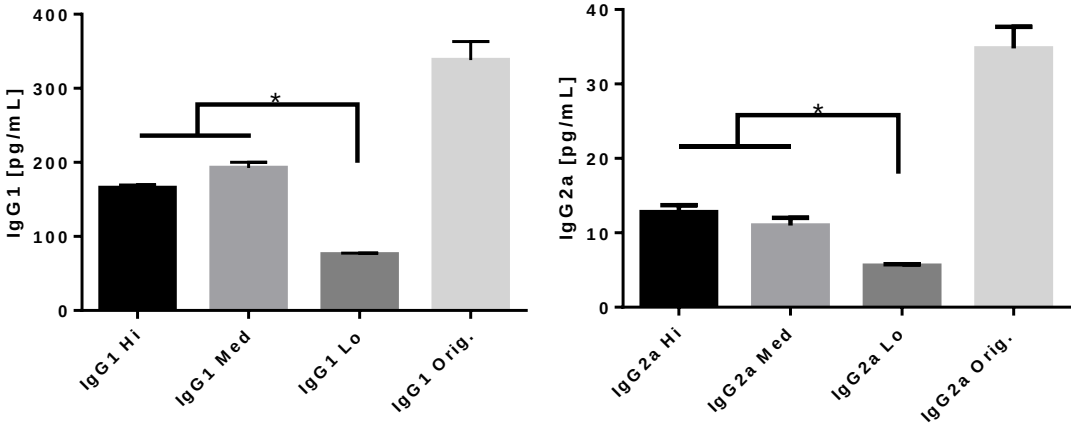

Figure 57. IgG density on OVA-OVA nanoparticles was measured by ELISA. Error bars represent the standard deviation of three technical replicates (* = $p < 0.05$). IgG coated on bare OVA cores (IgG Orig.) is included for reference.

All OVA-OVA nanoparticles had less IgG on the surface than uncoated OVA cores did (Figure 57). Despite this, all forms of IgG-coated OVA-OVA nanoparticles were able to induce strong TNF-α responses in BMDCs (Figure 58). In particular, IgG2a-coated OVA-OVA particles of all coating densities triggered significantly stronger IgG responses compared to IgG2a-coated OVA nanoparticles (Figure 58).

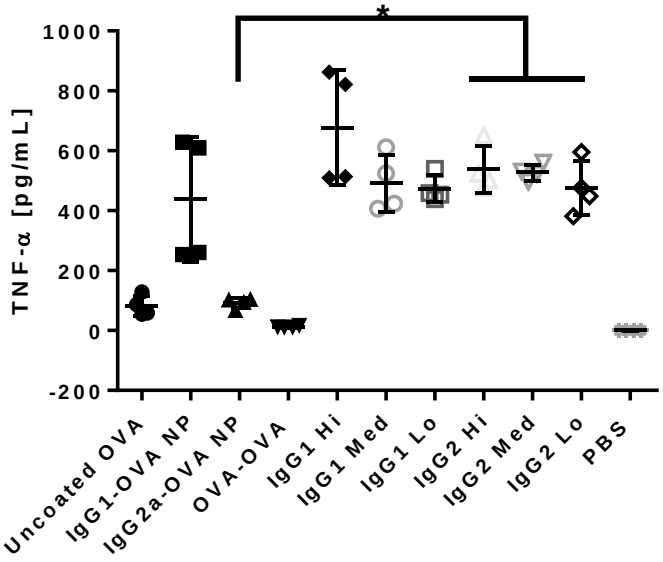

Figure 58. IgG1 and IgG2a coated at high, medium and low densities on OVA-OVA nanoparticles were used to stimulate BMDCs, and TNF-α was assessed by ELISA. Error bars represent the standard deviataion of 4 technical replicates. (* = $p < 0.05$)

5.3.13 IgG Adsorption versus Binding

To test whether OVA nanoparticles were non-specifically adsorbing IgG, antibodies were pre-incubated with soluble OVA first, then used to coat nanoparticles. With the Fab region of the antibodies blocked by soluble OVA, no antibodies should bind specifically, and any antibodies on the nanoparticle surface must be non-specifically adsorbed. At the same time, unquenched IgG is able to bind nanoparticles with its Fab region, and any difference in binding between unquenched and quenched IgG must be due to affinity-bound antibody. On both uncoated and coated OVA nanoparticles, non-specific IgG binding constituted a large portion of the antibodies on our nanoparticles (Figure 59). However, on OVA-OVA nanoparticles, we saw significant differences in antibody binding between quenched and unquenched antibodies, indicating significant amounts of properly-

bound antibody were obtained on the surface of coated OVA nanoparticles (Figure 59, right).

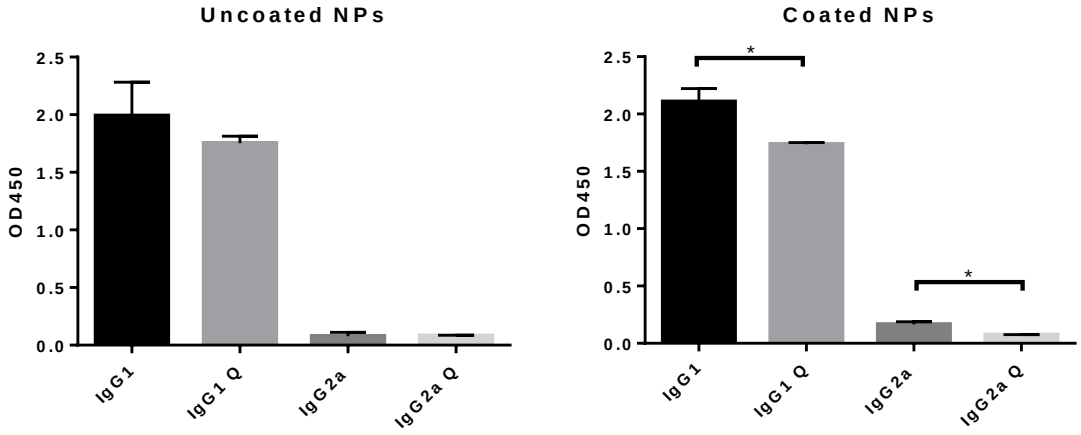

Figure 59. Uncoated OVA nanoparticles and OVA-OVA nanoparticles were coated with anti-OVA IgG or IgG-OVA immune complexes (IgG Q). Error bars represent the standard deviation of 3 technical replicates (* = $p < 0.05$)

5.4 Discussion

In Chapter 3, we found protein nanoparticle coating can alter dendritic cell inflammatory responses[45]. In addition to coating our nanoparticles with antigen, the studies in this chapter explore the *in vivo* immune responses to FliC, IgM, and IgG adjuvant coatings on nanoparticles.

5.4.1 Flagellin-Mediated Adjuvancy

When OVA-FliC nanoparticles and OVA nanoparticles admixed with soluble flagellin were used to immunize mice, both groups developed similar levels of anti-OVA IgG titers (Figure 48) and serum anti-OVA IgG1/IgG2a concentrations (Figure 50). Our FliC-coated nanoparticles elicited comparable antibody titers to other FliC-adjuvanted

nanovaccines [17, 49]. The production of high IgG2a levels after the boost immunization is consistent with other literature showing FliC on nanoparticles generates a T_H1-biased response[17]. However, the most drastic difference between the two forms of FliC adjuvant presentation was that affinity maturation of anti-OVA serum antibodies was triggered by OVA-FliC nanoparticles, but not by OVA nanoparticles with soluble FliC.

The phenomena of affinity maturation and class switching have classically been reported in the literature to occur in parallel upon immunization or infection[7]. To the best of our knowledge, only recently have the two phenomena been studied independently of one another[50]. Our observation that different modes of FliC presentation lead to differences in affinity maturation while not affecting class switching to IgG2a supports growing evidence that adjuvant presentation method can influence the resulting immune response[51]. Further work should examine whether affinity maturation is mediated by surface presentation of other TLR-based adjuvants on nanoparticles as well, since nanoparticles can facilitate ligand access to certain intracellular TLRs. A broader study of soluble vs nanoparticle-bound TLR ligands can also address whether stimulation of antigen-internalizing APCs or downstream immune effector cells is more immunogenic on an adjuvant-by-adjuvant basis.

5.4.2 IgM as a Host-Derived Adjuvant

Potential safety issues have been raised for TLR ligand-based adjuvants that may dissociate or diffuse away from the antigen[6]. Unlike FliC, host-derived IgM that may dissociate from the nanoparticles is probably not going to be seen as immunogenic as

soluble FliC, and thus an OVA nanoparticle + soluble IgM group was not included in the study design.

Antibodies have been proposed as host-derived adjuvants before[38, 52]. Most of these studies have been with soluble immune complexes consisting of soluble antigen bound to a cognate antibody[53, 54]. This strategy targets the antigen to Fc receptor-bearing antigen presenting cells, yet does not exploit a second feature of antibody-mediated adjuvancy – the activation of complement.

Complement activation can be triggered by the proximity of two IgG Fc domains, or one IgM Fc domain exposed upon antigen binding[36]. Activation of complement is necessary for vaccination not only as an innate host defense mechanism[7], but also for bridging innate and adaptive immune responses[55]. Triggering complement activation may further enhance the potency of immunoglobulin-adjuvanted vaccines, and the nanoparticle antigen delivery platform is well-suited to mediate this effect.

The IgM-coated OVA particles did not trigger significant complement activation as compared to uncoated OVA nanoparticles (Figure 44). While strategies for enhancing IgM density on the particle surface may increase the likelihood of stronger complement activation, OVA-IgM nanoparticles still significantly enhanced antibody and T cell responses even in the absence of significant complement activation.

Anti-OVA IgG endpoint titers significantly increased after one immunization with OVA-IgM nanoparticles, as compared to unadjuvanted OVA-OVA nanoparticles. Following the boost immunization, OVA-IgM nanoparticles induced elevated levels of IgG2a, whereas unadjuvanted OVA nanoparticles did not. Unexpectedly, unadjuvanted

OVA-OVA nanoparticles induced affinity maturation of antibodies, whereas OVA-IgM nanoparticles only triggered IgG2a antibody class switching and not affinity maturation. The inverse relationship between these phenomena has, to the best of our knowledge, never been reported before. If IgM could trigger a diversification of antibody effector functions, while at the same time preserving a pool of B cells that have not over-matured in their response to a particular antigen, IgM could be used to combat original antigenic sin. This phenomenon occurs when antibodies raised against an initial exposure of antigen are poorly protective against a slightly mutated version, and is a challenge in developing vaccines against highly mutable pathogens, such as influenza.

The strong IgG2a responses elicited by IgM were supported by the high levels of IFN-γ-producing T cells, both indicators of a strong T_H1 response. The T_H1 and T_H2 responses are mutually inhibitory[56], and during many infections, one response can be protective while the other can be fatal. The T_H1 response is induced in response to viral and bacterial infections[7], and therefore priming a T_H1-biased T cell response with anti-viral and anti-bacterial vaccines is critical for successful immunization.

Since successful vaccination requires immunological memory, the generation of memory T cell responses is crucial. CD44 and CD62L can be used to identify central memory T cells (T_{CM}, $CD44^+/CD62L^+$) and effector memory T cells (T_{EM}, $CD44^+/CD62L^-$)[20]. OVA-IgM nanoparticles stimulated strong T_{CM} differentiation (Figure 54) whereas the other nanoparticle formulations, including those with FliC, could not. This supports the case for IgM as an adjuvant for promoting cell-mediated immunity. However, none of the nanoparticle formulations induced strong T_{EM} responses (Figure 54), indicating that the nanoparticles and adjuvants used were unable to completely polarize the T cell response to

a T_H1 or T_H2 response[57]. These results are in contrast with those by Zhang et al., who found that immunizing mice with antigen encapsulated and admixed with PLGA nanoparticles triggered strong T_{EM} but not T_{CM} responses [20].

In the group combining both OVA-FliC and OVA-IgM particles (G5), we saw high IFN-γ production characteristic of OVA-IgM nanoparticles, low central memory T cell production characteristic of OVA-FliC nanoparticles, and high IL-4 production, which was uncharacteristic of either component nanoparticle alone. Although the benefits of combining these two types of adjuvanted nanoparticles are not immediately obvious, there is a synergistic effect as evidenced by the IL-4 response. Other work has shown that delivery of two types of adjuvants in separate particles elicits greater effects compared to adjuvant co-delivery in the same particle[9].

5.4.3 Challenges with IgG as an Adjuvant

IgG2a-coated nanoparticles triggered significantly greater complement activation than uncoated OVA particles, which is consistent with literature describing IgG2a but not IgG1 as a complement-activating antibody subtype [52]. Although IgG1-coated nanoparticles significantly enhanced BMDC TNF-α production in comparison to uncoated nanoparticles, neither *in vitro* metric translated into enhanced immunogenicity *in vivo*.

The fact that the combination group of IgG1- and IgG2a-coated nanoparticles showed significantly inferior IgG2a responses to mice immunized with IgG2a-coated nanoparticles alone or uncoated nanoparticles is surprising. Since uncoated OVA nanoparticles induce IgG1 and IgG2a antibodies, the immune system may perceive the presence of uncoated nanoparticles as an “unresolved insult” that requires an increased

antibody response. The introduction of IgG1- and IgG2a-coated nanoparticles may be perceived, therefore, as a pathogen that the body has already developed a response against, and consequently signals that an additional adaptive immune response is not required. The hypothesis that a combination of IgG1- and IgG2a-coated particulates promotes negative immunofeedback regulation would imply that this combination of antibodies is not suitable for enhancing nanovaccine adjuvancy. Experiments to test the negative immunofeedback hypothesis should examine the effects of IgG- and IgM-opsonized nanoparticle vaccines on IgG antibody responses. Opsonized nanoparticles could be given as a priming immunization or a boost immunization following an unopsonized nanoparticle prime immunization, in order to elucidate the potency of immunofeedback mechanisms in naïve and exposed populations.

The fact that IgG1 and IgG2a coating density was not consistent between the two types of coated nanoparticles confounds the effects of antibody isotype and density. Antibody density on OVA-OVA nanoparticles did not affect the TNF-α response, although the difference in density between the highest and lowest types of nanoparticles was only about a factor of 2. The greater than 30-fold discrepancy between IgG1 and IgG2a binding to uncoated nanoparticles means the TNF-α data cannot justify discounting density as a factor in explaining our *in vivo* results. High antibody densities on antigen, such as those of IgG1 on our nanoparticles, could occlude important epitopes needed by germinal center B cells to develop high affinity antibodies to conformational epitopes [58]. At the same time, too low of an antibody density on the nanoparticles could decrease complement activation, another important process in initiating adaptive immunity [34, 55]. Further

studies should investigate the role of antibody density on vaccine nanoparticles in triggering immune responses, as an optimal coating density probably exists.

The TNF-α responses observed in response to coated and uncoated OVA nanoparticles are very different than those observed in Chapter 3. In addition to using primary BMDCs instead of JAWS cells, the cells here were stimulated for 24 hours instead of 6. The discrepancy between the two data sets could represent, therefore, different timescales of DC inflammation associated with different types of nanoparticles, although future comparisons would have to be made using the same types of cells at each timepoint for conclusions about inflammation patterns to be drawn.

In our quenched antibody coating studies, we found that a large portion of bound IgG1 and IgG2a was non-specifically bound, even on coated OVA nanoparticles. We chose mouse anti-OVA antibodies for coating our nanoparticles to allow the Fc region of the antibody to interface with the host's immune system, and non-specifically bound IgG may not be able to interact with the cells and proteins of the immune system as efficiently. Supporting evidence for this was recently published by Holt et al., examining complement activation by IgG specifically or non-specifically adsorbed to microparticles [35]. IgG with Fc domains oriented outwards was able to sequester complement on the surface of the nanoparticle, while randomly adsorbed IgG generated soluble TCC away from the nanoparticles' surface, which could decrease the adjuvancy of the nanoparticle. Additionally, given that Fc sequestration is a strategy employed by pathogens to evade the host's immune response [59], it is important that antibody-coated nanoparticle vaccines retain the Fc-out conformation. Future studies should look into minimizing improper binding of antibodies during the coating process.

When equal coating concentrations of IgG1 and IgG2a were mixed with coated and uncoated nanoparticles, IgG1 bound to the nanoparticles much more efficiently than IgG2a did. This may suggest that the large discrepancy in coating density may be a fundamental property of the immunoglobulin subclasses themselves, potentially due to IgG2a being hypothesized to have more effector functions than IgG1 [60], and thus requiring tighter regulation of its binding. Future studies should design nanoparticles with comparable coating densities of IgG on nanoparticles' surfaces to not only deconvolve the effects of Fc density on immunostimulation, but to also reduce the possibility of antigen occlusion by antibodies reducing the immunogenicity of the nanoparticles.

Our finding that all uncoated, IgG1- and IgG2a-coated nanoparticles all triggered BMDC maturation is consistent with our results in Chapters 2 and 3 showing upregulation of CD86 in JAWS dendritic cells in response to OVA and 3HA nanoparticles. CD86 upregulation in primary BMDCs was much more dramatic than upregulation by the JAWS cell line, suggesting that BMDCs should be used in future studies. Taken together, the upregulation findings suggest that a fundamental component of protein nanoparticle adjuvancy is triggering dendritic cell maturation. Molecular adjuvants that are used to coat protein nanoparticle vaccines should therefore primarily be triggers of inflammation, rather than maturation, to maximize synergistic effects between the two.

To the best of our knowledge, the exact function of each of the IgG subtypes remains unclear and a subject of active investigation. Though the pentameric IgM molecule is conserved between humans and mice, the diversity of IgG subtype numbers, ranging from one in rabbits to 4 in humans and mice to 8 in elephants may suggest that the existence of IgG subtypes is a coincidence rather than a conserved evolutionary trait [60]. Though our

data suggest that IgM could act as a host-derived adjuvant, more information on the immunological processes associated with each IgG subtype will be needed to determine whether IgG-mediated immunofeedback is subtype dependent. Additionally, controlling for the effects of antigen occlusion and antibody density through particle design will be necessary to provide conclusive insight into IgG-mediated immunofeedback.

5.4.4 A Note on Controls Across Studies

Comparing the FliC/IgM and IgG studies, it is important to highlight the differences between the G1 control groups. In the FliC/IgM study, OVA-OVA nanoparticles were used as the unadjuvanted control, whereas in the IgG study, uncoated OVA cores were the unadjuvanted control. The motivation for the FliC/IgM study came from the observation in Chapter 2 that coated 3HA nanoparticles triggered protective immunity, and we sought to replace the antigen coating on the nanoparticles with an adjuvant coating instead. The IgG study was designed to answer a more fundamental question; if IgG on nanoparticles would bias the resulting immune response. Though both coated and uncoated particles could be considered valid controls for either study, a crucial difference between the two was that uncoated OVA cores in the second study triggered strong IgG1 and IgG2a responses, while OVA-OVA nanoparticles only triggered IgG1 production. An explanation for this may lie in our observation in Chapter 3 that uncoated OVA nanoparticles bind serum proteins better than coated OVA nanoparticles do, which could lead to a more immunogenic nanoparticle. Nevertheless, the IgG2a response to uncoated OVA cores calls into question whether IgM-coated OVA nanoparticles triggered class switching, or whether this was an artefact of an incomplete coating of IgM on the surface of an uncoated nanoparticle. While direct comparisons across the two studies are difficult to draw because

of the different conditions under which they were conducted, the higher levels of $CD44^+/CD62L^+$ T_{CM} proliferation in response to IgM-OVA nanoparticles than uncoated OVA nanoparticles would seem to suggest that IgM at the very least is responsible for enhancing central memory T cell responses.

The uncoated OVA control also calls into question whether the OVA cores + soluble FliC experienced enhanced adjuvancy due to the FliC adjuvant or to the uncoated nanoparticles. Without ELISPOT or biolayer interferometry data for the uncoated OVA particle group, it is hard to answer that question. However, because administering a soluble adjuvant inherently meant administering an uncoated nanoparticle, our comparison between adsorbed and detached flagellin still remains valid. Follow-up experiments to compare flagellin adsorbed to or detached from other types of nanoparticles to could further support or refute our conclusions drawn here.

Finally, it is important to note the diversity of immunological metrics measured inherently translates into a wide range of effect sizes and, consequently, many measurements with overlapping error bars and differences of low significance. Since serum antibody levels are one of the terminal outputs that many immunological pathways converge upon, these should be regarded as the primary results from which to draw statistical conclusions. Other mechanistic measurements, such as those of helper T cells, can further describe the immune responses observed, but their effect sizes will be inherently lower as a result of their upstream position in the immunological pathway, and are harder to draw statistical conclusions from.

5.5 Conclusions

In this work, we tested the efficacy of host-derived adjuvants, IgM and IgG, as well as the use of a pathogen-derived adjuvant both on nanoparticles and admixed with them. Given the enhanced adjuvancy we observed with IgM, our finding that IgG did not enhance the immune response in comparison to uncoated OVA nanoparticles was surprising. The large amount of non-specifically adsorbed IgG may have played a role, and future studies should investigate methods to minimize non-specific IgG binding by altering reaction time, IgG concentration, rate of IgG addition, and other parameters. Additionally, studies to ensure proper IgM orientation should also be performed in conjunction with IgM density optimization. The finding that the combination of IgG1- and IgG2a-coated nanoparticles reduced IgG2a responses may suggest a negative feedback mechanism involving both subtypes regulates antibody class switching. From a therapeutic development perspective, our results suggest combinations of antibody coatings should be avoided until individual antibody subtypes have their adjuvant effects established.

Perhaps our most surprising finding was that antibody affinity maturation and IgG2a class switching did not correlate with one another. The two processes are normally associated with each other in the development of an antibody response [7]. We found all nanoparticle types except OVA-OVA nanoparticles and IgG1-OVA/IgG2a-OVA nanoparticles triggered class switching. Unadjuvanted OVA-OVA nanoparticles and FliC-coated OVA nanoparticles triggered affinity maturation, while IgM- and soluble FliC-adjuvanted nanoparticles did not. Our results stand in contrast to those by Corley, et al., who showed that IgM-bound soluble antigen (IgM-ICs) accelerates affinity maturation responses to T-dependent antigens[39]. Future work should examine the differences in

immune responses to soluble and nanoparticulate immune complexes, and whether such a difference can be exploited to tune the affinity of the humoral immune response. Affinity maturation is necessary for generating high affinity, neutralizing antibodies, which can be protective against highly conserved pathogens[61]. For pathogens that mutate or change yearly, such as influenza, however, the generation of high-affinity neutralizing antibodies results in a loss of antibody diversity, and can contribute to the phenomenon known as original antigenic sin, in which antibodies are only made to epitopes found on the first strain of virus the immune system encountered[7]. If vaccine adjuvants can delay the affinity maturation process while promoting diversification of antibody effector functions via class switching, it is possible that the memory B cell repertoire generated from the immunization will be more effective at combatting rapidly mutating pathogens.

The work of this chapter confirms the hypothesis set forth in Chapters 2 and 3 – that molecular adjuvants can be used as coatings on protein nanoparticle vaccines to bias the resulting immune response. In particular, host-derived immunoglobulins are a promising new class of adjuvants that can interact with multiple parts of the immune system. Given the role that Fc receptors play in proper presentation of antigen by follicular dendritic cells to germinal center B cells [62], it is possible that immunoglobulin-opsonized nanoparticles enhance the germinal center response. Flow cytometry or immunohistochemical studies could elucidate the exact role of opsonizing immunoglobulin in the germinal center response. Immunoglobulin coatings on nanoparticle vaccines is consistent with the pathogen-mimetic paradigm of nanovaccine development, and is a relatively unexplored field. If the challenge of optimizing specific antibody binding can be

met, these host-derived proteins could provide the next generation of safe and effective vaccine adjuvants.

REFERENCES

[1] J. Leleux, K. Roy, Micro and Nanoparticle-Based Delivery Systems for Vaccine Immunotherapy: An Immunological and Materials Perspective, Adv Healthc Mater 2(1) (2013) 72-94.

[2] J.M. Brewer, K.G.J. Pollock, L. Tetley, D.G. Russell, Vesicle size influences the trafficking, processing, and presentation of antigens in lipid vesicles, J Immunol 173(10) (2004) 6143-6150.

[3] M. Lundqvist, J. Stigler, G. Elia, I. Lynch, T. Cedervall, K.A. Dawson, Nanoparticle size and surface properties determine the protein corona with possible implications for biological impacts, P Natl Acad Sci USA 105(38) (2008) 14265-14270.

[4] S. Kumar, A.C. Anselmo, A. Banerjee, M. Zakrewsky, S. Mitragotri, Shape and size-dependent immune response to antigen-carrying nanoparticles, J Control Release 220(Pt A) (2015) 141-148.

[5] K.A. Beningo, Y.L. Wang, Fc-receptor-mediated phagocytosis is regulated by mechanical properties of the target, J Cell Sci 115(4) (2002) 849-856.

[6] D.J. Irvine, M.A. Swartz, G.L. Szeto, Engineering synthetic vaccines using cues from natural immunity, Nat Mater 12(11) (2013) 978-990.

[7] K. Murphy, P. Travers, M. Walport, C. Janeway, Janeway's immunobiology, Garland Science, New York, 2012.

[8] D.T. Fearon, R.M. Locksley, Elements of immunity - The instructive role of innate immunity in the acquired immune response, Science 272(5258) (1996) 50-54.

[9] S.P. Kasturi, I. Skountzou, R.A. Albrecht, D. Koutsonanos, T. Hua, H.I. Nakaya, R. Ravindran, S. Stewart, M. Alam, M. Kwissa, F. Villinger, N. Murthy, J. Steel, J. Jacob, R.J. Hogan, A. Garcia-Sastre, R. Compans, B. Pulendran, Programming the magnitude and persistence of antibody responses with innate immunity, Nature 470(7335) (2011) 543-U136.

[10] L. Wang, A. Hess, T.Z. Chang, Y.C. Wang, J.A. Champion, R.W. Compans, B.Z. Wang, Nanoclusters self-assembled from conformation-stabilized influenza M2e as broadly cross-protective influenza vaccines, Nanomed-Nanotechnol 10(2) (2014) 473-482.

[11] S.B. Mizel, J.T. Bates, Flagellin as an Adjuvant: Cellular Mechanisms and Potential, J Immunol 185(10) (2010) 5677-5682.

[12] M. Kwissa, H.I. Nakaya, H. Oluoch, B. Pulendran, Distinct TLR adjuvants differentially stimulate systemic and local innate immune responses in nonhuman primates, Blood 119(9) (2012) 2044-2055.

[13] S. Lee, Nguyen, M.T., Recent Advances of Vaccine Adjuvants for Infectious Diseases, Immune Network 15(2) (2015) 51-57.

[14] J.Z. Oh, R. Ravindran, B. Chassaing, F.A. Carvalho, M.S. Maddur, M. Bower, P. Hakimpour, K.P. Gill, H.I. Nakaya, F. Yarovinsky, R.B. Sartor, A.T. Gewirtz, B. Pulendran, TLR5-Mediated Sensing of Gut Microbiota Is Necessary for Antibody Responses to Seasonal Influenza Vaccination, Immunity 41(3) (2014) 478-492.

[15] J.R. Kim, B.C. Holbrook, S.L. Hayward, L.K. Blevins, M.J. Jorgensen, N.D. Kock, K. De Paris, R.B. D'Agostino, S.T. Aycock, S.B. Mizel, G.D. Parks, M.A. Alexander-Miller, Inclusion of Flagellin during Vaccination against Influenza Enhances Recall Responses in Nonhuman Primate Neonates, J Virol 89(14) (2015) 7291-7303.

[16] C.B. Turley, R.E. Rupp, C. Johnson, D.N. Taylor, J. Wolfson, L. Tussey, U. Kavita, L. Stanberry, A. Shaw, Safety and immunogenicity of a recombinant M2e-flagellin influenza vaccine (STF2.4xM2e) in healthy adults, Vaccine 29(32) (2011) 5145-5152.

[17] B.Z. Wang, F.S. Quan, S.M. Kang, J. Bozja, I. Skountzou, R.W. Compans, Incorporation of Membrane-Anchored Flagellin into Influenza Virus-Like Particles Enhances the Breadth of Immune Responses, J Virol 82(23) (2008) 11813-11823.

[18] H.H. Salman, J.M. Irache, C. Gamazo, Immunoadjuvant capacity of flagellin and mannosamine-coated poly(anhydride) nanoparticles in oral vaccination, Vaccine 27(35) (2009) 4784-4790.

[19] ClinicalTrials.gov, U.S. National Institutes of Health, 2016, p. Database searched for "flagellin" and "fusion".

[20] W. Zhang, L. Wang, Y. Liu, X. Chen, Q. Liu, J. Jia, T. Yang, S. Qiu, G. Ma, Immune responses to vaccines involving a combined antigen–nanoparticle mixture and nanoparticle-encapsulated antigen formulation, Biomaterials 35(23) (2014) 6086-6097.

[21] E.T. Weimer, S.E. Ervin, D.J. Wozniak, S.B. Mizel, Immunization of young African green monkeys with OprF epitope 8–OprI–type A- and B-flagellin fusion proteins promotes the production of protective antibodies against nonmucoid Pseudomonasaeruginosa, Vaccine 27(48) (2009) 6762-6769.

[22] B. Roic, S. Cajavec, N. Ergotic, Z. Lipej, J. Madic, M. Lojkic, B. Pokric, Immune complex-based vaccine for pig protection against parvovirus, J Vet Med B 53(1) (2006) 17-23.

[23] K. Rafiq, A. Bergtold, R. Clynes, Immune complex-mediated antigen presentation induces tumor immunity, J Clin Invest 110(1) (2002) 71-79.

[24] G. Fossati, R.C. Bucknall, S.W. Edwards, Insoluble and soluble immune complexes activate neutrophils by distinct activation mechanisms: changes in functional responses induced by priming with cytokines, Ann Rheum Dis 61(1) (2002) 13-19.

[25] M.Y. Kim, R. Reljic, J. Kilbourne, I. Ceballos-Olvera, M.S. Yang, J. Reyes-del Valle, H.S. Mason, Novel vaccination approach for dengue infection based on recombinant immune complex universal platform, Vaccine 33(15) (2015) 1830-1838.

[26] A. Getahun, J. Dahlstrom, S. Wernersson, B. Heyman, IgG2a-mediated enhancement of antibody and T cell responses and its relation to inhibitory and activating Fc gamma receptors, J Immunol 172(9) (2004) 5269-5276.

[27] F. Hjelm, F. Carlsson, A. Getahun, B. Heyman, Antibody-mediated regulation of the immune response, Scand J Immunol 64(3) (2006) 177-184.

[28] C.A. Clarke, W. Kulke, J.R. Krevans, D. Lehane, R.B. Mcconnell, P.M. Sheppard, W.T.A. Donohoe, J.C. Woodrow, R. Finn, Further Experimental Studies on Prevention of Rh Haemolytic Disease, Brit Med J (533) (1963) 979-&.

[29] C. Gunawan, M. Lim, C.P. Marquis, R. Amal, Nanoparticle-protein corona complexes govern the biological fates and functions of nanoparticles, J Mater Chem B 2(15) (2014) 2060-2083.

[30] L.J. Cruz, F. Rueda, B. Cordobilla, L. Simon, L. Hosta, F. Albericio, J.C. Domingo, Targeting Nanosystems to Human DCs via Fc Receptor as an Effective Strategy to Deliver Antigen for Immunotherapy, Mol Pharmaceut 8(1) (2011) 104-116.

[31] J. Banchereau, R.M. Steinman, Dendritic cells and the control of immunity, Nature 392(6673) (1998) 245-252.

[32] A. Shibuya, S. Honda, Immune regulation by Fc alpha/mu receptor (CD351) on marginal zone B cells and follicular dendritic cells, Immunol Rev 268(1) (2015) 288-295.

[33] A. Sorman, L. Zhang, Z.J. Ding, B. Heyman, How antibodies use complement to regulate antibody responses, Mol Immunol 61(2) (2014) 79-88.

[34] P.M. Pacheco, B. Le, D. White, T. Sulchek, TUNABLE COMPLEMENT ACTIVATION BY PARTICLES WITH VARIABLE SIZE AND Fc DENSITY, Nano LIFE 3(2) (2013) 1341001.

[35] B.A. Holt, M.C. Bellavia, D. Potter, D. White, S.R. Stowell, T. Sulchek, Fc microparticles can modulate the physical extent and magnitude of complement activity, Biomater Sci-Uk (2017).

[36] W.F. Rosse, Quantitative immunology of immune hemolytic anemia: I. The fixation of C1 by autoimmune antibody and heterologous anti-IgG antibody, The Journal of Clinical Investigation 50(4) (1971) 727-733.

[37] M.R. Ehrenstein, T.L. O'Keefe, S.L. Davies, M.S. Neuberger, Targeted gene disruption reveals a role for natural secretory IgM in the maturation of the primary immune response, P Natl Acad Sci USA 95(17) (1998) 10089-10093.

[38] L.L. Ilag, Immunoglobulin M as a vaccine adjuvant, Medical Hypotheses 77(4) (2011) 473-478.

[39] R.B. Corley, E.M. Morehouse, A.R. Ferguson, IgM accelerates affinity maturation, Scand J Immunol 62 (2005) 55-61.

[40] P.G. Harte, A. Cooke, J.H.L. Playfair, Specific Monoclonal Igm Is a Potent Adjuvant in Murine Malaria Vaccination, Nature 302(5905) (1983) 256-258.

[41] H.W. Schroeder, L. Cavacini, Structure and function of immunoglobulins, J. Allergy Clin. Immunol. 125(2) (2010) S41-S52.

[42] A. Regnault, D. Lankar, V. Lacabanne, A. Rodriguez, C. Thery, M. Rescigno, T. Saito, S. Verbeek, C. Bonnerot, P. Ricciardi-Castagnoli, S. Amigorena, Fc gamma receptor-mediated induction of dendritic cell maturation and major histocompatibility complex class I-restricted antigen presentation after immune complex internalization, J Exp Med 189(2) (1999) 371-380.

[43] M. Guilliams, P. Bruhns, Y. Saeys, H. Hammad, B.N. Lambrecht, The function of Fc gamma receptors in dendritic cells and macrophages, Nat Rev Immunol 14(2) (2014) 94-108.

[44] T.R. Mosmann, R.L. Coffman, Th1-Cell and Th2-Cell - Different Patterns of Lymphokine Secretion Lead to Different Functional-Properties, Annu Rev Immunol 7 (1989) 145-173.

[45] T.Z. Chang, Stadmiller, S.S., Staskevicius, E., Champion, J.A. , Effects of Ovalbumin Protein Nanoparticle Vaccine Size and Coating on Dendritic Cell Processing, Biomater Sci-Uk (in review) (2016).

[46] H.C. Chaung, L.T. Cheng, L.H. Hung, P.C. Tsai, I. Skountzou, B.Z. Wang, R.W. Compans, Y.Y. Lien, Salmonella flagellin enhances mucosal immunity of avian influenza vaccine in chickens, Vet Microbiol 157(1-2) (2012) 69-77.

[47] T.Z. Chang, S.S. Stadmiller, E. Staskevicius, J.A. Champion, Effects of ovalbumin protein nanoparticle vaccine size and coating on dendritic cell processing, Biomater Sci-Uk (2017).

[48] V. Baron, C. Bouneaud, A. Cumano, A. Lim, T.P. Arstila, P. Kourilsky, L. Ferradini, C. Pannetier, The Repertoires of Circulating Human CD8+ Central and Effector Memory T Cell Subsets Are Largely Distinct, Immunity 18(2) (2003) 193-204.

[49] F. Dakterzada, A. Mohabati Mobarez, M. Habibi Roudkenar, A. Mohsenifar, Induction of humoral immune response against Pseudomonas aeruginosa flagellin(1-161) using gold nanoparticles as an adjuvant, Vaccine 34(12) (2016) 1472-1479.

[50] A.D. Gitlin, L. von Boehmer, A. Gazumyan, Z. Shulman, T.Y. Oliveira, M.C. Nussenzweig, Independent Roles of Switching and Hypermutation in the Development and Persistence of B Lymphocyte Memory, Immunity 44(4) (2016) 769-781.

[51] S. Manmohan, Vaccine adjuvants and delivery systems, Wiley-Interscience, Hoboken, N.J., 2007.

[52] A. Getahun, B. Heyman, How antibodies act as natural adjuvants, Immunol Lett 104(1-2) (2006) 38-45.

[53] C.E. Hioe, M.L. Visciano, R. Kumar, J. Liu, E.A. Mack, R.E. Simon, D.N. Levy, M. Tuen, The use of immune complex vaccines to enhance antibody responses against neutralizing epitopes on HIV-1 envelope gp120, Vaccine 28(2) (2009) 352-360.

[54] J.R. Janczy, C. Ciraci, S. Haasken, Y. Iwakura, A.K. Olivier, S.L. Cassel, F.S. Sutterwala, Immune Complexes Inhibit IL-1 Secretion and Inflammasome Activation, J Immunol 193(10) (2014) 5190-5198.

[55] A. Ghannam, M. Pernollet, J.L. Fauquert, N. Monnier, D. Ponard, M.B. Villiers, J. Peguet-Navarro, A. Tridon, J. Lunardi, D. Gerlier, C. Drouet, Human C3 deficiency associated with impairments in dendritic cell differentiation, memory B cells, and regulatory T cells, J Immunol 181(7) (2008) 5158-5166.

[56] T.R. Mosmann, S. Sad, The expanding universe of T-cell subsets: Th1, Th2 and more, Immunol Today 17(3) (1996) 138-146.

[57] F. Sallusto, J. Geginat, A. Lanzavecchia, Central memory and effector memory T cell subsets: Function, generation, and maintenance, Annu Rev Immunol 22 (2004) 745-763.

[58] A. Aguzzi, J. Kranich, N.J. Krautler, Follicular dendritic cells: origin, phenotype, and function in health and disease, Trends Immunol 35(3) 105-113.

[59] P.R. Widders, CHAPTER 31 - Fc receptors and the pathogenesis of bacterial infections in animals A2 - Boyle, Michael D.P, Bacterial Immunoglobulin-binding Proteins, Academic Press1990, pp. 375-396.

[60] A.M. Collins, IgG subclass co-expression brings harmony to the quartet model of murine IgG function, Immunol Cell Biol 94(10) (2016) 949-954.

[61] R.N. Germain, Vaccines and the Future of Human Immunology, Immunity 33(4) (2010) 441-450.

[62] B.A. Heesters, P. Chatterjee, Y.A. Kim, S.F. Gonzalez, M.P. Kuligowski, T. Kirchhausen, M.C. Carroll, Endocytosis and Recycling of Immune Complexes by

Follicular Dendritic Cells Enhances B Cell Antigen Binding and Activation, Immunity 38(6) (2013) 1164-1175.

CHAPTER 6. CONCLUSIONS AND FUTURE DIRECTIONS

The studies performed in this work establish protein nanoparticles as a promising platform technology for enhancing recombinant antigen adjuvancy. The simple method of desolvation employs a non-toxic solvent, ethanol, to generate a high yield of nanoparticles that consist primarily of antigen. As we demonstrated in Chapters 2, 3 and 5, desolvated nanoparticles can be further modified by coating with antigen or adjuvant to enhance or alter the immune response. As immunologists learn more about the protective immunological correlates associated with different pathogens, the immunomodulatory capacity of coated protein nanoparticles, and coated nanoparticle vaccines in general, will become increasingly relevant. Outlined below are the key insights this thesis contributes to the growing literature on nanoparticle vaccines.

6.1 Mechanistic Insights into Protein Nanoparticle Adjuvancy

In Chapter 3, the *in vitro* studies of OVA nanoparticle-dendritic cell interactions established that protein nanoparticles enhance antigen uptake and reduce antigen acidification by dendritic cells, but these markers alone did not lead to increased inflammatory responses. Inflammation was instead found to depend on size and coating, with nanoparticles between 270-350 nm in size more inflammatory than 500 nm nanoparticles. This inflammatory size range, which overlaps with that of some viruses, is consistent with the pathogen-mimetic paradigm of nanoparticle vaccine design.

The *in vivo* studies with 3HA nanoparticles show that components of the immune system that are downstream of dendritic cells also play a role in interacting with protein nanoparticle vaccines. While antigen retention at the site of injection did not play a role in enhancing adjuvancy, nanoparticles were retained better than soluble protein in the spleen after 8 days. In the spleen and draining lymph nodes, nanoparticles also enhanced germinal center B cell responses better than soluble protein did. Further evidence for B cell involvement was found in Chapter 4, as fresh and aged 3HA nanoparticles induced higher levels of neutralizing antibodies than soluble 3HA did. The enhanced ability of nanoparticles to induce neutralizing antibodies is additional supporting evidence for the pathogen-mimetic design strategy of multimeric antigen display on the nanoparticle surface. Taken together, our results implicate dendritic cells, B cells, and splenic antigen retention in mediating protein nanoparticle adjuvancy.

6.2 Flagellin Adjuvancy

The findings in Chapter 2 that FliC-M2e fusion protein nanoparticles are capable of inducing protective immune responses suggested that flagellin may not need to be incorporated in a 1:1 ratio with antigen protein. We explored this idea further in Chapter 5, using full-length flagellin to coat desolvated protein nanoparticles. Our results showed that FliC-coated nanoparticles retained their TLR-5-stimulating activity, and enhanced the immune response to the underlying antigen core. Corroboration of these findings by using FliC-coated antigen nanoparticles in an influenza challenge study would establish adjuvant coatings as an adjuvant dose-sparing alternative to FliC-fusion proteins.

6.3 Nanoparticle Stability

Our successful extended cold chain-independent storage of 3HA nanoparticles in Chapter 4 suggests the viability of protein nanoparticles as an appropriate vaccine technology for the developing world. To further validate its potential, future studies should examine how to extend viable storage at 37°C beyond 2 weeks, as storage at elevated temperatures is especially important for transport to tropical and sub-tropical regions of the world. Given the importance of adjuvant coatings on protein nanoparticles that we observed in Chapter 5, storage of different types of adjuvant-coated protein nanoparticles should also be tested to ensure that the molecular adjuvants used can retain their stimulatory abilities outside of the cold-chain.

Wherever stability cannot be maintained, a screen of stabilizing excipient compounds could be used to find sugars and buffer salts that assist in preservation of protein structure. Alternatively, protein nanoparticles with components prone to hydrolysis could be entrapped in a non-aqueous vaccine delivery vehicle, such as in microneedle patches [1]. In addition to enhancing protein stability, microneedles can provide an easier means of vaccine administration than hypodermic needles, and provide access to the antigen presenting cell-rich layers of the dermis [2].

6.4 Immunoglobulins as Nanoparticle-Bound Adjuvants

Although FliC showed promising results as an adjuvant coating, we tested the adjuvant efficacy of the host-derived proteins IgG and IgM because of potential issues with pathogen-derived adjuvant toxicity. IgM-coated OVA nanoparticles significantly enhanced memory T cell responses *in vivo*, and triggered IgG class switching but not affinity

maturation. Future studies should examine the hypothesis that delayed affinity maturation responses translate into more cross-protective immune responses in *in vivo* challenge models of highly mutable pathogens.

Contrary to observations in the literature, the IgM coating on our nanoparticles did not significantly induce complement activation. Future studies should vary IgM density on the nanoparticle surface to look for complement activation *in vitro* and other immunomodulatory effects *in vivo*.

Though IgG2a-coated nanoparticles were able to activate complement, we did not observe any enhancement of antibody or memory T cell responses *in vivo* in response to IgG-coated nanoparticles. Upon further study, OVA nanoparticles were found to have a significant amount of non-specifically adsorbed antibodies, which may have led to non-immunogenic clearance instead of immunostimulatory antigen presentation. By adding antibodies to OVA-coated-OVA particles, we were able to both increase the amount of properly-oriented antibodies and enhance TNF-α secretion in response to nanoparticles by BMDCs. This leads us to believe IgG may still prove useful as an adjuvant, though care needs to be taken in future work to minimize non-specifically adsorbed antibodies.

6.5 Perspectives and Future Work

Vaccine design is moving away from the isolate-inactive-inject paradigm and toward more engineered vaccine formulations for directing the immune response. Protein nanoparticles made from crosslinked antigen could be a safe, effective, and cold-chain-independent platform technology for enhancing recombinant antigen immunogenicity. The combination of particulate and molecular adjuvants holds great potential for engineering

specific immune responses to antigens from different pathogens, and the findings of this thesis can help guide molecular adjuvant choice for other types of vaccine nanoparticles. Specifically, molecular adjuvants should focus on generating APC inflammation and biasing APC inflammatory responses toward generating the desired adaptive immune responses. While multimeric epitope and TLR-ligand display can be used to generate immunogenic nanoparticles in line with the pathogen-mimetic design strategy, immunoglobulin-coated nanoparticles are also consistent with the pathogen-mimetic design strategy. Host-derived immunoglobulins could be a safer alternative to pathogen-derived adjuvants, and the synergistic effects between nanoparticulate and immunoglobulin-mediated adjuvancy is a promising area of investigation.

Future work to build on our FliC-coated nanoparticles should look at other TLR ligand-coated nanoparticles versus admixed TLR ligands. Additionally, dose-sparing studies should be performed comparing FliC-coated nanoparticles to FliC-fusion proteins to confirm whether nanoparticle colocalization can reduce the amount of adjuvant needed for an immunization.

Building on our stability studies, strategies to extend the 37°C wet storage of protein nanoparticles should be investigated. Methods for prolonging storage can include the addition of excipient salts, disaccharides, or biodegradable polymers that can bind to the protein nanoparticles and shield them from nanoparticle collision-induced denaturation. The wet storage of immunoglobulin-coated nanoparticles or other adjuvant-coated nanoparticles should also be tested. If wet storage is not possible for certain types of adjuvanted nanoparticles, excipients should also be tested for enhancing extended wet

storage. At the same time, the stable incorporation of nanoparticles into microneedle patches should also be pursued for enhancing delivery of vaccine to the APCs of the dermis.

Of particular interest is the future development of immunoglobulin coatings of nanoparticulate vaccines. The following sections outline three studies that could be undertaken to further develop immunoglobulins as adjuvants.

6.6 Hapten-Mediated Immunoglobulin Coupling

To avoid the necessity of developing new types of antibodies for each new antigen nanoparticle, a chemically conjugated hapten coating on the surface of the vaccine nanoparticles can serve as an adapter between the antibody coating and the antigen core. Figure 60 illustrates how the small molecule trinitrobenzenesulfonic acid (TNBS) can be used to chemically add trinitrophenol (TNP) groups to the surface of a nanoparticle, which can then be bound by anti-hapten antibodies. Instead of relying on affinity interactions between antibodies with different target epitopes, a standard anti-hapten affinity interaction can be optimized and used across many different vaccine nanoparticle types.

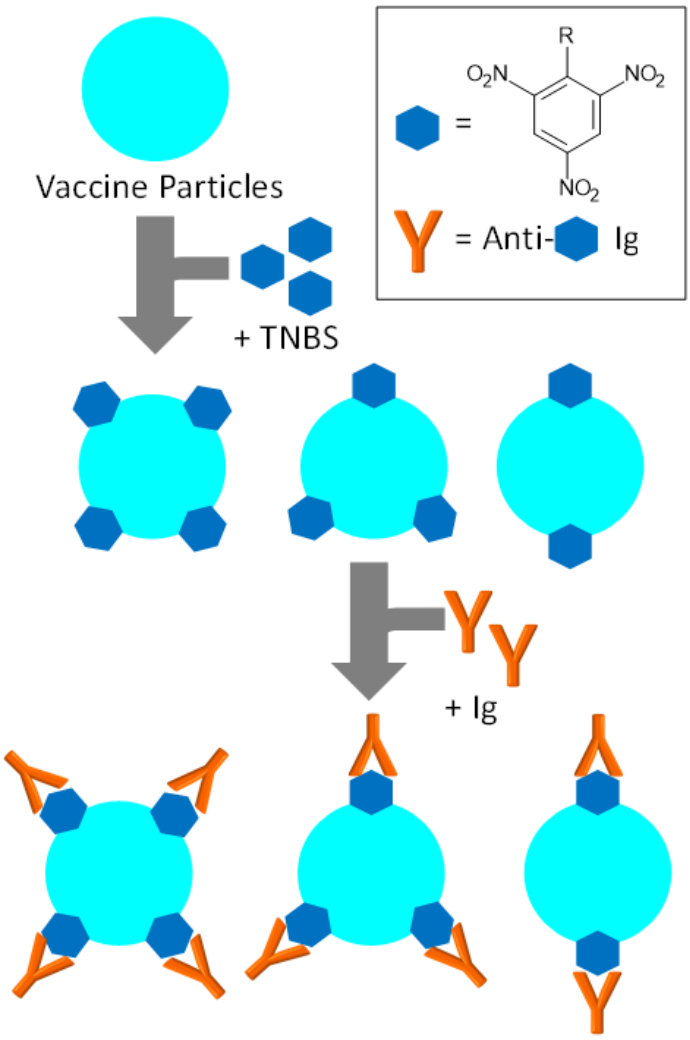

Figure 60. Proposed coating scheme involving conjugating protein nanoparticles with a small molecule hapten (TNP) first, then binding anti-TNP immunoglobulin to the surface. This plan should allow for better antibody density control, greater fraction of properly-oriented antibodies, and increased versatility of the immunoglobulin adjuvant as a platform technology.

6.7 Examining Density Effects

Once the hapten coating protocol is established, different densities of hapten and antibody can be used to coat the nanoparticles. By controlling hapten conjugation density, we can theoretically achieve a much higher antibody coating density than would be possible through only binding native antigen epitopes. Varying antibody density on the particle surface should reveal an optimal coating density – too many antibodies can mask epitopes needed for B cell antigen presentation, too few antibodies could be insufficient for complement activation or other Fc-mediated adjuvant effects. In addition to exploring antibody density effects, controlling antibody density across different subtypes will allow for conclusions on subtype-mediated immunofeedback to be drawn. As monoclonal antibodies are still relatively expensive compared to influenza vaccines [3], cost considerations should also be taken into account for minimizing immunoglobulin use.

6.8 Additional Antibody Isotype Testing

Other antibody isotypes may also be immunogenic on protein nanoparticles, and should be investigated for their adjuvant potential as well. In particular, IgE and IgA are especially important in providing mucosal protection. Recently, IgE has been identified as a potent weapon in cancer immunotherapy [4, 5], although IgE-adjuvanted vaccines have so far been limited to intravenous administration of IgE-opsonized cancer cells [6], and recombinant, Fcε-expressing cancer cells [7]. Immunoglobulin E is most commonly associated with anti- parasite and allergic responses. It is the last antibody isotype in the class-switching series, and can trigger powerful immune responses that can range from parasite neutralization to systemic anaphylaxis [8]. Of all the antibody classes, IgE has the

greatest potential for generating strong immune responses, and the administration route needs to be carefully examined to avoid the risk of anaphylaxis.

Immunoglobulin A is predominantly found in mucosal secretions [8], IgA-NPs administered through mucosal routes (i.e. intra-nasal) may be more immunogenic than IgA-NPs administered through the traditional intra-muscular route. Given the importance of mucosal immunity in influenza and other respiratory diseases, and the fact that our protein nanoparticles have generated immune responses through both of these routes previously [9, 10], IgA would seem to be a reasonable choice of adjuvant for an influenza vaccine.

Although our studies are primarily motivated by vaccine development, testing various antibody isotypes and densities as nanoparticle coatings can yield fundamental insight into the feedback-based regulation of the immune system. Using antibodies on nanoparticles to downregulate the antibody response could eventually have implications in treating autoimmune diseases and organ transplant recipients, while therapeutics that upregulate anti-cancer antibodies could become a cornerstone of the next generation of ADCC-dependent cancer therapies.

APPENDIX A. SEQUENCES OF RECOMBINANT INFLUENZA PROTEINS USED

6.9 M2e Peptides

M2e sequence from

H1N1:SLLTEVETPTRSEWESRSSDSSDP

H3N2:SLLTEVETPIRNEWGSRSNDSSDP

H5N1:SLLTEVETPTRTEWESRSSDSSDP

H7N9:SLLTEVETPTRTGWESNSSGSSEP

6.10 H7 Hemagglutinin Sequences

Red = H7 Hemagglutinin Sequence, Green = GCN4 Trimerization Motif, Blue = His Tag

3HA Sequence : 62.86 kDa, 33 free amines

MNTQILVFALIAIIPTNADKICLGHHAVSNGTKVNTLTERGVEVVNATETVERTNI
PRICSKGKRTVDLGQCGLLGTITGPPQCDQFLEFSADLIIERREGSDVCYPGKFVN
EEALRQILRESGGIDKEAMGFTYSGIRTNGATSACRRSGSSFYAEMKWLLSNTDN
AAFPQMTKSYKNTRKSPALIVWGIHHSVSTAEQTKLYGSGNKLVTVGSSNYQQS
FVPSPGARPQVNGLSGRIDFHWLMLNPNDTVTFSFNGAFIAPDRASFLRGKSMGI
QSGVQVDANCEGDCYHSGGTIISNLPFQNIDSRAVGKCPRYVKQRSLLLATGMK
NVPEIPKGRGLFGAIAGFIENGWEGLIDGWYGFRHQNAQGEGTAADYKSTQSAI
DQITGKLNRLIEKTNQQFELIDNEFNEVEKQIGNVINWTRDSITEVWSYNAELLVA

MENQHTIDLADSEMDKLYERVKRQLRENAEEDGTGCFEIFHKCDDDCMASIRNN
TYDHSKYREEAMQNRIQIDPVKLSSGYKDRMKQIEDKIEEILSKIYHIENEIARIKK
LVGERHHHHHH

HA Sequence ; 58.85 kDa, 28 free amines

MNTQILVFALIAIIPTNADKICLGHHAVSNGTKVNTLTERGVEVVNATETVERTNI
PRICSKGKRTVDLGQCGLLGTITGPPQCDQFLEFSADLIIERREGSDVCYPGKFVN
EEALRQILRESGGIDKEAMGFTYSGIRTNGATSACRRSGSSFYAEMKWLLSNTDN
AAFPQMTKSYKNTRKSPALIVWGIHHSVSTAEQTKLYGSGNKLVTVGSSNYQQS
FVPSPGARPQVNGLSGRIDFHWLMLNPNDTVTFSFNGAFIAPDRASFLRGKSMGI
QSGVQVDANCEGDCYHSGGTIISNLPFQNIDSRAVGKCPRYVKQRSLLLATGMK
NVPEIPKGRGLFGAIAGFIENGWEGLIDGWYGFRHQNAQGEGTAADYKSTQSAI
DQITGKLNRLIEKTNQQFELIDNEFNEVEKQIGNVINWTRDSITEVWSYNAELLVA
MENQHTIDLADSEMDKLYERVKRQLRENAEEDGTGCFEIFHKCDDDCMASIRNN
TYDHSKYREEAMQNRIQIDPVKLSSGYKDHHHHHH

6.11 FliC-Fusion Proteins with PR8 and AiChi Stalk Domains

PR8 24-184 amino acid sequences:

MAQVINTNSLSLLTQNNLNKSQSALGTAIERLSSGLRINSAKDDAAGQAIANRFTANI
KGLTQASRNANDGISIAQTTEGALNEINNNLQRVRELAVQSANSTNSQSDLDSIQAEI
TQRLNEIDRVSGQTQFNGVKVLAQDNTLTIQVGANDGETIDIDLKQINSQTLGLDTLN
VGAPVGSAAAYQHQNEQGSGYAADQKSTQNAINGITNKVNSVIEKMNTQFTAVGKE
FNKLEKRMENLNKKVDDGFLDIWTYNAELLVLLENERTLDFHDSNVKNLYEKVKSQ
LKNNAKEIGNGCFEFYHKCDNECMESVRNGTYDYPKYSEESKLNREKVDGVKLESM
GIY VDELKL ASPWTTTENPLQKIDAALAQVDTLRSDLGAVQNR
FNSAITNLGNTVNNLTSARSRIEDSDYATEVSNMSRAQILQQ
AGTSVLAQANQVPQNVLSLLRLEHHHHHH

Black: Nde+1-176 aa of sflic
Green: BamHI
Red: linker region
Blue: PR8 insertion
Orange SalI, SacI and HindIII
Purple: C terminus+xhoI+his tag

Aichi 24-184-flic fusion protein sequence:

MAQVINTNSLSLLTQNNLNKSQSALGTAIERLSSGLRINSAKDDAAGQAIANRFTAN
IKGLTQASRNANDGISIAQTTEGALNEINNNLQRVRELAVQSANSTNSQSDLDSIQAE
TQRLNEIDRVSGQTQFNGVKVLAQDNTLTIQVGANDGETIDIDLKQINSQTLGLDTL
VGAPVGSAAA FRHQNSEGTGQAADLKSTQAAIDQINGKLNR
IEKTNEKFHQIEKEFSEVEGRIQDLEKYVEDTKIDLWSYN
ELLVALENQHTIDLTDSEMNKLFEKTRRQLRENAEEMGN
CFKIYHKCDNACIESIRNGTYDHDVYRDEALNNRFQIKG
ELKSGYKDVDELKL ASPWTTTENPLQKIDAALAQVDTLRSDL
AVQNRFNSAITNLGNTVNNLTSARSRIEDSDYATEVSNMSR
QILQQAGTSVLAQANQVPQNVLSLLRLEHHHHHH

6.12 Flagellin (FliC) for Nanoparticle Coating

MAQVINTNSLSLLTQNNLNKSQSALGTAIERLSSGLRINSAKDD

AAGQAIANRFTANIKGLTQASRNANDGISIAQTTEGALNEINNNLQRVRELAVQS

ANSTNSQSDLDSIQAEITQRLNEIDRVSGQTQFNGVKVLAQDNTLTIQVGANDGE

TIDIDLKQINSQTLGLDTLNVQQKYKVSDTAATVTGYADTTIALDNSTFKASATG

LGGTDQKIDGDLKFDDTTGKYYAKVTVTGGTGKDGYYEVSVDKTNGEVTLAG

GATSPLTGGLPATATEDVKNVQVANADLTEAKAALTAAGVTGTASVVKMSYTD

NNGKTIDGGLAVKVGDDYYSATQNKDGSISINTTKYTADDGTSKTALNKLGGA

DGKTEVVSIGGKTYAASKAEGHNFKAQPDLAEAAATTTENPLQKIDAALAQVDT

LRSDLGAVQNRFNSAITNLGNTVNNLTSARSRIEDSDYATEVSNMSRAQILQQAG

TSVLAQANQVPQNVLSLLRHHHHHH

REFERENCES

[1] M.D. Martin, W.C. Weldon, V.G. Zarnitsyn, D.G. Koutsonanos, H. Akbari, I. Skountzou, J. Jacob, M.R. Prausnitz, R.W. Compans, Local Response to Microneedle-Based Influenza Immunization in the Skin, Mbio 3(2) (2012).

[2] R.T. Kenney , S.A. Frech , L.R. Muenz , C.P. Villar , G.M. Glenn Dose Sparing with Intradermal Injection of Influenza Vaccine, New Engl J Med 351(22) (2004) 2295-2301.

[3] B. Kelley, Industrialization of mAb production technology The bioprocessing industry at a crossroads, Mabs 1(5) (2009) 443-452.

[4] L.S. Leoh, T.R. Daniels-Wells, M.L. Penichet, IgE Immunotherapy Against Cancer, Ige Antibodies: Generation and Function 388 (2015) 109-149.

[5] J. Singer, E. Jensen-Jarolim, IgE-based immunotherapy of cancer: challenges and chances, Allergy 69(2) (2014) 137-149.

[6] E.A. Nigro, A.T. Brini, E. Soprana, A. Ambrosi, D. Dombrowicz, A.G. Siccardi, L. Vangelista, Antitumor IgE Adjuvanticity: Key Role of Fc epsilon RI, J Immunol 183(7) (2009) 4530-4536.

[7] E.A. Nigro, E. Soprana, A.T. Brini, A. Ambrosi, V.A. Yenagi, D. Dombrowicz, A.G. Siccardi, L. Vangelista, An Antitumor Cellular Vaccine Based on a Mini-Membrane IgE, J Immunol 188(1) (2012) 103-110.

[8] K. Murphy, P. Travers, M. Walport, C. Janeway, Janeway's immunobiology, Garland Science, New York, 2012.

[9] L. Wang, A. Hess, T.Z. Chang, Y.C. Wang, J.A. Champion, R.W. Compans, B.Z. Wang, Nanoclusters self-assembled from conformation-stabilized influenza M2e as broadly cross-protective influenza vaccines, Nanomed-Nanotechnol 10(2) (2014) 473-482.

[10] L. Wang, T.Z. Chang, Y. He, J.R. Kim, S. Wang, T. Mohan, Z. Berman, S.M. Tompkins, R.A. Tripp, R.W. Compans, J.A. Champion, B.-Z. Wang, Coated protein nanoclusters from influenza H7N9 HA are highly immunogenic and induce robust protective immunity, Nanomedicine: Nanotechnology, Biology and Medicine 13(1) (2016) 253-262.